Acoustically induced spin relaxation in two-dimensional electronic systems

Dissertation

zur Erlangung des akademischen Grades
Dr. rer. nat.
eingereicht an der
Mathematisch-Naturwissenschaftlichen-Technischen Fakultät
der Universität Augsburg

von
Johannes Wanner

Augsburg, September 14, 2015

Erstgutachter:	Prof. Dr. Ulrich Eckern
Zweitgutachter:	Prof. Dr. Gert-Ludwig Ingold
Tag der mündlichen Prüfung:	25.11.2015

Contents

1. Introduction

Nowadays, electronic devices such as the central processing unit CPU of a computer are based on the flow of electric currents. Electronic switches inside the microprocessors are interconnected to build up logical gates, which consist mainly of transistors and diodes. Since the first transistor by Bardeen, Brattain and Shockley in 1947, many types of transistors have been developed mostly with the goal to improve their switching speed and also to reduce their size. The rapid technological progress over the last decades can thus be ascribed in a large part to the increase of the number of transistors within electronic devices. Already forty years ago, in 1975, Gordon E. Moore predicted a doubling of the number of transistors on a chip every two years [1]. This exponential growth, known as Moore's law, is valid until today. However, to maintain this rate in the future, new concepts have to be established.

The development of spintronics [2–5] represents a promising candidate for upcoming devices. As implied by its name, spintronics is the idea of manipulating the spin polarisation of charge carriers instead of their motion. The information is then no longer carried by the charge but the spin of an electron. One of the appealing aspects of semiconductor spintronic devices is the prospect of a possible combination with conventional electronic systems.

For a successful inclusion of existing approaches to spin manipulation into electronic systems some obstacles have to be overcome. A major task for the engineering of future devices is to generate and reliably detect an ensemble of spins. A local spin polarisation can be generated by shining polarized light onto a semiconductor sample. If the energy of the light matches the band gap of the semiconductor, the photons are able to create electron-hole pairs. As the angular momentum of the photons is preserved during the excitation process, the spin of the electron is oppositely aligned to the spin of the holes. Hence, a spin polarization can be obtained and by that information can be written. In practice, such a spin density is only stable within confined systems like quantum dots, where electrons are not able to couple to extra degrees of freedom. A disadvantage of such zero-dimensional systems is the confinement of the spins to the quantum

dot, as for spintronic devices controlled transport of the spin density is desirable. In unconfined systems, however, relaxation processes remove all stored information previously encoded in the spin density within the spin lifetime. For a working quantum computing device a reliable storage of information is mandatory, i.e., the lifetime of the spins has to be longer than one writing-reading cycle [6].

One of the main sources of spin relaxation in undoped semiconductors has its origin in the electron-hole exchange interaction known as the Bir-Aronov-Pikus spin dephasing mechanism [7]. This mechanism is especially important for excitons, which are bound pairs of electrons and holes [8] analogous to a hydrogen atom.

In this thesis, we discuss an approach which spatially separates the electrons from the holes, and thus effectively suppresses the Bir-Aronov-Pikus relaxation mechanism, namely the spin dynamics of a two-dimensional electron gas in a quantum well. Such heterostructures confine electrons within a thin layer of a material with a smaller band gap than the surrounding semiconducting material. Gallium arsenide (GaAs) is – next to silicon – presumably the most prominent material for semiconductor applications. It is a III-V direct band gap semiconductor with zinc blende crystal structure. Contrary to silicon, GaAs consists of two distinct elements and is therefore piezoelectric.

Piezoelectricity can be expediently exploited for the generation of surface acoustic waves (SAW). These are sound waves, which are confined to the surface of a sample in the sense that the amplitude decays exponentially with the distance to the surface. An acoustic wave represents an oscillation of the density and thus a spatiotemporal deformation of the material. Hence, in piezoelectric materials a time and space-dependent electric field is induced, and the electrons and holes within the quantum well are accelerated by the in-plane component of the electric field, yet in different directions. As a consequence, electrons and holes tend to accumulate at distinct phase points of the sinusoidal electric potential of the SAW. Due to this separation, the Bir-Aronov-Pikus relaxation mechanism is suppressed and the spin lifetime is enhanced.

As a further important source of spin relaxation, for moving electrons the Dyakonov-Perel spin-dephasing mechanism [9] has to be taken into account. This mechanism arises from the spin-orbit interaction which couples the spin of an electron to its momentum. The spin density is therefore susceptible to scattering processes of the electrons, and an initial spin polarization relaxes to zero.

A SAW is able to influence the relaxation rate in basically two ways.

On the one hand, the piezoelectric field controls the momentum of the electrons and thus reduces the motional degree of freedom, and hence decreases effectively the spin relaxation rate. On the other hand, a SAW induced deformation of the material leads to additional spin-orbit interactions which enhance the relaxation rate.

In order to study these competing processes, this work is organized as follows:

- In Chap. 2 the basic properties of a SAW are reviewed. The piezoelectric field responsible for the modulation of the two dimensional electron gas, as well as the components of the strain tensor are obtained for a wave propagating in the [110] direction of an $Al_{0.3}Ga_{0.7}As$ semiconductor surface.

- Starting with the Schrödinger equation of a single electron, in Chap. 3 we will develop a description of the charge carriers which takes the properties of the crystal into account by effective Hamiltonians. For the construction of these effective Hamiltonians we will exploit the symmetry of the crystal to obtain all relevant types of effective spin-orbit couplings. Contrary to the approaches used in the literature, our method is free of any unnecessary approximations.

- In Chap. 4 we summarize the basic concepts of many-particle physics to generalize the description of single electrons by effective Hamiltonians to a quantum mechanical ensemble of electrons.

- The resulting Boltzmann-like equation, derived in Chap. 4, will eventually be utilized in Chap. 5 for the calculation of the charge dynamics as well as the spin dynamics of the two-dimensional electron gas under the influence of a SAW.

2. Surface acoustic waves

Although surface acoustic waves (SAW) came into focus in many experiments over the last decades, they were already discussed by Lord Rayleigh in 1885 [10]. In this early work, Rayleigh investigated the case of elastic waves at the surface of an isotropic medium. Rayleigh found waves where the displacement of a point describes an ellipse in the sagittal plane, which is spanned by the surface normal and the wave vector. Moreover, the amplitude of these waves is decaying exponentially with increasing distance from the surface. Additional to such waves, which are referred to as Rayleigh surface waves, Love [11] discovered another type of surface acoustic wave, where transverse shear deformation occurs. At that time, work on the field of surface acoustic waves was mainly inspired by seismology and geophysics. For the description of, e.g., earth quakes the effects of anisotropy can be neglected. Thus, in the following decades, there were hardly any further contributions to the topic of SAW. The situation changed in 1949, when Stoneley reopened the issue by discussing surface acoustic waves in hexagonal crystals [12]. In the 1950s further anisotropic materials were investigated by considering elastic waves in media with various crystal symmetries (see [13–17]).

For piezoelectric materials, such as GaAs, the theory of elastic surface acoustic waves had to be modified. An acoustic wave in piezoelectric materials is in general accompanied by an electric field, induced by the deformation of the media. Hence, additionally to the continuum mechanics of the elastic waves, Maxwell's equations have to be taken into account. The first treatment of surface acoustic waves in piezoelectric materials was carried out by Tseng and White [18] in 1967, where they discussed waves in the basal plane of hexagonal crystals.

In this chapter, we will apply the theory of SAW to materials with zinc blende structure for various crystal directions compared to the surface normal. In the first part Sec. 2.1, we therefore discuss the general concept of elastic waves in piezoelectric bulk materials. The influence of the surface boundary on the propagation of waves will then be investigated in the second part, Sec. 2.2, of this chapter.

2.1. Acoustic waves in the bulk

In principle, the vibrational motion of a lattice of atoms in solids is described by phonons, and sound waves therefore by a collective excitation of them. The wave length of a usual SAW is of the order of $\lambda_{\mathrm{SAW}} \sim 5\,\mu\mathrm{m}$ and therefore about a factor 10^4 larger than the lattice constant. In this limit of long wave length, sound waves can be described within continuum mechanics, where solids are assumed to consist of continuous material rather than discrete atoms. A large wave length corresponds to a small wave vector $\mathbf{k}_{\mathrm{SAW}}$. Hence, the dispersion relation in continuum mechanics is described by the dispersion relation of phonons near the center of the Brillouin zone. It is therefore purely linear $\omega_{\mathrm{SAW}} = v_{\mathrm{SAW}}(\hat{e}_{\mathbf{k}})k_{\mathrm{SAW}}$, where the velocity of sound depends only on the direction $\hat{e}_{\mathbf{k}}$ of the sound wave. Since in this chapter all quantities refer to acoustic waves, there is no danger of confusing the wave vector $\mathbf{k}_{\mathrm{SAW}}$ with the wave vector of the electron $\mathbf{k}$ of the following chapter. We will therefore drop the indices and denote the wave vector $\mathbf{k}_{\mathrm{SAW}} = \mathbf{k}$ throughout this chapter.

As a first step, we will neglect piezoelectricity. In continuum mechanics, a material with density ρ can be subdivided into infinitesimally small volume elements. The displacement $\mathbf{u}(\mathbf{r}, t)$ (see Fig. 2.1) of an infinitesimally small volume element exerts forces on the adjacent volume elements, and the dynamics of such an element is thus coupled to the displacement of the surrounding volume elements. The time dependence of the vector field $\mathbf{u}(\mathbf{r}, t)$ is then described analogously to Newton's equation of motion:

$$\rho \frac{\partial^2 u_i}{\partial t^2} = \frac{\partial T_{ij}}{\partial x_j}, \tag{2.1}$$

with the symmetric stress tensor T_{ij}, which includes all mechanical forces induced by deformation, implying a connection to the strain tensor ε_{ij}. The components of the strain tensor, which are defined according to

$$\varepsilon_{ij} = \frac{1}{2}\left(\frac{\partial u_i}{\partial x_j} + \frac{\partial u_j}{\partial x_i}\right), \tag{2.2}$$

describe infinitesimal deformations of a continuum body (see Fig. 2.1). Note that by definition the strain tensor is symmetric, $\varepsilon_{ij} = \varepsilon_{ji}$. The corresponding antisymmetric quantity $(\partial u_i/\partial x_j - \partial u_j/\partial x_i)/2$ is not included in the strain tensor as it corresponds to a rotation instead of a deformation.

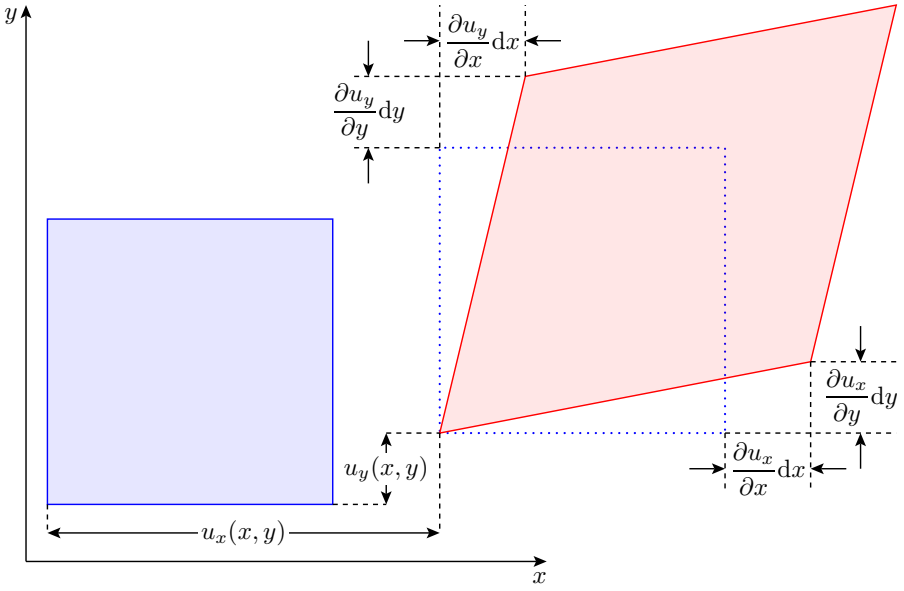

Figure 2.1.: Deformation of an infinitesimal two-dimensional volume element under strain.

For acoustic waves, one usually considers the case of small deformations, which according to Hooke's law are linearly related to stress:

$$T_{ij} = c_{ijkl}\varepsilon_{kl}, \tag{2.3}$$

where the components of the fourth order stiffness tensor c_{ijkl} are material dependent constants. Apparently from its definition, the stiffness tensor is symmetric in the first two indices, $c_{ijkl} = c_{jikl}$, as well as in the last two indices, $c_{ijkl} = c_{ijlk}$. In elastic deformations, the energy is preserved and the stress-strain relation can be derived from a strain energy density functional U:

$$T_{ij} = \frac{\partial U}{\partial \varepsilon_{ij}}, \tag{2.4}$$

or with Hooke's law:

$$c_{ijkl} = \frac{\partial^2 U}{\partial \varepsilon_{ij}\partial \varepsilon_{kl}}. \tag{2.5}$$

Since the elements of the stiffness tensor are independent of the order of differentiation, it possesses one further symmetry, $c_{ijkl} = c_{klij}$. In general, the number of independent components is thus only 21 instead of $3^4 = 81$. As we are interested in materials with zinc blende structure, the material dependent stiffness tensor has to reflect the symmetry properties of the

underlying crystal, and the number of independent components is further decreased. Material constants have to be invariant under all symmetry operations that map the crystal on itself. Hence, the stiffness tensor has to transform according to the irreducible representation Γ^1 of the point group T_d. For more details of the point group T_d and its irreducible representations, see Sec. 3.2. Each index then transforms according to the irreducible representation Γ^5 of a vector, and a general fourth rank tensor can be decomposed into

$$\Gamma^5_i \otimes \Gamma^5_j \otimes \Gamma^5_k \otimes \Gamma^5_l = 4\Gamma^1_{ijkl} \oplus 3\Gamma^2_{ijkl} \oplus 7\Gamma^3_{ijkl} \oplus 10\Gamma^4_{ijkl} \oplus 10\Gamma^5_{ijkl}. \quad (2.6)$$

Apart from the symmetries of the tensor, there are therefore only 4 independent components possible for the zinc blende structure. Considering now the symmetry of the first and the last two indices, there is no combination of these indices ($\Gamma^5_i \otimes \Gamma^5_j = \Gamma^1_{ij} \oplus \Gamma^3_{ij} \oplus \Gamma^5_{ij}$) that transforms according to Γ^4. This reduces the number of material constants c_i further to 3 independent components:

$$c_1 \equiv c_{1111} \sim \Gamma^1_{ij} \otimes \Gamma^1_{kl}, \quad (2.7)$$

$$c_2 \equiv c_{1122} \sim \Gamma^3_{ij} \otimes \Gamma^3_{kl}, \quad (2.8)$$

$$c_3 \equiv c_{1212} \sim \Gamma^5_{ij} \otimes \Gamma^5_{kl}, \quad (2.9)$$

of the stiffness tensor. These constants are of course equal to components derived by cyclic permutations (e.g., $c_{1122} = c_{2233} = c_{3311}$).

For this fourth rank tensor the notation is somewhat inconvenient. Since the stiffness tensor is symmetric in the first as well as in the last two indices, for each pair of indices ij and kl of $c_{(ij)(kl)}$ only six distinct combinations are possible. With the definitions

$$\begin{array}{ccc} 11 \to 1, & 22 \to 2, & 33 \to 3, \\ 23, 32 \to 4, & 31, 13 \to 5, & 12, 21 \to 6, \end{array} \quad (2.10)$$

one is able to map the fourth rank tensor c_{ijkl} on a 6×6 matrix:

$$c_{mn} = \begin{pmatrix} c_1 & c_2 & c_2 & 0 & 0 & 0 \\ c_2 & c_1 & c_2 & 0 & 0 & 0 \\ c_2 & c_2 & c_1 & 0 & 0 & 0 \\ 0 & 0 & 0 & c_3 & 0 & 0 \\ 0 & 0 & 0 & 0 & c_3 & 0 \\ 0 & 0 & 0 & 0 & 0 & c_3 \end{pmatrix}. \quad (2.11)$$

This kind of representation is referred to as Voigt notation.

Now including piezoelectricity, additional forces due to the piezoelectric field **E** arise, which additionally contribute to the stress tensor. Augmented by these supplementary terms, the stress tensor for piezoelectric materials reads

$$T_{ij} = c_{ijkl}\varepsilon_{kl} - e_{kij}E_k, \tag{2.12}$$

with the third order piezoelectric tensor e_{kij}, which is by definition symmetric in the last two indices. The same symmetry discussion as above:

$$\Gamma_k^5 \otimes \Gamma_i^5 \otimes \Gamma_j^5 = \Gamma_{kij}^1 \oplus \Gamma_{kij}^3 \oplus 2\Gamma_{kij}^4 \oplus 3\Gamma_{kij}^5, \tag{2.13}$$

yields that there is only one independent constant

$$e \equiv e_{123} \sim \Gamma_k^5 \otimes \Gamma_{ij}^5, \tag{2.14}$$

of the $3^3 = 21$ components of the piezoelectric tensor. Using again the Voigt notation for the last two indices, the piezoelectric tensor can, similarly to the stiffness tensor, also be expressed in matrix form:

$$e_{im} = \begin{pmatrix} 0 & 0 & 0 & e & 0 & 0 \\ 0 & 0 & 0 & 0 & e & 0 \\ 0 & 0 & 0 & 0 & 0 & e \end{pmatrix}. \tag{2.15}$$

Additionally to the deformation generated by piezoelectric fields, there is the reversed effect of electric fields induced by strain. Hence, the dynamics of sound waves is coupled to the electromagnetic field, which is described by Maxwell's equations in matter. In the following, we consider acoustic waves in magnetically isotropic materials and also neglect free charge carriers. The Maxwell equations then read:

$$\nabla \cdot \mathbf{D} = 0, \tag{2.16}$$

$$\nabla \cdot \mathbf{B} = 0, \tag{2.17}$$

$$\nabla \times \mathbf{E} = -\frac{\partial \mathbf{B}}{\partial t}, \tag{2.18}$$

$$\nabla \times \mathbf{B} = \mu_0 \frac{\partial \mathbf{D}}{\partial t}, \tag{2.19}$$

with the dielectric displacement

$$D_i = e_{ijk}\varepsilon_{jk} + \epsilon_{ij}E_j, \tag{2.20}$$

and the dielectric tensor, ϵ_{ij}. In materials with zinc blende structure the symmetry implies that this tensor has to be diagonal $\epsilon_{ij} = \epsilon\delta_{ij}$.

These are, however, more equations than needed for the derivation of the wave equation. Inserting (2.12) into (2.1) yields

$$\rho\frac{\partial^2 u_j}{\partial t^2} = c_{ijkl}\frac{\partial^2 u_k}{\partial x_i \partial x_l} - e_{kij}\frac{\partial E_k}{\partial x_i}, \tag{2.21}$$

and by combining the last two Maxwell equations one obtains

$$\nabla \times \nabla \times \mathbf{E} = -\mu_0 \frac{\partial^2 \mathbf{D}}{\partial t^2}. \tag{2.22}$$

This last equation describes the electromagnetic waves excited by the temporally changing electric field. By an estimation of the order of magnitude of the involved quantities in this last two equations, and by neglecting the spatial anisotropy of the material ($c_{ijkl} \approx c'$), one can deduce

$$\hat{e}_\mathbf{k} \times \hat{e}_\mathbf{k} \times \mathbf{E} \approx -\left(\frac{v}{c}\right)^2 \left(1 + \frac{e^2}{\epsilon_0 c'}\right)\mathbf{E} \ll \frac{e_{ijk}\varepsilon_{jk}}{\epsilon_0}, \tag{2.23}$$

where c is the speed of light in vacuum. As the velocity of the sound wave is much slower than the speed of light in vacuum, $(v/c)^2 \sim 10^{-10}$, the rotation of the electric field vanishes; in other words, there is no mutual coupling between these waves. It is therefore well justified to work with the electrostatic Maxwell equations, where the electric field can be expressed by a potential:

$$E_i = -\frac{\partial \Phi}{\partial x_i}. \tag{2.24}$$

Note that with this approximation waves, which are referred to as "uncoupled transverse mode" (see, e.g., [18]) are no longer possible. This approximation is thus equivalent to a restriction to Rayleigh waves. With the discussion above, only the first Maxwell equation is of importance for the characterization of sound waves in piezoelectric materials. By using (2.24) in (2.16) and (2.21) one obtains eventually:

$$\rho\frac{\partial^2 u_j}{\partial t^2} = c_{ijkl}\frac{\partial^2 u_k}{\partial x_i \partial x_l} + e_{kij}\frac{\partial^2 \Phi}{\partial x_i \partial x_k}, \tag{2.25}$$

$$0 = e_{ijk}\frac{\partial^2 u_j}{\partial x_i \partial x_k} - \epsilon_{ij}\frac{\partial^2 \Phi}{\partial x_i \partial x_j}, \tag{2.26}$$

the so-called constitutive equations.

A Fourier transformation turns these coupled differential equations into a set of coupled algebraic equations. Expressed by a symmetric matrix,

they read

$$M = \begin{pmatrix} \rho\omega^2 - c_{i11j}k_ik_j & -c_{i12j}k_ik_j & -c_{i13j}k_ik_j & -e_{ij1}k_ik_j \\ -c_{i12j}k_ik_j & \rho\omega^2 - c_{i22j}k_ik_j & -c_{i23j}k_ik_j & -e_{ij2}k_ik_j \\ -c_{i13j}k_ik_j & -c_{i23j}k_ik_j & \rho\omega^2 - c_{i33j}k_ik_j & -e_{ij3}k_ik_j \\ -e_{ij1}k_ik_j & -e_{ij2}k_ik_j & -e_{ij3}k_ik_j & \epsilon_{ij}k_ik_j \end{pmatrix}. \tag{2.27}$$

Evaluating the characteristic equation $\det M = 0$, one obtains an equation which is cubic in ω^2, with three $\mathbf{k}$-dependent solutions ω_i^2, which correspond to three distinct modes. For materials with zinc blende structure, we will discuss this now in detail for a sound wave propagation in $\mathbf{k} \parallel [100]$ and $\mathbf{k} \parallel [110]$.

In the first case, $\mathbf{k} = k\hat{e}_x$, the matrix M simplifies to

$$M_{[100]} = \begin{pmatrix} \rho\omega^2 - c_1k^2 & 0 & 0 & 0 \\ 0 & \rho\omega^2 - c_3k^2 & 0 & 0 \\ 0 & 0 & \rho\omega^2 - c_3k^2 & 0 \\ 0 & 0 & 0 & \epsilon k^2 \end{pmatrix}, \tag{2.28}$$

and the wave is decoupled from the piezoelectric field. The three solutions of $\det M_{[100]} = 0$ correspond then to one longitudinal wave with velocity

$$v_{l,[100]} = \sqrt{\frac{c_1}{\rho}}, \tag{2.29}$$

and to two transversal waves with

$$v_{t,[100]} = \sqrt{\frac{c_3}{\rho}}. \tag{2.30}$$

The situation changes in the second case, $\mathbf{k} = k(\hat{e}_x + \hat{e}_y)/\sqrt{2}$. Considering the matrix M:

$$M_{[110]} = \begin{pmatrix} \rho\omega^2 - \frac{1}{2}(c_1 + c_3)k^2 & -\frac{1}{2}(c_2 + c_3)k^2 & 0 & 0 \\ -\frac{1}{2}(c_2 + c_3)k^2 & \rho\omega^2 - \frac{1}{2}(c_1 + c_3)k^2 & 0 & 0 \\ 0 & 0 & \rho\omega^2 - c_3k^2 & -ek^2 \\ 0 & 0 & -ek^2 & \epsilon k^2 \end{pmatrix} \tag{2.31}$$

of this propagation direction, evidently two modes with velocities

$$v_{l,[110]} = \sqrt{\frac{c_1 + c_2 + 2c_3}{2\rho}}, \tag{2.32}$$

and

$$v_{t1,[110]} = \sqrt{\frac{c_1 - c_2}{2\rho}}, \tag{2.33}$$

are again independent of the piezoelectric field, whereas one new transversal mode with velocity

$$v_{t2,[110]} = \sqrt{\frac{c_3\epsilon + e^2}{\epsilon\rho}}, \tag{2.34}$$

couples to it. Comparing this velocity with its associated value $v^*_{t2,[110]} = \sqrt{c_3/\rho}$ for vanishing piezoelectricity ($e = 0$), the coupling to the electric field increases therefore the speed of sound. In other words, due to piezoelectricity, the material appears to be "stiffer". Note that for waves propagating in other directions one obtains of course similar results.

2.2. Surface acoustic waves

After discussing sound waves in an infinite spatially extended material, we now focus on the description of surface acoustic waves. We assume a medium, which is infinitely extended along the x and y axis, and also for $z < 0$. The half space $z > 0$ is assumed to consist of vacuum.

The surface at $z = 0$ is then taken into account by mechanical and electrical boundary conditions. The lack of adjacent volume elements at the boundary averts forces perpendicular to the surface. Hence, the components

$$T_{31} = T_{32} = T_{33} = 0|_{z=0} \tag{2.35}$$

of the stress tensor have to vanish for $z = 0$. Contrary to the motion of particles inside of the crystal, the electromagnetic field is not restricted to the lower half space. The tangential components of the electric field as well as the normal component of the electric displacement have therefore to be continuous at the surface, i.e.

$$E_x(z = 0^-) = E_x(z = 0^+), \quad E_y(z = 0^-) = E_y(z = 0^+), \tag{2.36}$$

and

$$D_z(z = 0^-) = \epsilon_0 E_z(z = 0^+). \tag{2.37}$$

Surface acoustic waves are confined to the surface in the sense that their amplitudes are decaying exponentially with the depth z (see Fig. 2.2). We employ therefore the ansatz

$$\mathbf{u}(\mathbf{r}, t) = \mathbf{u}_0 \exp(\Omega k z) \exp[\mathrm{i}(kx - \omega t)], \tag{2.38}$$

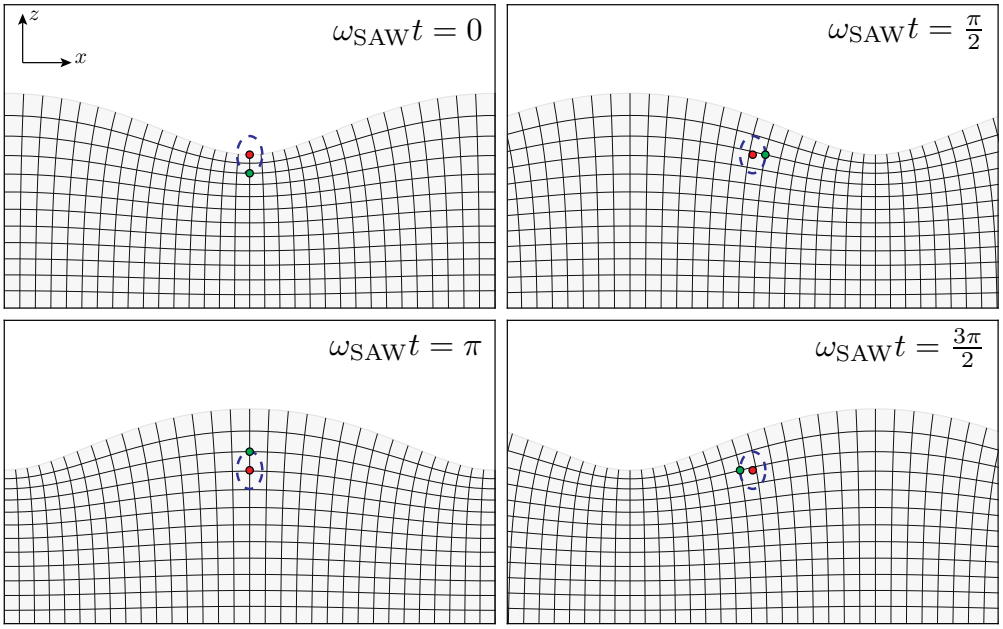

Figure 2.2.: Scheme of a SAW for four distinct times. The red circle indicates a fixed point in space, whereas the green circle marks the displacement of a particle for various times within one period. The amplitude of the displacement vanishes exponentially with the depth.

for the displacement, and

$$\Phi(\mathbf{r}, t) = \Phi_0 \exp(\Omega k z) \exp[\mathrm{i}(kx - \omega t)], \tag{2.39}$$

for the electric potential, where Ω denotes a dimensionless decay constant.

As a first step, we want to determine the electric field in the vacuum above the medium. In order to ensure continuity at the surface, the electric field has to have a similar form compared to the one inside the medium. Assuming

$$\mathbf{E}^{+} = \mathbf{E}_0^{+} \exp(\beta k z) \exp[\mathrm{i}(kx - \omega t)], \tag{2.40}$$

and substituting this into

$$\nabla \times \nabla \times \mathbf{E} = -\frac{1}{c^2} \frac{\partial^2 \mathbf{E}}{\partial t^2}, \tag{2.41}$$

one finds easily for the electric field coupled to the Rayleigh mode

$$\beta = -\sqrt{1 - \left(\frac{v}{c}\right)^2} \approx -1, \tag{2.42}$$

and

$$E_z^+ \approx \mathrm{i}E_x^+. \tag{2.43}$$

Hence, the phase between E_x^+ and E_z^+ amounts to $\pi/2$. Note that the positive solution for β has been discarded, since the electric fields have to vanish for $z \to \infty$. By choosing $E_x^+ = -\mathrm{i}k\Phi_0$ the boundary condition $E_x(z = 0^-) = E_x(z = 0^+)$ is automatically fulfilled.

For the derivation of the wave inside the material, we substitute the ansatz (2.38) and (2.39) into (2.27). The characteristic equation $\det M = 0$ yields then an equation of fourth order in Ω^2 with a so far unknown velocity $v = \omega/k$. Denoting by Ω_i^2 the roots of the characteristic equation, we keep only the set of decay constants Ω_i with positive real parts in order to satisfy the assumption of vanishing wave amplitudes for $z \to -\infty$. To each decay constant Ω_i belongs a set of amplitudes $\mathbf{u}^{(i)}$ and $\Phi^{(i)}$, and the ansatz can be rewritten as

$$\mathbf{u}(\mathbf{r}, t) = \sum_i A_i \mathbf{u}^{(i)} \exp(\Omega_i k z) \exp[\mathrm{i}(kx - \omega t)], \tag{2.44}$$

and

$$\Phi(\mathbf{r}, t) = \sum_i A_i \Phi^{(i)} \exp(\Omega_i k z) \exp[\mathrm{i}(kx - \omega t)], \tag{2.45}$$

where the prefactors A_i of each solution have to be determined by the residual four boundary conditions (2.35) and (2.37). This set of solutions together with the boundary condition form a matrix N with dimensions 4×4. From the matrix equation

$$N_{ij} A_j = 0 \tag{2.46}$$

the non-trivial solutions can then be derived by setting $\det N = 0$.

In principle, solving the second determinantal equation (2.46) yields the velocity of the SAW. In practice, however, due to the fourth order roots of the characteristic equations, this is not feasible. One therefore relies usually on a numerical iteration procedure. As a starting point, an arbitrary velocity v is chosen to solve the first characteristic equation $\det M = 0$. If the resulting set of amplitudes, $\mathbf{u}^{(i)}$ and $\Phi^{(i)}$, also solves the second determinant $\det N = 0$ of the boundary conditions, the solution is found and the iteration ends. Otherwise the iteration continues.

In the following we discuss in detail a SAW propagating in the (001) plane along the [110] direction for $Al_{0.3}Ga_{0.7}As$. The calculations are thus performed in the coordinate system, $\hat{e}_x \parallel [110]$, $\hat{e}_y \parallel [1\bar{1}0]$, and $\hat{e}_z \parallel [001]$. Note that the parameters given in Table 2.1 correspond to the

coordinate system, $\hat{e}_x \parallel [100]$, and $\hat{e}_y \parallel [010]$. Hence, before we determine the solution of a SAW propagating in [110] direction, we have to transform these parameters into the new basis. The rotation of the stiffness tensor

Parameter	$Al_xGa_{1-x}As$	$Al_{0.3}Ga_{0.7}As$
$c_{1111} = c_1\,[10^{10}\,\mathrm{N/m^2}]$	$11.88 + 0.14x$	11.92
$c_{1122} = c_2\,[10^{10}\,\mathrm{N/m^2}]$	$5.38 + 0.32x$	5.48
$c_{1212} = c_3\,[10^{10}\,\mathrm{N/m^2}]$	$5.94 - 0.05x$	5.93
$e_{123} = e\,[\mathrm{C/m^2}]$	$-0.16 - 0.065x$	-0.18
$\varepsilon_{11} = \varepsilon\,[\varepsilon_0]$	$13.18 - 3.12x$	10.77
$\rho\,[\mathrm{kg/m^3}]$	$5360 - 1600x$	4880

Table 2.1.: The bulk parameters of $Al_xGa_{1-x}As$ are taken from [19, 20]. The data for GaAs can be obtained from the values of $Al_xGa_{1-x}As$ by setting $x = 0$.

to the new coordinate system reads in the new basis:

$$c_{mn} = \begin{pmatrix} \frac{c_1+c_2+2c_3}{2} & \frac{c_1+c_2-2c_3}{2} & c_2 & 0 & 0 & 0 \\ \frac{c_1+c_2-2c_3}{2} & \frac{c_1+c_2+2c_3}{2} & c_2 & 0 & 0 & 0 \\ c_2 & c_2 & c_1 & 0 & 0 & 0 \\ 0 & 0 & 0 & c_3 & 0 & 0 \\ 0 & 0 & 0 & 0 & c_3 & 0 \\ 0 & 0 & 0 & 0 & 0 & \frac{c_1-c_2}{2} \end{pmatrix}. \tag{2.47}$$

The change of the reference frame also influences the piezoelectric tensor e_{ijk}. The symmetry discussion above remains of course valid, and there is still only one independent constant e. The only non vanishing components within the new system (Voigt notation) are then:

$$e_{15} = -e_{24} = e_{31} = -e_{32} = e. \tag{2.48}$$

As the dielectric tensor ϵ_{ij} is diagonal, it obviously remains invariant under any change of the coordinate system.

With the parameters given, we are in the position to obtain the matrix

$$M = \begin{pmatrix} \rho v^2 + c_{55}\Omega^2 - c_{11} & 0 & \mathrm{i}(c_{13} + c_{55})\Omega & 2\mathrm{i}e\Omega \\ 0 & \rho v^2 + c_{44}\Omega^2 + c_{66} & 0 & 0 \\ \mathrm{i}(c_{13} + c_{55})\Omega & 0 & \rho v^2 + c_{33}\Omega^2 - c_{55} & -e \\ 2ie\Omega & 0 & -e & \epsilon(1 - \Omega^2) \end{pmatrix}, \tag{2.49}$$

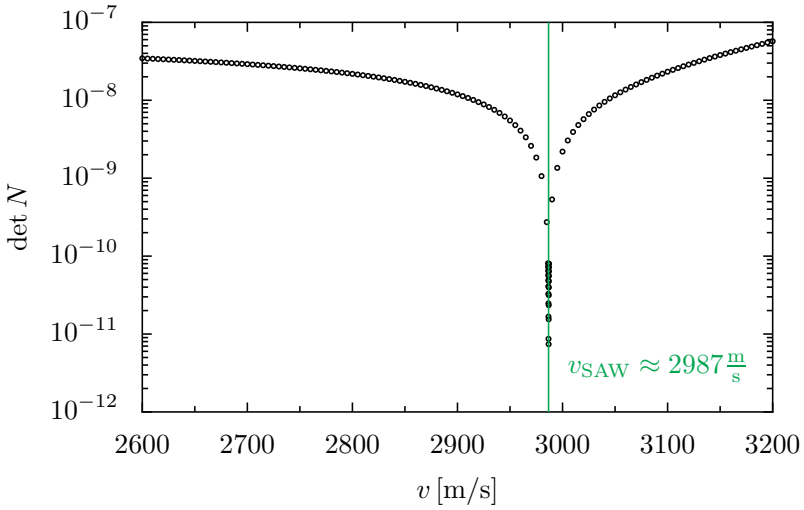

Figure 2.3.: The sharp minimum of the determinant $\det N$ versus the velocity v is associated with the velocity of the Rayleigh surface acoustic wave. For $Al_{0.3}Ga_{0.7}As$ the characteristic equation $\det N = 0$ is fulfilled for $v_{\mathrm{SAW}} \approx 2987\,\mathrm{m/s}$.

where the components for the y direction are completely decoupled from the residual directions. The solution of $\rho v^2 + c_{44}\Omega^2 + c_{66} = 0$, which is independent of the piezoelectric field, corresponds to a sound wave propagating in y direction. Since it is not related to the Rayleigh surface acoustic wave, we will not consider it any further.

As the y components are decoupled, the boundary condition $T_{23} = 0$ is already fulfilled. Thus, instead of four independent equations, only three are left, and

$$N_{mn} = \begin{pmatrix} c_{55}\left(u_z^{(n)} - \mathrm{i}\Omega_n u_x^{(n)}\right) - e\Phi^{(n)} \\ c_{31}u_x^{(n)} - \mathrm{i}c_{33}\Omega_n u_z^{(n)} \\ eu_x^{(n)} + \mathrm{i}(\varepsilon\Omega_n + \varepsilon_0)\Phi^{(n)} \end{pmatrix}. \tag{2.50}$$

The characteristic equation $\det M = 0$ is therefore only cubic in Ω^2 and for, $v = v_{\mathrm{SAW}} = 2987\,\mathrm{m/s}$ (see Fig. 2.3), the three roots with positive real part are given by

$$\Omega_1 = 0.49 - 0.48\mathrm{i}, \quad \Omega_2 = 0.49 + 0.48\mathrm{i}, \quad \Omega_3 = 1.02, \tag{2.51}$$

with their associated amplitudes (in units of $10^{-10}\,\mathrm{m}$)

$$\mathbf{u}^{(1)} = \begin{pmatrix} 1.26 - 3.77\mathrm{i} \\ 0 \\ -1.04 - 5.26\mathrm{i} \end{pmatrix}, \quad \mathbf{u}^{(2)} = \begin{pmatrix} -1.26 - 3.77\mathrm{i} \\ 0 \\ -1.04 + 5.26\mathrm{i} \end{pmatrix}, \tag{2.52}$$

$$\mathbf{u}^{(3)} = \begin{pmatrix} 6.69\mathrm{i} \cdot 10^{-2} \\ 0 \\ 5.55 \cdot 10^{-2} \end{pmatrix}, \tag{2.53}$$

where we have chosen $\Phi^{(1)} = \Phi^{(2)} = \Phi^{(3)} = 1\,\mathrm{V}$. The corresponding prefactors A_i, resulting from the solution of the second determinantal equation (2.46), are:

$$A_1 = 0.305 + 0.276\mathrm{i}, \quad A_2 = 0.305 - 0.276\mathrm{i}, \quad A_3 = -0.813. \tag{2.54}$$

Inserting these prefactors together with the amplitudes into (2.44) and (2.45), one obtains the solution of the surface acoustic wave. Eventually, the components of the electric field can be derived from (2.24). The phase relations of the displacement and the electric field as well as the dependence of the amplitudes on the distance z from the surface are depicted in Fig. 2.4.

In the following, we will be interested in the effect of a SAW on electrons in a quantum well (see Chap. 3). We therefore already state explicitly the displacement and the electric field in a quantum well with a quite typical depth of $z = 100\,\mathrm{nm}$. Since the components of the electric field are the spatial derivation of the potential, they are proportional to the wave vector $k = 2\pi/\lambda$. In practice, a SAW is generated by interdigital transducers (IDT) (see Fig. 5.1), which in many experiments [21–28] are designed for an acoustic wavelength of $\lambda_{\mathrm{SAW}} = 5.6\,\mu\mathrm{m}$. Within such a setup, the components of the displacement and the electric field read

$$\mathbf{u}(x,t) = \mathcal{C} \begin{pmatrix} -2.1\cos[kx - \omega t] \\ 0 \\ 3.5\sin[kx - \omega t] \end{pmatrix} \mathrm{pm}, \tag{2.55}$$

and

$$\mathbf{E}(x,t) = \mathcal{C} \begin{pmatrix} 3.0\cos[kx - \omega t] \\ 0 \\ 3.4\sin[kx - \omega t] \end{pmatrix} \frac{\mathrm{kV}}{\mathrm{m}}, \tag{2.56}$$

where $\mathcal{C}$ denotes a dimensionless constant of the order of one representing the strength of the SAW (see Sec. 5.3). For the calculation of spin-dependent spin-orbit coupling (see Sec. 3.5) we also need the components

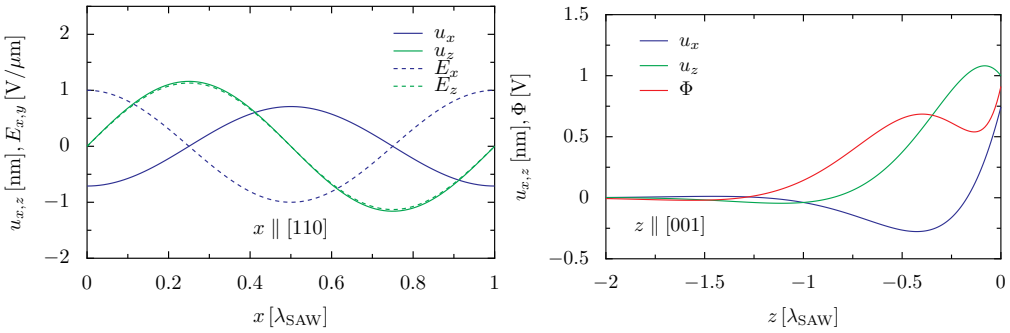

(a) Phase relations between the components of the displacement **u** and the electric field **E**

(b) Exponential decay of the amplitudes.

Figure 2.4.: The left figure a) shows the phase relation of the displacement and the electric field in a depth of $z = 100\,\mathrm{nm}$ and $\lambda_{\mathrm{SAW}} = 5.6\,\mu\mathrm{m}$ for $Al_{0.3}Ga_{0.7}As$. As shown in b), the amplitudes of the displacement u_x, u_z as well as the amplitude of the potential Φ basically vanish on the length scale of the wavelength λ_{SAW}.

of the strain tensor. Eventually, these components are easily obtained from the general solution (2.44):

$$\boldsymbol{\varepsilon} = 10^{-7}\mathcal{C} \begin{pmatrix} 24\sin[kx-\omega t] & 0 & 2.0\cos[kx-\omega t] \\ 0 & 0 & 0 \\ 2.0\cos[kx-\omega t] & 0 & -9.6\sin[kx-\omega t] \end{pmatrix}. \tag{2.57}$$

3. Effective Hamiltonian of a two-dimensional electron gas

For a proper description of charge carriers within a quantum well under an external SAW perturbation, the properties of the underlying material has to be considered. Whereas the previous chapter on surface acoustic waves was formulated exclusively in terms of classical continuum mechanics, for the dynamics of charge carriers and their associated spin, quantum mechanics has to be taken into account. In the next section we will therefore start with the Schrödinger equation of an electron in a perfect crystal structure. However, in the semiconductors we have in mind, say GaAs, a complete solution of the Schrödinger equation – if possible after all – contains too much information for our purposes. Typically, the band gap between the conduction and the uppermost valence band is of the order of electron volts ($\sim 1.5\,\mathrm{eV}$ for GaAs). Such a relatively large energetic separation, compared to the external influences of the SAW, effectively hampers transitions of the electrons between bands, enabling thus a description of carriers in a particular band independently of the others. This point motivates the derivation of effective Hamiltonians, where the information of the band structure is taken into account by effective quantities such a the effective mass.

As a further consequence, at room temperature and below, there are hardly any charge carriers in the conduction band. In the experiments we have in mind (see Chap. 5), therefore a laser is used to excite an ensemble of electrons in the conduction band. These electrons, together with the thereby generated holes, occupy states at the bottom (top) of the conduction (valence) band. Hence, only the neighbourhood of these band extrema is of importance for our purposes. This feature is especially addressed within the $\mathbf{k}\cdot\mathbf{p}$ theory, which can be considered as an expansion in terms of the wave vector $\mathbf{k}$. Within the envelope function approximation this theory is furthermore capable to describe the reaction of charge carriers on the external perturbations arising from the SAW.

The $\mathbf{k}\cdot\mathbf{p}$ theory becomes even more powerful by taking into account all the information provided by pure symmetry arguments. Hence, after we

provided a short introduction to group theory, we will utilize symmetry arguments to derive all allowed effective Hamiltonians up to second order in $\mathbf{k}$. Furthermore, we will pay special attention to all possible spin-orbit interactions that couple to the strain tensor.

3.1. The $\mathbf{k} \cdot \mathbf{p}$ theory

3.1.1. $\mathbf{k} \cdot \mathbf{p}$ theory and envelope function approximation

The $\mathbf{k} \cdot \mathbf{p}$ theory is especially well suited for the expansion of the band structure at points of high symmetry within the Brillouin zone. If the temperature is sufficiently low, the carriers are concentrated near the band extrema. Hence, we will employ $\mathbf{k} \cdot \mathbf{p}$ theory in order to determine the band structure of a zinc blende semiconductor in the neighbourhood of its fundamental band gap, which for III-V semiconductors such as GaAs is the gamma point.

The $\mathbf{k} \cdot \mathbf{p}$ theory is based on the Hamiltonian of an electron in a periodic potential $V_0(\mathbf{r})$, with additional external fields $\mathbf{A}(\mathbf{r})$ and $V(\mathbf{r})$

$$\hat{H} = \frac{(\mathbf{p} + e\mathbf{A})^2}{2m_0} + V_0(\mathbf{r}) + \frac{g_0}{2}\mu_B \boldsymbol{\sigma} \cdot \mathbf{B} + V(\mathbf{r}) + \hat{H}_{\mathrm{so}}, \tag{3.1}$$

where m_0 denotes the mass of a free electron. The last term

$$\hat{H}_{\mathrm{so}} = \frac{\hbar}{4m_0^2c^2}(\mathbf{p} + e\mathbf{A}) \cdot \boldsymbol{\sigma} \times (\nabla V_0) \tag{3.2}$$

has its origin in the Pauli equation and takes the effects of relativity into account by a correction to the Schrödinger equation of the order of $(m_0c^2)^{-1}$. As it couples the motion of an electron with its spin, it is known as the Hamiltonian of the spin-orbit interaction. We deliberately neglected here the contribution of the external potential $V(\mathbf{r})$ to the spin orbit interaction, since the main part originates from $V_0(\mathbf{r})$ in the region close to the atomic cores. Note, however, that this approximation may not be justified in semiconductors with a high impurity concentration. The inclusion of impurity potentials into the spin-orbit Hamiltonian results in an additional relaxation mechanism, known as Elliot-Yafet relaxation mechanism [29, 30].

The influence of electromagnetic fields or the fields from crystal defects are then summed up in the potential $V(\mathbf{r})$ and the vector potential $\mathbf{A}(\mathbf{r})$,

where both potentials are assumed to be slowly varying functions on the length scale of the lattice constant.

Instead of calculating the eigenfunctions of the Hamiltonian in the basis of Bloch or Wannier functions, Luttinger and Kohn [31] proposed

$$\chi_{nk\sigma}(\mathbf{r}) = \mathrm{e}^{\mathrm{i}\mathbf{k}\cdot\mathbf{r}} u_{n0\sigma}(\mathbf{r}), \tag{3.3}$$

as a complete and orthogonal set of basis functions. The lattice periodic functions $u_{n0\sigma}(\mathbf{r})$ are the Bloch functions for $\mathbf{k} = 0$, n is the band index and $\sigma = \uparrow, \downarrow$ is the quantum number of the spin. The wave vectors $\mathbf{k}$ are, similarly to the Bloch functions, restricted to the first Brillouin zone. A main advantage of the basis (3.3) is the lattice periodicity of the functions $u_{n0\sigma}(\mathbf{r})$ as well as their independence on external fields. As they depend merely on the crystal symmetry of the potential $V_0(\mathbf{r})$, they have to transform according to one of the irreducible representations Γ^a. The characteristics of this Bloch functions under symmetry transformations will be thus discussed in full detail in Sec. 3.3.

With the help of the basis (3.3), every wave function

$$\begin{aligned}
\Psi(\mathbf{r}) &= \langle \mathbf{r}|\Psi\rangle = \sum_{n\sigma} \int \mathrm{d}\mathbf{k}\, \langle \chi_{\mathrm{n}\mathbf{k}\sigma}|\Psi\rangle \chi_{\mathrm{n}\mathbf{k}\sigma}(\mathbf{r}) \\
&= \sum_{n\sigma} \int \mathrm{d}\mathbf{k}\, \langle \chi_{\mathrm{n}\mathbf{k}\sigma}|\Psi\rangle \mathrm{e}^{\mathrm{i}\mathbf{k}\cdot\mathbf{r}} \mathrm{u}_{\mathrm{n}0\sigma}(\mathbf{r}) \\
&= \sum_{n\sigma} F_{n\sigma}(\mathbf{r}) u_{n0\sigma}(\mathbf{r}),
\end{aligned} \tag{3.4}$$

can be split up into a sum of products of functions

$$F_{n\sigma}(\mathbf{r}) := \int \mathrm{d}\mathbf{k}\, \langle \chi_{\mathrm{n}\mathbf{k}\sigma}|\Psi\rangle \mathrm{e}^{\mathrm{i}\mathbf{k}\cdot\mathbf{r}}. \tag{3.5}$$

and $u_{n0\sigma}(\mathbf{r})$. The functions $F_n(\mathbf{r})$ contain, according to their definition, only Fourier components of the first Brillouin zone and are thus slowly varying functions on the length scale of the crystal lattice. As the products $F_{n\sigma}(\mathbf{r})u_{n0\sigma}(\mathbf{r})$ describe a modulation of the quickly oscillating Bloch functions $u_{n0\sigma}(\mathbf{r})$ by the functions $F_{n\sigma}(\mathbf{r})$, the latter are called envelope functions.

The envelope functions $F_{n\sigma}(\mathbf{r})$ contain the information about the reaction of the electrons on the external fields. Thus, it is sufficient to focus on the envelope functions in order to describe the electron and spin dynamics in a macroscopic crystal. Within the envelope function approximation

one assumes furthermore all external potentials, as well as the envelope functions, to be constant on the length scale of the lattice constant

$$\langle u_{n'0\sigma'} F_{n\sigma}(\mathbf{r}) | u_{n0\sigma} \rangle = \int_{\text{cell}} \mathrm{d}\mathbf{r}\, u^*_{n'0\sigma'}(\mathbf{r}) F_{n\sigma}(\mathbf{r}) u_{n0\sigma}(\mathbf{r}) \approx F_{n\sigma}(\mathbf{r})\, \delta_{nn'}\delta_{\sigma\sigma'}, \tag{3.6}$$

where we used the orthogonality of the Bloch functions.

Within the envelope function approximation the Schrödinger equation $\hat{H}\Psi = E\Psi$ becomes thus a system of coupled differential equations of envelope functions $F_{n\sigma}(\mathbf{r})$. This set of equations reads

$$\sum_{n\sigma} \left\{ \left[E_n(0) + \frac{\hbar^2\mathbf{k}^2}{2m_0} + V(\mathbf{r}) \right] \delta_{nn'}\delta_{\sigma\sigma'} + \Delta^{\sigma\sigma'}_{nn'} + \right.$$
$$\left. + \frac{\hbar\mathbf{k}}{m_0} \cdot \boldsymbol{\pi}^{\sigma\sigma'}_{nn'} + \frac{g_0}{2}\mu_B \boldsymbol{\sigma} \cdot \mathbf{B}\, \delta_{nn'} \right\} F_{n\sigma}(\mathbf{r}) = E\, F_{n\sigma}(\mathbf{r}), \tag{3.7}$$

where

$$\mathbf{k} = -\mathrm{i}\nabla + \frac{e}{\hbar}\mathbf{A}, \tag{3.8}$$

is now an operator acting on the envelope functions. Here, $E_n(0)$ denotes the energy of the n-th band without spin-orbit interaction. These band edge energies are modified by the matrix elements of the spin orbit interaction

$$\Delta^{\sigma\sigma'}_{nn'} = \frac{\hbar}{4m_0^2c^2} \left\langle u_{n0\sigma} \,|\, \mathbf{p} \cdot \boldsymbol{\sigma} \times (\nabla V_0) \,|\, u_{n'0\sigma'} \right\rangle, \tag{3.9}$$

which in general, due to the coupling of different bands and spins, lead to a splitting of degenerate energy levels (see Sec. 3.4.2 for more details). The matrix elements of the vector

$$\begin{aligned} \boldsymbol{\pi}^{\sigma\sigma'}_{nn'} &= \langle u_{n0\sigma} \,|\, \boldsymbol{\pi} \,|\, u_{n'0\sigma'} \rangle \\ &= \left\langle u_{n0\sigma} \left| \mathbf{p} + \frac{\hbar}{4m_0c^2} \boldsymbol{\sigma} \times (\nabla V_0) \right| u_{n'0\sigma'} \right\rangle, \end{aligned} \tag{3.10}$$

are responsible for a coupling of band edge states. Thus, in order to solve this set of differential equations, one has to decouple them. In general, this is not possible, and one has to resort to perturbation theoretical methods. These – at least to a given order in $\mathbf{k}$ – decoupled differential equations are then independent of each other and (3.7) becomes:

$$\sum_j \left[E_j + \frac{\hbar^2\mathbf{k}^2}{2m_0} + V(\mathbf{r}) + h_j(\mathbf{k}) \right] F_j(\mathbf{r}) \equiv \sum_j \mathcal{H}_j(\mathbf{k}) F_j(\mathbf{r}) = E\, F_j(\mathbf{r}), \tag{3.11}$$

where j denotes a generalized band index, since due to the spin-orbit interaction σ is no longer a good quantum number. For any band index j (3.11) resembles the Schrödinger equation. Hence, each $\mathcal{H}_j(\mathbf{k})$ can be identified with a Hamiltonian; the effective Hamiltonian $\hat{\mathcal{H}}_j$ of the band j.

As a consequence of the operator behaviour of $\mathbf{k}$, its components in general do not commute and, i.e.,

$$\mathrm{i}\mathbf{k}\times\mathbf{k}=\frac{e}{\hbar}\mathbf{B}, \tag{3.12}$$

yields the magnetic field, whereas the components of the electric field are obtained by

$$[\mathbf{k},V(\mathbf{r})]=-\mathrm{i}e\mathbf{E}. \tag{3.13}$$

Note that although $\mathbf{p}$ and $\mathbf{k}$ are both operators with the same appearance, as a consequence of the envelope function approximation they act on different functions $u_{n0\sigma}(\mathbf{r})$, and $F_{n\sigma}(\mathbf{r})$, respectively:

$$\mathbf{k}\cdot\mathbf{p}\,\Psi(\mathbf{r})=\sum_{n\sigma}\mathbf{k}\cdot\mathbf{p}\,F_{n\sigma}(\mathbf{r})u_{n0\sigma}(\mathbf{r})\approx\sum_{n\sigma}[\mathbf{k}F_{n\sigma}(\mathbf{r})]\cdot[\mathbf{p}\,u_{n0\sigma}(\mathbf{r})] \tag{3.14}$$

Keeping this in mind, (3.7) can be identified with a Hamiltonian, which acts on two distinct Hilbert spaces:

$$\hat{H}=\hat{H}_0+\hat{H}_{\mathrm{s.o}}+\hat{H}_{\mathbf{k}}+\hat{H}_{\mathbf{k}\cdot\mathbf{p}}+\hat{H}'_{\mathrm{s.o}}+V(\mathbf{r}), \tag{3.15}$$

with

$$\hat{H}_0=\frac{\mathbf{p}^2}{2m_0}+V_0(\mathbf{x}), \tag{3.16}$$

$$\hat{H}_{\mathrm{s.o}}\equiv\hat{H}_{\mathrm{I}}=\frac{\hbar}{4m_0^2c^2}(\nabla V_0)\times\mathbf{p}\cdot\boldsymbol{\sigma}, \tag{3.17}$$

$$\hat{H}_{\mathbf{k}}\equiv\hat{H}_{\mathrm{II}}=\frac{\hbar^2\mathbf{k}^2}{2m_0}, \tag{3.18}$$

$$\hat{H}_{\mathbf{k}\cdot\mathbf{p}}\equiv\hat{H}_{\mathrm{III}}=\frac{\hbar}{m_0}\mathbf{k}\cdot\mathbf{p}, \tag{3.19}$$

$$\hat{H}'_{\mathrm{s.o}}\equiv\hat{H}_{\mathrm{IV}}=\frac{\hbar^2}{4m_0^2c^2}\boldsymbol{\sigma}\times(\nabla V_0)\cdot\mathbf{k}. \tag{3.20}$$

In the following we will use this Hamiltonian for the derivation of the effective Hamiltonian of an electron in the conduction band as well as for

a hole in the valence band. Without external perturbations, this is of course equivalent to the calculation of the dispersion relation $E_n(\mathbf{k})$ in the neighbourhood of a band extremum. Note that this set of Hamiltonians was derived under the assumption of perfect lattice periodicity. In the presence of a SAW, however, due to deformations this is no longer the case. Nevertheless, for a deformation which is linear in the components of the strain tensor there is a relatively easy way to circumvent this difficulty.

3.1.2. Strained systems

As we will discuss in Chap. 5 in more detail, the surface acoustic waves of Chap. 2 are able to profoundly influence the dynamics of electrons as well as the dynamics of their spins. In piezoelectric materials there are in general two possible mechanisms how a SAW affects electrons. The major contribution arises from the piezoelectric field of the SAW, which is taken into account by the Hamiltonian

$$H_{\mathrm{pe}} = -e\Phi. \tag{3.21}$$

In the following, we will include the piezoelectric potential Φ within the general external potential $V(\mathbf{r})$.

In addition to the piezoelectric field, a SAW also deforms the material, which causes a displacement of the lattice ions,

$$\mathbf{R^i} = \mathbf{R_0^i} + \mathbf{u^i}(\mathbf{R_0^i}), \tag{3.22}$$

where $\mathbf{u^i}(\mathbf{R_0^i})$ denotes the displacement vector of lattice ion i, and $\mathbf{R_0^i}$ its equilibrium position. The wavelength of the SAW is in general of the order of $\sim 1\,\mu$m and thus much longer than the lattice constant of the crystal. Hence, we may neglect the discrete character of the displacement vectors $\mathbf{u^i}$ and describe them by a continuous vector field $\mathbf{u}(\mathbf{r})$. Specifically, one can expect that the wave functions of the electrons still possess a Bloch like character.

Within the Born-Oppenheimer approximation one assumes moreover that electrons are able to respond instantaneously to the motion of the lattice ions. The wave function of the stressed material thus reflects the motion of the lattice by a transformation of spatial coordinates:

$$\Psi(\mathbf{r}) \to \Psi'(\mathbf{r}') = \Psi'(\mathbf{r} + \mathbf{u}(\mathbf{r})). \tag{3.23}$$

In the presence of strain the symmetry of the crystal, and therefore also of the potential $V_0(\mathbf{r}) \to V_{\boldsymbol{\varepsilon}}(\mathbf{r})$, is reduced. As our aim is to construct

effective Hamiltonians from symmetry arguments, such a reduction is most inconvenient. We will therefore follow the method of Bir and Pikus [32–34], which restores the symmetry of the crystal. Instead of deforming the crystal, a transformation to a deformed coordinate system is performed in such a way that in this new system the wave function regains the old lattice periodicity. Since both sets of wave functions $\{|\Psi\rangle\}$ and $\{|\Psi'\rangle\}$ are complete and orthonormal, one can define a unitary transformation T relating each other:

$$|\Psi'\rangle = T|\Psi\rangle. \tag{3.24}$$

Instead of working with the primed wave functions $|\Psi'\rangle$, it is more convenient to use the unprimed Bloch wave functions $|\Psi\rangle$ and transform the Hamiltonian

$$H' = T^\dagger H T. \tag{3.25}$$

In many applications, the strain, e.g., due of a SAW, is relatively weak ($\sim 10^{-3}$) and it is sufficient to expand the transformed Hamiltonian up to linear order in terms of the strain $\boldsymbol{\varepsilon}$ (2.2) [32, 33, 35–39]:

$$\hat{H}' \approx \hat{H} + \hat{D}_0 + \hat{D}_{\mathbf{k}\cdot\mathbf{p}} + \hat{D}_{\text{s.o.}} + \hat{D}'_{\text{s.o.}}. \tag{3.26}$$

The recovery of symmetry thus results in additional terms in the Hamiltonian. These additional contributions finally are:

$$\hat{D}_0 \equiv \hat{H}_{\text{V}} = \sum_{ij}\left[-\frac{1}{m_0}p_i p_j + V_{ij}(\mathbf{r})\right]\varepsilon_{ij} \equiv \sum_{ij}\hat{D}_{ij}\varepsilon_{ij}, \tag{3.27}$$

$$\begin{aligned}\hat{D}_{\text{s.o.}} \equiv \hat{H}_{\text{VI}} = \frac{\hbar}{4m_0^2c^2}\Bigg[&\sum_{ij}\varepsilon_{ij}\nabla V_{ij}(\mathbf{r})\times\mathbf{p}\cdot\boldsymbol{\sigma} \\ &- (\nabla V_0(\mathbf{r})\cdot\boldsymbol{\varepsilon})\times\mathbf{p}\cdot\boldsymbol{\sigma} \\ &- \nabla V_0(\mathbf{r})\times(\boldsymbol{\varepsilon}\cdot\mathbf{p})\cdot\boldsymbol{\sigma}\Bigg],\end{aligned} \tag{3.28}$$

$$\hat{D}_{\mathbf{k}\cdot\mathbf{p}} \equiv \hat{H}_{\text{VII}} = -\frac{\hbar}{m_0}\mathbf{p}\cdot\boldsymbol{\varepsilon}\cdot\mathbf{k}, \tag{3.29}$$

$$\begin{aligned}\hat{D}'_{\text{s.o.}} \equiv \hat{H}_{\text{VIII}} = \frac{\hbar}{4m_0^2c^2}\Bigg[&\sum_{ij}\varepsilon_{ij}\nabla V_{ij}(\mathbf{r})\times\mathbf{k}\cdot\boldsymbol{\sigma} \\ &- (\nabla V_0(\mathbf{r})\cdot\boldsymbol{\varepsilon})\times\mathbf{k}\cdot\boldsymbol{\sigma}\Bigg].\end{aligned} \tag{3.30}$$

The potentials

$$V_{ij}(\mathbf{r}) = \frac{1}{2-\delta_{ij}} \lim_{\varepsilon \to 0} \frac{V_{\varepsilon}\left[(1+\boldsymbol{\varepsilon})\mathbf{r}\right] - V_0(\mathbf{r})}{\varepsilon_{ij}} \tag{3.31}$$

describe the reaction of the potential $V_0(\mathbf{r})$ to an infinitesimal strain. Together with the terms of the unstrained Hamiltonian (3.16)-(3.20), these terms will build the basis of the following discussions of charge carriers in zinc blende crystals in Sec. 3.3.

3.2. The point group T_d

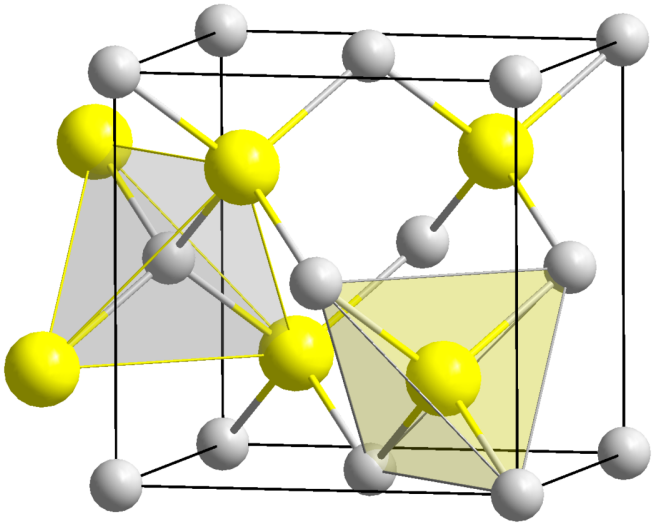

Figure 3.1.: Primitive cell of zinc blende crystal structure of GaAs. [40] The grey spheres represent Ga^{3+}, the yellow ones As^{3-}.

Group theory provides a very general approach for the description of symmetry operations [35, 41–45]. As depicted in Fig. 3.1, the zinc blende crystal structure has the symmetry of a tetrahedron. Considering the 4 vertices of a tetrahedron, one can easily convince oneself that there are $4! = 24$ possible symmetry operations. These 24 symmetry operations form the point group T_d. They can be divided into 5 distinct subclasses with similar symmetry operations. A list of this five classes is given in Tab. 3.1.

As we consider fermions, say electrons and holes, we also have to take the spin into account. Thus instead of the 24 symmetry operations, there

Table 3.1.: Classification of all 24 symmetry operations of the point group T_d. Overlined rotation angels denote improper rotations.

Class	Rotation angle	Rotation Axis
E	0	
$3C_2$	π	$[100], [010], [001]$
$6S_4$	$\overline{\pm\pi/2}$	$[100], [010], [001]$
6σ	$\overline{\pi}$	$[110], [1\bar{1}0], [101], [10\bar{1}], [011], [01\bar{1}]$
$8C_3$	$\pm 2\pi/3$	$[111], [\bar{1}11], [1\bar{1}1], [11\bar{1}]$

are 24 for each of the two possible spin directions, resulting in 48 symmetry operations. Regarding the quantum mechanical description of fermions, a rotation by 360° changes the sign of the wave function. Hence, the identity transformation is obtained by rotating by 720°, and the transformation characteristics of the spin is described by the symmetry group $D_{\frac{1}{2}}$. The symmetry properties of the spin are finally included by considering the double group $T_d \otimes D_{\frac{1}{2}}$ with 48 elements instead of the simple (geometric) symmetry group of the tetrahedron.

The full power of group theory reveals itself by considering the transformation properties of an arbitrary, complete set of basis functions. Representing each transformed function in terms of untransformed functions, one is able to define a transformation matrix $T(g)$ for each symmetry operation g. According to group theory, if such a transformation matrix is not already irreducible, it can be transformed into irreducible representations by a unitary matrix U:

$$U^\dagger T(g) U = \mathcal{D}^{(1)}(g) \oplus \mathcal{D}^{(2)}(g) \oplus \ldots = \begin{pmatrix} \mathcal{D}^{(1)}(g) & 0 & 0 \\ 0 & \mathcal{D}^{(2)}(g) & 0 \\ 0 & 0 & \ddots \end{pmatrix}. \quad (3.32)$$

Note that although U does not depend on a particular symmetry operation, it is not unique. An irreducible representation is therefore also not unique and can differ by a similarity transformation.

Let us now introduce the character of an irreducible representation, which is defined as the trace of the representation [45]:

$$\chi^{(i)}(g) = \mathrm{Tr}\left(\mathcal{D}^{(i)}(g)\right). \quad (3.33)$$

Since the trace of a matrix is invariant under any similarity transformation, the character of an irreducible representation is independent of the

choice of basis. Moreover, according to (3.32) the trace of a reducible transformation is obviously the sum of the characters of its irreducible representations:

$$\mathrm{Tr}\,(T(g)) = \chi^{(1)}(g) + \chi^{(2)}(g) + \ldots \tag{3.34}$$

In addition to the direct sum, the direct product of irreducible representations is defined by the Kronecker product of two matrices:

$$\mathcal{D}^{(1)}(g) \otimes \mathcal{D}^{(2)}(g) = \begin{pmatrix} \mathcal{D}^{(1)}_{11}(g)\mathcal{D}^{(2)}(g) & \ldots & \mathcal{D}^{(1)}_{1n}(g)\mathcal{D}^{(2)}(g) \\ \vdots & \ddots & \vdots \\ \mathcal{D}^{(1)}_{m1}(g)\mathcal{D}^{(2)}(g) & \ldots & \mathcal{D}^{(1)}_{mn}(g)\mathcal{D}^{(2)}(g) \end{pmatrix}. \tag{3.35}$$

The direct product of an irreducible representation Γ^i of dimension $\dim \Gamma^i = p$, with an irreducible representation Γ^j of dimension $\dim \Gamma^j = q$, results thus in a representation of dimension $p \cdot q$, which is in general reducible. Note that the character of the direct product of two representations is equal to the product of the characters:

$$\chi^{(1\otimes 2)}(g) = \chi^{(1)}(g) \cdot \chi^{(2)}(g). \tag{3.36}$$

Regarding now the double group $T_d \otimes D_{\frac{1}{2}}$, there are eight distinct irreducible representations. The first five of them are those of the simple spatial point group T_d, whereas the last three arise by taking the spin into account. These three additional representations are constructed by

$$\begin{array}{c|ccccc} \Gamma^i & \Gamma^1 & \Gamma^2 & \Gamma^3 & \Gamma^4 & \Gamma^5 \\ \Gamma^i \otimes D_{1/2} & \Gamma^6 & \Gamma^7 & \Gamma^8 & \Gamma^6 \oplus \Gamma^8 & \Gamma^7 \oplus \Gamma^8. \end{array} \tag{3.37}$$

The number of irreducible representations is equal to the number of classes. A set of symmetry operations forms a class, if the character of any given representation is the same for all members of the class. The symmetry properties of a point group can be neatly arranged in a character table. For the double group $T_d \otimes D_{\frac{1}{2}}$ this is depicted in Tab. 3.2, where each row of the character table displays the character of a given irreducible representation for a certain class. The (x, y, z) in $\Gamma^5(x, y, z)$ indicates that a vector transforms according to Γ^5. Note, however, that there is an ambiguity in the definition of the irreducible representations. In this work we adapted the notation of Ref. [46], where a vector transforms according to the irreducible representation Γ^5. See, e.g., Ref. [33] for more details.

Also note that the combination of Eqs. (3.34) and (3.36), together with the information of the character table, forms a set of linear equations. Solving this set, any direct product of irreducible representations can be decomposed into a direct sum of them.

Table 3.2.: Character table of the double group $T_d \otimes D_{\frac{1}{2}}$. The (x, y, z) indicates that a vector transforms according to Γ^5. The overline in the class names denote the same symmetry class as the one without overline, but after an addional rotation by 2π.

Γ	E	$\overline{E}$	$6C_2$	$8C_3$	$8\overline{C_3}$	$6S_4$	$6\overline{S_4}$	12σ
Γ^1	1	1	1	1	1	1	1	1
Γ^2	1	1	1	1	1	-1	-1	-1
Γ^3	2	2	2	-1	-1	0	0	0
Γ^4	3	3	-1	0	0	1	1	-1
$\Gamma^5(x, y, z)$	3	3	-1	0	0	-1	-1	1
Γ^6	2	-2	0	1	-1	$\sqrt{2}$	$-\sqrt{2}$	0
Γ^7	2	-2	0	1	-1	$-\sqrt{2}$	$\sqrt{2}$	0
Γ^8	4	-4	0	-1	1	0	0	0

3.3. Symmetric effective Hamiltonians

For the derivation of the effective Hamiltonians (3.11) one has to decouple the set of differential equations (3.7). In principle, one therefore needs to know all matrix elements of (3.9) and (3.10). With the group theoretical concepts of the previous section this is, however, not necessary. Basing solely on symmetry arguments, the theory of invariants [32, 35, 36, 39, 44] provides a very systematic approach for the determination of vanishing as well as identical matrix elements. Thus, due to symmetry arguments not all matrix elements of (3.10) are independent. This restriction is passed on to $\mathbf{k}$ by the scalar product and can be exploited for the decoupling of (3.7).

In this section, we will utilize the theory of invariants in order to derive effective Hamiltonians $\hat{\mathcal{H}}_j(\mathbf{k}, \boldsymbol{\varepsilon})$ (3.11) in a form that completely separates material specific quantities such as (3.9) and (3.10) from the parameters of the effective Hamiltonian $\mathbf{k}$ and $\boldsymbol{\varepsilon}$. Note that in order to avoid confusion, we denote in this section all quantities that operate on the Bloch functions (see Eq. (3.14)), e.g., $\mathbf{p}$ as operator, whereas, e.g., $\mathbf{k}$ which operates only on the envelope functions is referred to as parameter.

3.3.1. Spin independent Hamiltonians

We start with an arbitrary Hamiltonian $\hat{H}$ of an electron in a crystal environment. As discussed in the previous section 3.2, all symmetry operations map the whole lattice of the crystal onto itself. Hence, each representation of the Hamiltonian in an arbitrary basis has to stay invariant under any symmetry operation

$$\mathcal{D}(g)\hat{H}(g^{-1}\mathbf{K})\mathcal{D}^{-1}(g) = \hat{H}(\mathbf{K}) \qquad \forall g, \tag{3.38}$$

where $\mathbf{K}$ stands for a general tensor parameter, e.g., $\mathbf{k}$ or the strain tensor $\boldsymbol{\varepsilon}$.

Although we are especially interested in the various effective Hamiltonians describing spin-orbit coupling, as a starting point we consider only spin independent Hamiltonians and generalize the theory afterwards on the spin dependent case. From the general spin dependent Hamiltonian

$$\hat{\hat{H}} = \hat{H}^0 + \hat{H}^x\sigma^x + \hat{H}^y\sigma^y + \hat{H}^z\sigma^z = \hat{H}^0 + \sum_s \hat{H}^s\sigma^s, \tag{3.39}$$

we consider in this subsection thus only the Hamiltonian $\hat{H}^0$.

In the group theoretical language each matrix element of the Hamiltonian has to transform according to the irreducible representation Γ^1. In order to exploit this fact, one thus needs to know the behaviour of the operators contained in the Hamiltonian, as well as of the basis states under a symmetry operation.

Starting with the basis states, each eigenstate has to transform according to one particular irreducible representation Γ^a. Thus, one can choose a basis $|\Gamma_i^a(\delta)\rangle$, where all n_δ states with band index i transform under the symmetry operation g according to the same irreducible representation Γ^a:

$$g\,|\Gamma_i^a(\delta)\rangle = \sum_{\delta'}^{n_{\delta'}} \mathcal{D}^{\Gamma^a}_{\delta\delta'}(g)\,|\Gamma_i^a(\delta')\rangle\,. \tag{3.40}$$

Let us now express the Hamiltonian as a sum of operators

$$\hat{H}^0 = \sum_{o\mu\gamma} \mathrm{K}^{0,\mu}_{o;\gamma}\hat{\mathrm{O}}^{\mu}_{o;\gamma}, \tag{3.41}$$

where o sums over all operators $\hat{\mathrm{O}}^{\mu}_{o;\gamma}$ that transform according to $\sum_\gamma \mathcal{D}^{\Gamma^\mu}_{\gamma'\gamma}(g)\hat{\mathrm{O}}^{\mu}_{o;\gamma}$ under the symmetry transformation g. The prefactors $\mathrm{K}^{0,\mu}_{o;\gamma}$

are the components of the general tensor parameter **K** corresponding to $\hat{\mathrm{O}}^{\mu}_{o;\gamma}$. Since the Hamiltonian has to stay invariant under all symmetry operations only the matrix elements $H^{0,ab}_{ij;\delta\delta'} = \langle \Gamma^a_i(\delta)| \hat{H}^0 |\Gamma^b_j(\delta')\rangle$ that transform according to Γ^1 are non-vanishing. Hence, the matrix element $\mathrm{O}^{ab;\mu}_{o;\gamma;ij;\delta\delta'}$ of the operator $\hat{\mathrm{O}}^{\mu}_{o;\gamma}$ is only then non-zero, if the identity representation Γ^1 is contained in the direct product $\Gamma^a \otimes \Gamma^\mu \otimes \Gamma^b$.

According to the Wigner-Eckart-theorem, each matrix element of the Hamiltonian

$$H^{0;ab}_{ij;\delta\delta'} = \sum_{o\mu\gamma} \mathrm{K}^{0;\mu}_{o;\gamma}\, \mathrm{O}^{ab;\mu}_{o;\gamma;ij;\delta\delta'} = \sum_{o\mu\delta} \mathrm{I}^{ab;\mu}_{o;ij}\, \mathrm{K}^{0;\mu}_{o;\gamma}\, \mathrm{X}^{ab;\mu}_{\gamma;\delta\delta'}, \tag{3.42}$$

can be decomposed into a product of an invariant $\mathrm{I}^{ab;\mu}_{o;ij}$ and $\mathrm{X}^{ab;\mu}_{\gamma;\delta\delta'} = \langle \Gamma^a(\delta)\Gamma^b(\delta')|\Gamma^\mu(\gamma)\rangle$, which stands for the Clebsch-Gordan-coefficients (see Appendix A.3).

Before we continue, a few remarks on the matrices X are in order. In the literature (see, e.g., Ref. [35, 39]), often slightly different matrices are used (see Appendix A.10). The first difference consists in the normalization. All matrices X used in this work are orthogonal and normalized in the following sense:

$$\sum_{\delta\delta'} \mathrm{X}^{\alpha\beta;\mu}_{\gamma;\delta\delta'} \mathrm{X}^{\beta\alpha;\mu'}_{\gamma';\delta'\delta} = \sum_{\delta\delta'} \mathrm{X}^{\alpha\beta;\mu}_{\gamma;\delta\delta'} \left(\mathrm{X}^{\alpha\beta;\mu'}_{\gamma';\delta\delta'}\right)^* = \delta_{\mu\mu'}\delta_{\gamma\gamma'} \tag{3.43}$$

Whereas most matrices of Appendix A.10 are already orthogonal and this normalisation is thus expressed by a simple prefactor, the situation differs for the two sets of matrices J_γ and J^3_γ, which transform according to Γ^4. In order to ensure orthogonality of the matrices, we choose the linear combinations

$$\mathrm{X}^{88;5}_{\mathrm{A};\gamma} = \frac{1}{\sqrt{5}} J_\gamma, \tag{3.44}$$

and

$$\mathrm{X}^{88;5}_{\mathrm{B};\gamma} = \frac{1}{\sqrt{5}} \left(\frac{5}{3}\, J^3_\gamma - \frac{41}{12}\, J_\gamma \right). \tag{3.45}$$

A further deviation to the matrices X represents the number of matrices $\mathrm{X}^{68;3}_\gamma$ and $\mathrm{X}^{78;3}_\gamma$, respectively, which transform according to Γ^3. For the construction of a complete basis of matrices $\mathrm{X}^{68;\mu}_\gamma$, only two matrices, i.e., $\mathrm{X}^{68;3}_1$ and $\mathrm{X}^{68;3}_2$ with symmetry Γ^3 are necessary. For reasons not known to us, Ref. [35, 39]) defined three matrices, i.e., T_{xx}, T_{yy} and T_{zz}. As a

consequence of this additional matrix, they are linearly dependent and, e.g., $T_{zz} = -T_{xx} - T_{yy}$.

Returning to equation (3.42) and exploiting the orthonormality (3.43) of the matrices X, the invariants are obtained by

$$\mathrm{I}_{o;ij}^{ab;\mu} = \sum_{\delta\delta'} \mathrm{O}_{o;1;ij;\delta\delta'}^{ab;\mu}\, \mathrm{X}_{1;\delta'\delta}^{ba;\mu}, \tag{3.46}$$

where we took the first component $\gamma = 1$ for convenience.

For an infinite number of bands the matrix $\mathrm{I}_{o}^{ab;\mu}$ is infinite-dimensional and contains all relevant information of the operator O^{μ}. The matrices $\mathrm{X}_{\gamma}^{ab;\mu}$ depend, on the other hand, only on the chosen symmetry class. The expression (3.42) represents therefore a convenient separation of the material dependent quantities $\mathrm{I}_{o}^{ab;\mu}$ from parameter dependent matrices $\sum_{\gamma} \mathrm{K}_{o;\gamma}^{0;\mu}\, \mathrm{X}_{\gamma}^{\alpha\beta;\mu}$, which contain the information of the symmetry group. Using the Kronecker symbol $\otimes$, this separation can be directly conferred on each block of the Hamiltonian:

$$\hat{H}^{0;ab} = \sum_{o\mu\gamma} \mathrm{I}_{o}^{ab;\mu} \otimes \left(\mathrm{K}_{o;\gamma}^{0;\mu}\, \mathrm{X}_{\gamma}^{ab;\mu}\right). \tag{3.47}$$

3.3.2. Spin-dependent Hamiltonians

We will now transfer the above concepts on the full spin-dependent Hamiltonian $\hat{H}$. Including spin, the eigenstates of the full Hamiltonian have to transform according to one of the irreducible representations of the double group $\Gamma^{a} \otimes D_{1/2}$. In general, however, the spatial basis states (3.40) lack this requirement. An orthogonal basis that fulfils the time reversal symmetry, and whose states transform according to the irreducible representation Γ^{α}, can be constructed by using again Clebsch-Gordan coefficients:

$$\begin{aligned} |\Gamma_{i}^{\alpha a}(\delta)\rangle &= \sum_{\lambda} \left(\mathrm{X}_{\delta;\lambda 1}^{a\pi;\alpha}\, |\Gamma_{i}^{a}(\lambda)\rangle\, |\sigma = 1 \Leftrightarrow \uparrow\rangle + \mathrm{X}_{\delta;\lambda 2}^{a\pi;\alpha}\, |\Gamma_{i}^{a}(\lambda)\rangle\, |\sigma = 2 \Leftrightarrow \downarrow\rangle\right) \\ &= \sum_{\lambda\sigma} \mathrm{X}_{\delta;\lambda\sigma}^{a\pi;\alpha}\, |\Gamma_{i}^{a}(\lambda)\rangle\, |\sigma\rangle\,, \end{aligned} \tag{3.48}$$

where we assumed the states of the spins $|\sigma\rangle$ to transform according to Γ^{π} ($\pi = 6$ for point group T_d).

Analogously to the spin-independent case, the Hamiltonian $\hat{H}^{0}$ can then be written in the spin-dependent basis as

$$\hat{H}^{0;\alpha a\,\beta b} = \sum_{o\mu\gamma} \mathcal{I}_{o}^{\alpha a\,\beta b;\mu} \otimes \left(\mathcal{K}_{o;\gamma}^{\mu}\, \mathrm{X}_{\gamma}^{\alpha\beta;\mu}\right), \tag{3.49}$$

where we used calligraphic symbols in order to distinguish spin-dependent quantities from the spin-independent ones. The change of basis has of course no influence on the symmetry of the operators and the parameters, hence

$$\hat{\mathcal{O}}^{\mu}_{o;\gamma} \equiv \hat{\mathrm{O}}^{\mu}_{o;\gamma} \tag{3.50}$$

$$\hat{\mathcal{K}}^{\mu}_{o;\gamma} \equiv \hat{\mathrm{K}}^{0;\mu}_{o;\gamma}. \tag{3.51}$$

At this point the introduction of these calligraphic quantities seems somehow artificial, but will prove useful for the unification of spin-independent and spin-dependent quantities later on. The invariants that are determined analogously to (3.46) depend naturally on the invariants $\mathrm{I}^{ab;\mu}_{l;ij}$ of the spin-independent case

$$\mathcal{I}^{\alpha a\,\beta b;\mu}_{o;ij} = \sum_{\delta\delta'} \mathcal{O}^{\alpha a\,\beta b;\mu}_{o;1;ij;\delta\delta'}\,\mathrm{X}^{\beta\alpha;\mu}_{1;\delta'\delta} \equiv \mathrm{M}^{\alpha a\,\beta b;\mu}\,\mathrm{I}^{ab;\mu}_{o;ij}, \tag{3.52}$$

where we introduced the matrix

$$\mathrm{M}^{\alpha a\,\beta b;\mu} = \sum_{\substack{\delta\delta'\\ \lambda\lambda'\\ \sigma}} \mathrm{X}^{\pi a;\alpha}_{\delta;\sigma\lambda}\,\mathrm{X}^{ab;\mu}_{1;\lambda'\lambda}\,\mathrm{X}^{b\pi;\beta}_{\delta';\lambda'\sigma}\,\mathrm{X}^{\beta\alpha;\mu}_{1;\delta'\delta} \tag{3.53}$$

that maps the invariants $\mathrm{I}^{ab;\mu}_{o}$ of the spin-independent basis to the spin-dependent one. Similar to the matrices $\mathrm{X}^{\alpha\beta,\mu}_{\gamma}$ the matrix M depends also solely on the chosen symmetry class.

So far, we discussed only the spin-independent Hamiltonian $\hat{H}^0$. Considering now the spin-dependent part

$$\sum_{s} \hat{H}^{s}\sigma^{s} = \sum_{\substack{sp\\ \mu\gamma}} \mathrm{K}^{s;\mu}_{p;\gamma}\,\hat{\mathrm{O}}^{\mu}_{p;\gamma}\,\sigma^{s}, \tag{3.54}$$

some care is needed since one also has to take the transformation properties of the Pauli-matrices into account. Before we are able to re-use the above expressions, we therefore have to symmetrize the product $\hat{\mathrm{O}}^{\mu}_{p;\gamma}\,\sigma^{s}$. This can be achieved with the help of the identity

$$\begin{aligned}&\sum_{\gamma\gamma'} c_{\mu\gamma,\mu'\gamma'}\hat{\mathcal{A}}^{\mu}_{\gamma}\hat{\mathcal{B}}^{\mu'}_{\gamma'} = \\ &\sum_{\kappa\lambda}\left(\sum_{\gamma\gamma'} c_{\mu\gamma,\mu'\gamma'}\mathrm{X}^{\mu\mu';\kappa}_{\lambda;\gamma\gamma'}\right)\left(\sum_{\gamma\gamma'}\hat{\mathcal{A}}^{\mu}_{\gamma}\hat{\mathcal{B}}^{\mu'}_{\gamma'}\mathrm{X}^{\mu\mu';\kappa}_{\lambda;\gamma\gamma'}\right),\end{aligned} \tag{3.55}$$

which decomposes a product of two arbitrary operators $\hat{\mathcal{A}}$ and $\hat{\mathcal{B}}$ that transform according to μ and μ', in a sum of operators that transform according to the irreducible representations contained in the direct product $\Gamma^{\mu} \otimes \Gamma^{\mu'}$.

Assuming that the Pauli matrices transform according to the spatial irreducible representation $\Gamma^{\mu'}$ ($\mu' = 4$ for point group T_d), the symmetrized spin-dependent Hamiltonian is thus

$$\begin{aligned} \hat{H}^s \sigma^s &= \sum_{p\kappa\lambda} \left[\left(\sum_{\mu\gamma s} \mathrm{K}^{s;\mu}_{p;\gamma} \mathrm{X}^{\mu\mu';\kappa}_{\lambda;\gamma s} \right) \left(\sum_{\mu\gamma s} \hat{\mathrm{O}}^{\mu}_{p;\gamma} \sigma^s \mathrm{X}^{\mu\mu';\kappa}_{\lambda;\gamma s} \right) \right] \\ &\equiv \sum_{p\kappa\lambda} \mathcal{K}^{\kappa}_{p;\lambda} \hat{\mathcal{O}}^{\kappa}_{p;\lambda} \end{aligned} \tag{3.56}$$

with

$$\mathcal{K}^{\kappa}_{p;\lambda} = \sum_{\mu\gamma s} \mathrm{K}^{s;\mu}_{p;\gamma} \mathrm{X}^{\mu\mu';\kappa}_{\lambda;\gamma s}, \tag{3.57}$$

and

$$\hat{\mathcal{O}}^{\kappa}_{p;\lambda} = \sum_{\mu\gamma s} \hat{\mathrm{O}}^{\mu}_{p;\gamma} \sigma^s \mathrm{X}^{\mu\mu';\kappa}_{\lambda;\gamma s}. \tag{3.58}$$

Equivalently to equation (3.52), the invariants of the spin-dependent Hamiltonian are obtained by

$$\mathcal{I}^{\alpha a\,\beta b;\mu}_{p;ij} = \sum_{\delta\delta'} \mathcal{O}^{\alpha a\,\beta b;\mu}_{p;1;ij;\delta\delta'}\, \mathrm{X}^{\beta\alpha;\mu}_{1,\delta'\delta} \equiv \sum_{\tau} \mathrm{N}^{\alpha a\,\beta b;\mu\tau}\, \mathrm{I}^{ab;\tau}_{p;ij}\,, \tag{3.59}$$

where we introduced the matrix

$$\mathrm{N}^{\alpha a\,\beta b;\mu\tau} = \sum_{\substack{\delta\delta'\lambda\lambda' \\ \tau\gamma s\sigma\sigma'}} \mathrm{X}^{\pi a;\alpha}_{\delta;\sigma\lambda}\, \mathrm{X}^{ab;\tau}_{\gamma;\lambda\lambda'}\, \mathrm{X}^{b\pi;\beta}_{\delta';\lambda'\sigma'}\, \mathrm{X}^{\beta\alpha;\mu}_{1;\delta'\delta}\, \mathrm{X}^{\tau\mu';\mu}_{1;\gamma s}\, \sigma^s_{\sigma\sigma'} \tag{3.60}$$

which transforms the "spatial" invariants

$$\mathrm{I}^{ab;\tau}_{p;ij} \equiv \sum_{\delta\delta'} \mathrm{O}^{ab;\tau}_{p;1;ij;\delta\delta'}\, \mathrm{X}^{ba;\tau}_{1;\delta'\delta}, \tag{3.61}$$

to the invariants $\mathcal{I}^{\alpha a\,\beta b;\mu}_{p;}$ of the spin-dependent basis.

Each block of the full spin-dependent Hamiltonian

$$\hat{H}^{\alpha a\,\beta b} = \sum_{l\mu\gamma} \mathcal{I}^{\alpha a\,\beta b;\mu}_{l} \otimes \left(\mathrm{K}^{\mu}_{l;\gamma}\, \mathrm{X}^{\alpha\beta;\mu}_{\gamma} \right), \tag{3.62}$$

with $l \in (o,p)$ is then a simple sum of the invariants associated with $\hat{H}^0$ and $\hat{H}^s$, respectively.

The fact that the separation of the material specific matrices $\mathcal{I}_l^{\alpha a\,\beta b;\mu}$ and the parameter-dependent matrices $\mathcal{K}^{\mu}_{l;\gamma}\,\mathrm{X}^{\alpha\beta;\mu}_{\gamma}$ keeps its form even after applying quasi-degenerate Löwdin perturbation theory (see Appendix B), renders it especially convenient for calculating, e.g., the effective mass or the effective g-factor of charge carriers. Up to second order Löwdin perturbation theory, the effective Hamiltonian $\hat{\mathcal{H}}_i^{\alpha a}$ of the $|\Gamma_i^{\alpha a}\rangle$ band is then given by:

$$\begin{aligned}\hat{\mathcal{H}}_i^{\alpha a} =& E_{\alpha a;i} + \sum_{l\mu\gamma} \mathcal{I}^{\alpha a\,\alpha a;\mu}_{l;ii}\mathcal{K}^{\mu}_{l;\gamma}\,\mathrm{X}^{\alpha\alpha;\mu}_{\gamma} \\ &+ \sum_{\substack{l\mu\gamma \\ l'\mu'\gamma' \\ (\beta b) \\ j\neq i}} \frac{\mathcal{I}^{\alpha a\,\beta b;\mu}_{l;ij}\mathcal{I}^{\beta b\,\alpha a;\mu'}_{l';ji}}{E_{\alpha a;i} - E_{\beta b;j}} \otimes \left(\mathcal{K}^{\mu}_{l;\gamma}\mathcal{K}^{\mu'}_{l';\gamma'}\,\mathrm{X}^{\alpha\beta;\mu}_{\gamma}\mathrm{X}^{\beta\alpha,\mu'}_{\gamma'}\right) + \ldots \end{aligned} \tag{3.63}$$

However, the above perturbative approach has one disadvantage, since by construction the basis states (3.48) are eigenstates of the spin-independent Hamiltonian $\hat{H}^0$, and thus not necessarily of the full Hamiltonian $\hat{H}$. This point is, for example, important for the determination of the effective mass, which is quadratic in the parameters $\mathcal{K}^{\mu}_{l;\gamma}$. As we will discuss in more detail in the next section, off-diagonal matrix elements of the parameter independent spin-orbit Hamiltonian $\hat{H}_{\mathrm{so}}$ are able to contribute to the effective mass in every order of perturbation theory.

In order to circumvent this problem, we introduce the eigenbasis of the full Hamiltonian $\hat{H}$:

$$\begin{aligned}|\Gamma_i^{\alpha}(\delta)\rangle &= \sum_{\substack{\alpha'\delta' \\ aj}} \left\langle \Gamma_j^{\alpha' a}(\delta') \,\middle|\, \Gamma_i^{\alpha}(\delta)\right\rangle \left|\Gamma_j^{\alpha' a}(\delta')\right\rangle \\ &\equiv \sum_{aj} \eta^a_{ji} \left|\Gamma_j^{\alpha a}(\delta)\right\rangle, \end{aligned} \tag{3.64}$$

which represents a better starting point for the derivation of the effective Hamiltonians. Note that the symmetry of the state is unaltered under the change of basis and thus only the invariants $\mathcal{I}_l^{\alpha a\,\beta b;\mu}$ are affected, whereas the parameters $\mathcal{K}^{\mu}_{l;\delta}$ are unchanged. The invariants associated with $\hat{H}^0$ are then given in the eigenbasis of the full Hamiltonian $\hat{H}$ by

$$\mathcal{I}^{\alpha\beta;\mu}_{o;ij} = \sum_{\substack{ai' \\ bj'}} \mathrm{M}^{\alpha a\,\beta b,\mu}\,(\eta^a_{i'i})^*\,\eta^b_{j'j}\,\mathrm{I}^{ab;\mu}_{o;i'j'} \equiv \sum_{ab} \mathrm{M}^{\alpha a\,\beta b,\mu}\,\tilde{\mathrm{I}}^{ab;\mu}_{o;ij}, \tag{3.65}$$

and equivalently for the invariants

$$\mathcal{I}_{p;ij}^{\alpha\beta;\mu} = \sum_{ab\tau} \mathrm{N}^{\alpha a\,\beta b,\mu\tau}\, \tilde{\mathrm{I}}_{p;ij}^{ab;\tau}, \tag{3.66}$$

of spin-dependent Hamiltonian $\hat{H}^s$.

3.4. Effective Hamiltonians of the zinc blende structure

Although the method derived in the previous section is very general and valid for every symmetry group, as we are interested in GaAs, we will now stick to the point group T_d of the zinc blende structure. Without strain, the Hamiltonian of the $\mathbf{k}\cdot\mathbf{p}$ model is given by (3.15). As a starting point, we introduce in Subsec. 3.4.1 the 14×14 extended Kane model, which considers only the neighbouring bands of the fundamental band gap.

Following the extended Kane model, we employ the general concepts of the previous Sec. 3.3 on the Hamiltonian of the $\mathbf{k}\cdot\mathbf{p}$ model. The first two $\mathbf{k}$-independent Hamiltonians $\hat{H}_0$ and $\hat{H}_\mathrm{I}$ describe the energy spectrum at the gamma point. As the Hamiltonian of the spin-orbit interaction depends on the Pauli matrices, we have to deal with the situation described in Sec. 3.3 and choose between the basis (3.48) and (3.64), respectively. In Subsec. 3.4.2, the spin-splitting at the gamma point, we stick to the usual choice of basis (3.48) (see e.g. Ref. [31, 36, 42, 47]). As this basis is ill-suited for Löwdin perturbation theory, beginning with Subsec. 3.4.2, the basis (3.64) is used henceforth to derive analytical expressions for important quantities, such as effective masses, effective g-factors or spin-orbit coupling constants. The latter will be of major interest in the last Subsec. 3.4.6, where we examine additional spin-orbit interactions in the presence of strain.

3.4.1. Extended Kane model

For many applications, the bands near the fundamental band gap are of most importance, especially if the coupling to more remote bands is only weak. Although all residual, more remote bands are neglected, several important aspects of the band structure are at least qualitatively incorporated. Within the tight-binding picture, the neighbouring bands to the s-like conduction band are the p-like valence bands and the anti-bonding p-like conduction bands.

Including spin, Kane took in his model 1957 [47] the two s-like conduction bands $|S\sigma =\uparrow,\downarrow\rangle$, and the six p-like valence bands $|X\sigma\rangle$, $|Y\sigma\rangle$, $|Z\sigma\rangle$ into account. The model, also known as 8×8 Kane model, was later extended by six p-like conduction bands $|X'\sigma\rangle$, $|Y'\sigma\rangle$, $|Z'\sigma\rangle$ to the 14×14 extended Kane model [35, 48–50]. Within the extended Kane model the infinite-dimensional Hamiltonian (3.26) is therefore approximated by a 14×14 matrix.

Considering the definition (3.48) of the spin-dependent basis the s-like states $|S\uparrow\rangle$ and $|S\downarrow\rangle$ already transform according to Γ^6, whereas by the inclusion of the spin, the p-like states split up into two states which transform according to Γ^7 and four which transform according to Γ^8. This separation is also often characterized by considering the total angular momentum of the wave functions. The total angular momentum of the s-like states

$$\left|\Gamma_c^{61}(1)\right\rangle = \left|\frac{1}{2},\quad \frac{1}{2}\right\rangle_c = |S\uparrow\rangle\,, \tag{3.67}$$

$$\left|\Gamma_c^{61}(2)\right\rangle = \left|\frac{1}{2},-\frac{1}{2}\right\rangle_c = |S\downarrow\rangle\,, \tag{3.68}$$

is $j=\frac{1}{2}$ (orbital momentum $l=0$, $s=\frac{1}{2}$). The p-like functions ($l=1$) split up into two functions with total angular momentum $j=\frac{1}{2}$, and four functions with $j=\frac{3}{2}$. Thus, in the extended Kane model the symmetrized basis states (3.48) coincide with the usual definitions of the angular momentum eigenstates (see e.g. [51, 52]). Note, however, that arbitrary eigenstates $|\Gamma_i^{\alpha a}(\delta)\rangle$ are not necessarily also eigenstates of the angular momentum operator. The states of the valence band ($i=v$) and the conduction bands ($i=c'$) with total angular momentum $j=1/2$ that transform according to Γ^7 are

$$\left|\Gamma_i^{75}(1)\right\rangle = \left|\frac{1}{2},\quad \frac{1}{2}\right\rangle_i = -\frac{1}{\sqrt{3}}\left(|X\downarrow\rangle + \mathrm{i}\,|Y\downarrow\rangle + |Z\uparrow\rangle\right), \tag{3.69}$$

$$\left|\Gamma_i^{75}(2)\right\rangle = \left|\frac{1}{2},-\frac{1}{2}\right\rangle_i = -\frac{1}{\sqrt{3}}\left(|X\uparrow\rangle - \mathrm{i}\,|Y\uparrow\rangle - |Z\downarrow\rangle\right), \tag{3.70}$$

whereas the states with total angular momentum $j=3/2$, which transform

according to Γ^8 read:

$$\left|\Gamma_i^{85}(1)\right\rangle = \left|\frac{3}{2}, \quad \frac{3}{2}\right\rangle_i = -\frac{1}{\sqrt{2}}\left(|X\uparrow\rangle + \mathrm{i}|Y\uparrow\rangle\right), \tag{3.71}$$

$$\left|\Gamma_i^{85}(2)\right\rangle = \left|\frac{3}{2}, \quad \frac{1}{2}\right\rangle_i = \sqrt{\frac{2}{3}}|Z\uparrow\rangle - \frac{1}{\sqrt{6}}\left(|X\downarrow\rangle + \mathrm{i}\,|Y\downarrow\rangle\right), \tag{3.72}$$

$$\left|\Gamma_i^{85}(3)\right\rangle = \left|\frac{3}{2}, -\frac{1}{2}\right\rangle_i = \sqrt{\frac{2}{3}}|Z\downarrow\rangle + \frac{1}{\sqrt{6}}\left(|X\uparrow\rangle - \mathrm{i}\,|Y\uparrow\rangle\right), \tag{3.73}$$

$$\left|\Gamma_i^{85}(4)\right\rangle = \left|\frac{3}{2}, -\frac{3}{2}\right\rangle_i = \frac{1}{\sqrt{2}}\left(|X\downarrow\rangle - \mathrm{i}|Y\downarrow\rangle\right). \tag{3.74}$$

For many applications the limitation to these 14 states constitutes a quite good approximation and many observable quantities can be expressed by matrix elements of these states. There are, however, also exceptions (see e.g. Sec. 3.4.6) where additional bands have to be considered. Note that in order to improve accuracy, for the valence bands these remote bands are frequently taken into account by second order Löwdin perturbation theory [35, 47]. A direct diagonalization of the 14×14 Kane Hamiltonian then yields the energy spectrum in the vicinity of the band gap (Fig. 3.4). Instead of calculating all non-vanishing matrix, we postpone this to the next parts of this section, where we exploit the general approach outlined in the previous section 3.3. These non-vanishing quantities will then turn out to be special elements of the infinite-dimensional matrices of invariants.

3.4.2. Spin-splitting at the gamma point

At the gamma point, only the first two Hamiltonians of (3.15) are of relevance, where $\hat{H}_0$ is spin-independent and $\hat{H}_\mathrm{I}$ is responsible for spin-orbit interaction. Following the general discussion of Sec. 3.3, we have to determine the symmetry properties of the operators contained in the Hamiltonians. As both Hamiltonians are independent of an external parameter, the first Hamiltonian reads

$$\mathrm{O}_0^1 = \mathcal{O}_0^1 = \hat{H}_0, \tag{3.75}$$

with $\mathrm{K}_0^{0;1} = \mathcal{K}_0^1 = 1$. This statement is of course also true for the Hamiltonian $\hat{H}_\mathrm{I}^s \sigma^s$, which also transforms according to Γ^1. Since the Pauli matrices transform according to Γ^4, the "spatial" operators $\hat{\mathrm{O}}_{\mathrm{I};\gamma}^4$ of $\hat{H}^s$ must behave

equally under a symmetry operation and we obtain

$$\hat{H}_{\mathrm{I}}^{s} = \sum_{\gamma} \mathrm{K}_{\mathrm{I};\gamma}^{s;4} \hat{\mathrm{O}}_{\mathrm{I};\gamma}^{4} = \frac{\hbar^2}{4m_0^2c^2} \mathbf{e}_s \cdot (\nabla V_0) \times \mathbf{p}, \tag{3.76}$$

with

$$\mathrm{K}_{\mathrm{I};\gamma}^{s;4} = \mathrm{X}_{1;s\gamma}^{44;1}, \tag{3.77}$$

$$\hat{\mathrm{O}}_{\mathrm{I};\gamma}^{4} = \frac{\sqrt{3}\hbar^2}{4m_0^2c^2} \mathbf{e}_\gamma \cdot (\nabla V_0) \times \mathbf{p}. \tag{3.78}$$

Transforming these operators to spin-dependent, calligraphic expressions, one finds the expected result of

$$\mathcal{O}_{\mathrm{I}}^{1} = \hat{H}_{\mathrm{I}}. \tag{3.79}$$

Note that, as the Hamiltonian (3.76) is given by a product of parameters and operators, we are of course free to choose any non-zero prefactor for (3.78). The at first glance irritating additional prefactor of $\sqrt{3}$, due to the matrix elements of $\mathrm{X}_{1;s\gamma}^{44;1}$, is thus chosen in order to ensure $\mathcal{K}_0^1 = \mathcal{K}_{\mathrm{I}}^1 = 1$.

For the choice of basis we stick to the eigenbasis of $\hat{H}_0$, which is commonly used in the literature [31, 36, 42, 47]. To obtain the necessary invariants of (3.62), we need the relevant elements of the matrices M (3.53) and N (3.60). As $\hat{H}_0$ contains only the operator $\mathrm{O}_{0;1}^{1}$, for M, only the elements $\mathrm{M}^{\alpha a\, \alpha b;1}$ are of interest, which written in matrix form read:

$$\mathrm{M}^{66;1} = \begin{pmatrix} \mathrm{M}^{6161;1} & \mathrm{M}^{6164;1} \\ \mathrm{M}^{6461;1} & \mathrm{M}^{6464;1} \end{pmatrix} = \begin{pmatrix} \sqrt{2} & 0 \\ 0 & \sqrt{\frac{2}{3}} \end{pmatrix}, \tag{3.80}$$

$$\mathrm{M}^{77;1} = \begin{pmatrix} \mathrm{M}^{7272;1} & \mathrm{M}^{7275;1} \\ \mathrm{M}^{7572;1} & \mathrm{M}^{7575;1} \end{pmatrix} = \begin{pmatrix} \sqrt{2} & 0 \\ 0 & \sqrt{\frac{2}{3}} \end{pmatrix}, \tag{3.81}$$

$$\mathrm{M}^{88;1} = \begin{pmatrix} \mathrm{M}^{8383;1} & \mathrm{M}^{8384;1} & \mathrm{M}^{8385;1} \\ \mathrm{M}^{8483;1} & \mathrm{M}^{8484;1} & \mathrm{M}^{8485;1} \\ \mathrm{M}^{8583;1} & \mathrm{M}^{8584;1} & \mathrm{M}^{8585;1} \end{pmatrix} = \begin{pmatrix} \sqrt{2} & 0 & 0 \\ 0 & \frac{2}{\sqrt{3}} & 0 \\ 0 & 0 & \frac{2}{\sqrt{3}} \end{pmatrix}. \tag{3.82}$$

With a similar argumentation for N, the only relevant matrices are

$$\mathrm{N}^{66;14} = \mathrm{N}^{77;14} = \begin{pmatrix} 0 & -\sqrt{2} \\ -\sqrt{2} & -\mathrm{i}\frac{2}{\sqrt{3}} \end{pmatrix}, \tag{3.83}$$

and

$$\mathrm{N}^{88;14} = \begin{pmatrix} 0 & \sqrt{2} & -\sqrt{2} \\ \sqrt{2} & \mathrm{i}\sqrt{\frac{2}{3}} & \sqrt{2}\mathrm{i} \\ -\sqrt{2} & -\sqrt{2}\mathrm{i} & \mathrm{i}\sqrt{\frac{2}{3}} \end{pmatrix}, \tag{3.84}$$

where the elements of the matrices are defined analogously to the elements of M.

Using (3.52) and (3.59), one finally obtains all possible invariant matrix elements of the spin-orbit Hamiltonian. A special representative of them, which is of fundamental importance to semiconductors, is the constant of the spin-orbit splitting Δ_0 between the Γ_v^{85} valence band and the Γ_v^{75} spin-orbit split-off valence band. In first order Löwdin perturbation theory, it is given by [35, 47]

$$\begin{aligned} \Delta_0 &= \frac{1}{2}\mathcal{I}_{\mathrm{I};vv}^{85\,85;1} - \frac{1}{\sqrt{2}}\mathcal{I}_{\mathrm{I};vv}^{75\,75;1} = \mathrm{i}\sqrt{\frac{3}{2}}\mathrm{I}_{\mathrm{I};vv}^{55;4} \\ &= -\frac{3\hbar}{4m_0^2c^2}\,\mathrm{Im}(\langle Z \,|\, [(\nabla V_0)\times\mathbf{p}]_x \,|\, Y\rangle), \end{aligned} \tag{3.85}$$

where in the last term we used the basis functions (3.69)-(3.74). In the extended Kane model, there are two further invariants of the same type. The first one describes the spin-orbit splitting $\Delta_0' = \mathrm{i}\sqrt{3/2}\,\mathrm{I}_{\mathrm{I};cc}^{55;4}$ between the Γ_c^{85} and the Γ_c^{75} conduction band, whereas $\Delta^- = \mathrm{i}\sqrt{3/2}\,\mathrm{I}_{\mathrm{I};vc}^{55;4}$ is responsible for a coupling between these bands. We depict the band splitting within the extended Kane model in Fig. 3.2.

The matrix of the invariants $\mathrm{I}_{\mathrm{I},ij}^{55,4}$ can thus be understood as a generalization of all these special representatives. Furthermore, with this systematic approach of invariant matrices, all additional possible matrix elements resulting in a spin-splitting of bands are summed up in the invariant matrix $\mathcal{I}_{\mathrm{I}}^{\alpha a\,\alpha b;4}$ (3.59). This matrix represents therefore an ideal starting point for perturbation theories with the goal to diagonalize the whole external parameter-independent Hamiltonian $\hat{H}_0 + \hat{H}_{\mathrm{I}}$. Up to second order in Löwdin perturbation theory we obtain, e.g., as a correction to the $|\Gamma_c^{61}\rangle$ conduction bands

$$\mathcal{H}_{cc}^{61\,61} = E_{61;c} + \frac{1}{2}\sum_{j\neq c}\frac{\mathcal{I}_{\mathrm{I};cj}^{61\,64;1}\mathcal{I}_{\mathrm{I};jc}^{64\,61;1}}{E_{61;c} - E_{64;j}} + \ldots, \tag{3.86}$$

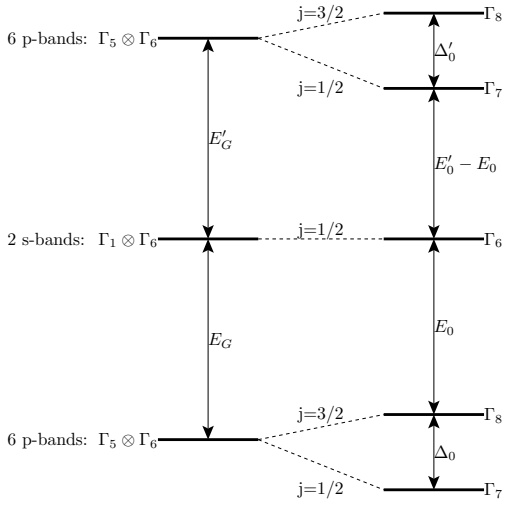

Figure 3.2.: Shift of the band extrema of the doubly degenerate p-like bands due to spin orbit interaction. The energy of the bottom of the s-like conduction band is not affected by spin orbit interaction.

and for the $|\Gamma_v^{85}\rangle$ valence bands

$$\mathcal{H}_{vv}^{85\,85} = E_{85;v} + \frac{1}{2}\mathcal{I}_{\mathrm{I};vv}^{85\,85;1} + \frac{1}{4}\sum_{\substack{b\\ j\neq v}} \frac{\mathcal{I}_{\mathrm{I};vj}^{85\,8b;1}\mathcal{I}_{\mathrm{I};jv}^{8b\,85;1}}{E_{85;v} - E_{8b;j}} + \dots \tag{3.87}$$

The diagonalized Hamiltonian thus couples states with different spatial symmetry Γ^a, albeit no states with distinct symmetry Γ^α, and the resulting basis states are naturally given by (3.64). Finally, we want to emphasize that the eigenvalues of the full Hamiltonian $\hat{H}_0 + \hat{H}_\mathrm{I}$ are the energies of the bands at the band extrema, which can be measured in experiments, contrary to the eigenenergies of the Hamiltonian $\hat{H}_0$.

3.4.3. Second order perturbation theory of Γ^6 bands

We will now utilize the general concepts of Sec. 3.3 to determine the band structure in the vicinity of the gamma point. Note that at the time being, we still focus on unstrained crystals and the **k**-dependent Hamiltonian is given by (3.15). As the term $\hat{H}_\mathrm{II}$ (3.18) is proportional to the identity operator, it is already diagonal and can easily be added to all effective Hamiltonians $\hat{\mathcal{H}}_i$. We are therefore left to deal with the

Hamiltonians $\hat{H}_{\mathrm{III}}$ (3.19) and $\hat{H}_{\mathrm{IV}}$ (3.20). Analogously to the procedure in the previous section 3.4.2, we determine the symmetry properties of the involved operators. Since $\mathbf{p}$ has the transformation properties of a vector it transforms according to Γ^5, and the operators and parameters of the spin-independent Hamiltonian $\hat{H}_{\mathrm{III}}$ are:

$$\mathrm{K}^{0;5}_{\mathrm{III};\gamma} = k_\gamma, \tag{3.88}$$

$$\mathrm{O}^{5}_{\mathrm{III};\gamma} = \frac{\hbar}{m_0} p_\gamma. \tag{3.89}$$

In the spin-dependent Hamiltonian $\hat{H}_{\mathrm{IV}}$ the spatial operator is constituted by the gradient of the potential, ∇V_0, which also transforms as a vector and thus also according to Γ^5. Similarly to the discussions that led us to the definition of (3.77), we define:

$$\mathrm{K}^{s;5}_{\mathrm{IV};\gamma} = \sum_\lambda \mathrm{X}^{45;5}_{\lambda;s\gamma}\, k_\lambda, \tag{3.90}$$

$$\mathrm{O}^{5}_{\mathrm{IV};\gamma} = \frac{\sqrt{2}\hbar^2}{4m_0^2c^2}\partial_\gamma V_0, \tag{3.91}$$

as a set of parameters and operators, which build up the Hamiltonians $\hat{H}^s_{\mathrm{IV}}$. Using (3.57), we are again able to unify the spin-independent parameters with the dependent ones and we obtain

$$\mathcal{K}^5_{\mathbf{k};\gamma} \equiv \mathcal{K}^5_{\mathrm{III};\gamma} = \mathcal{K}^5_{\mathrm{IV};\gamma} = k_\gamma. \tag{3.92}$$

With the deliberations of Sec. 3.3, we now choose the basis (3.64). For the derivation of the required invariants we need again matrix elements of M and N. As we deal here only with operators that transform according to Γ^5, we need only the matrices $\mathrm{M}^{\alpha a\,\beta b;5}$ and $\mathrm{N}^{\alpha a\,\beta b;55}$. According to Tab. A.9, in all combinations of α, β except $\alpha = \beta = 6$ and $\alpha = \beta = 7$, matrix elements of an operator with Γ^5 symmetry are possible. Writing M and N in an equivalent form compared to (3.80)-(3.82), the off-diagonal matrices read

$$\mathrm{M}^{67;5} = \begin{pmatrix} 0 & -\sqrt{\frac{2}{3}} \\ -\sqrt{\frac{2}{3}} & -\frac{2}{3}\mathrm{i} \end{pmatrix}, \tag{3.93}$$

$$\mathrm{M}^{68;5} = \begin{pmatrix} 0 & 0 & \frac{2}{\sqrt{3}} \\ \sqrt{\frac{2}{3}} & \sqrt{\frac{2}{3}}\mathrm{i} & -\frac{\sqrt{2}}{3}\mathrm{i} \end{pmatrix}, \tag{3.94}$$

$$\mathrm{M}^{78;5} = \begin{pmatrix} 0 & -\frac{2}{\sqrt{3}}\mathrm{i} & 0 \\ \sqrt{\frac{2}{3}}\mathrm{i} & \frac{\sqrt{2}}{3} & -\sqrt{\frac{2}{3}} \end{pmatrix}, \tag{3.95}$$

where $\mathrm{M}^{76;5}$, $\mathrm{M}^{86;5}$ and $\mathrm{M}^{87;5}$ are easily obtained by transposing and taking the complex conjugate.

Note, as a consequence of the direct product

$$\Gamma^{8*} \otimes \Gamma^{8} = \Gamma^{1} \oplus \Gamma^{2} \oplus \Gamma^{3} \oplus 2\Gamma^{4} \oplus 2\Gamma^{5}, \tag{3.96}$$

there are two sets of matrices $\mathrm{X}^{88;5}_{\mathrm{A};\gamma;\delta\delta'}$ and $\mathrm{X}^{88;5}_{\mathrm{B};\gamma;\delta\delta'}$ that transform according to Γ^5. Hence, for both, M and N, also two matrices are needed. We obtain for M

$$\mathrm{M}^{88;5}_{\mathrm{A}} = \begin{pmatrix} 0 & \sqrt{\frac{2}{3}}\mathrm{i} & \sqrt{\frac{2}{3}}\mathrm{i} \\ -\sqrt{\frac{2}{3}}\mathrm{i} & -\sqrt{\frac{2}{3}} & -\frac{\sqrt{2}}{3} \\ -\sqrt{\frac{2}{3}}\mathrm{i} & -\frac{\sqrt{2}}{3} & -\sqrt{\frac{2}{3}} \end{pmatrix}, \tag{3.97}$$

$$\mathrm{M}^{88;5}_{\mathrm{B}} = \begin{pmatrix} 0 & \sqrt{\frac{2}{3}} & -\sqrt{\frac{2}{3}} \\ \sqrt{\frac{2}{3}} & 0 & \frac{2\sqrt{2}}{3}\mathrm{i} \\ -\sqrt{\frac{2}{3}} & -\frac{2\sqrt{2}}{3}\mathrm{i} & 0 \end{pmatrix}, \tag{3.98}$$

and for the matrices N

$$\mathrm{N}^{67;55} = \begin{pmatrix} 0 & \frac{2}{\sqrt{3}}\mathrm{i} \\ -\frac{2}{\sqrt{3}}\mathrm{i} & 0 \end{pmatrix}, \tag{3.99}$$

$$\mathrm{N}^{68;55} = \begin{pmatrix} 0 & 0 & \sqrt{\frac{2}{3}}\mathrm{i} \\ -\frac{\mathrm{i}}{\sqrt{3}} & \frac{1}{\sqrt{3}} & 1 \end{pmatrix}, \tag{3.100}$$

$$\mathrm{N}^{78;55} = \begin{pmatrix} 0 & \sqrt{\frac{2}{3}} & 0 \\ \frac{1}{\sqrt{3}} & \mathrm{i} & \frac{\mathrm{i}}{\sqrt{3}} \end{pmatrix}, \tag{3.101}$$

$$\mathrm{N}^{88;55}_{\mathrm{A}} = \begin{pmatrix} 0 & \frac{2}{\sqrt{3}} & \frac{2}{\sqrt{3}} \\ \frac{2}{\sqrt{3}} & 0 & 0 \\ \frac{2}{\sqrt{3}} & 0 & 0 \end{pmatrix}, \quad \mathrm{N}^{88;55}_{\mathrm{B}} = \begin{pmatrix} 0 & \frac{2}{\sqrt{3}}\mathrm{i} & -\frac{2}{\sqrt{3}}\mathrm{i} \\ -\frac{2}{\sqrt{3}}\mathrm{i} & \frac{2}{\sqrt{3}} & 0 \\ \frac{2}{\sqrt{3}}\mathrm{i} & 0 & -\frac{2}{\sqrt{3}} \end{pmatrix}. \tag{3.102}$$

Using the definitions (3.52) and (3.59) we are now able to determine all needed invariants $\mathcal{I}^{\alpha\beta;5}_{\mathbf{k}}$. In this subsection we intend to obtain the effective Hamiltonian $\hat{\mathcal{H}}_c$ of an electron in the $|\Gamma^6_c\rangle$ conduction band by

using Löwdin perturbation theory. Due to symmetry arguments a first order contribution is not possible ($\mathrm{M}^{66;5} = \mathrm{N}^{66;55} = 0$) and the first non-vanishing term arises by second order perturbation theory,

$$\sum_{j\neq c}\left[\frac{\mathcal{I}^{67;5}_{\mathbf{k},cj}\mathcal{I}^{76;5}_{\mathbf{k},jc}}{E_{6,c}-E_{7,j}}\frac{(\mathbf{k}\cdot\boldsymbol{\sigma})(\mathbf{k}\cdot\boldsymbol{\sigma})^\dagger}{2}+\frac{\mathcal{I}^{68;5}_{\mathbf{k},cj}\mathcal{I}^{86;5}_{\mathbf{k},jc}}{E_{6,c}-E_{8,j}}\frac{9}{4}(\mathbf{k}\cdot\mathbf{T})(\mathbf{k}\cdot\mathbf{T})^\dagger\right], \quad (3.103)$$

where we used the matrices $\boldsymbol{\sigma}$ and $\mathbf{T}$ of Tab. A.10 instead of the matrices $\mathrm{X}^{\alpha\beta;5}_{\gamma;\delta\delta'}$. Utilizing now the identities

$$(\mathbf{k}\cdot\boldsymbol{\sigma})(\mathbf{k}'\cdot\boldsymbol{\sigma})^\dagger = \mathbf{k}\cdot\mathbf{k}' + \mathrm{i}\mathbf{k}\times\mathbf{k}'\cdot\boldsymbol{\sigma}, \quad (3.104)$$

$$(\mathbf{k}\cdot\mathbf{T})(\mathbf{k}'\cdot\mathbf{T})^\dagger = \frac{2}{9}\mathbf{k}\cdot\mathbf{k}' - \frac{1}{9}\mathrm{i}\mathbf{k}\times\mathbf{k}'\cdot\boldsymbol{\sigma}, \quad (3.105)$$

and remembering (3.12), the second order effective Hamiltonian can be written as

$$\hat{\mathcal{H}}^{\mathbf{k}}_c = E_{6,c} + \frac{\hbar^2\mathbf{k}^2}{2m_c} + \frac{g_c}{2}\mu_\mathrm{B}\mathbf{B}\cdot\boldsymbol{\sigma}, \quad (3.106)$$

with the effective mass

$$\frac{\hbar^2}{2m_c} = \frac{\hbar^2}{2m_0} + \frac{1}{2}\sum_{j\neq c}\left(\frac{\mathcal{I}^{67,5}_{\mathbf{k},cj}\mathcal{I}^{76,5}_{\mathbf{k},jc}}{E_{6,c}-E_{7,j}} + \frac{\mathcal{I}^{68,5}_{\mathbf{k},cj}\mathcal{I}^{86,5}_{\mathbf{k},jc}}{E_{6,c}-E_{8,j}}\right), \quad (3.107)$$

and the effective g-factor

$$g_c = \frac{2m_0}{\hbar^2}\sum_{j\neq c}\left(\frac{\mathcal{I}^{67,5}_{\mathbf{k},cj}\mathcal{I}^{76,5}_{\mathbf{k},jc}}{E_{6,c}-E_{7,j}} - \frac{1}{2}\frac{\mathcal{I}^{68,5}_{\mathbf{k},cj}\mathcal{I}^{86,5}_{\mathbf{k},jc}}{E_{6,c}-E_{8,j}}\right). \quad (3.108)$$

The first term of the effective mass has its origin in the Hamiltonian $\hat{H}_\mathrm{II}$ (3.18). We emphasize that the above expressions are exact, contrary to the expressions used in the literature (see, e.g., Ref. [31, 35, 36, 42, 47]), and that they include also the often neglected contributions of the Hamiltonian $\hat{H}_\mathrm{IV}$ (3.20).

Before we derive the second order effective Hamiltonians of bands with Γ^7 and Γ^8 symmetry, we state the difference of the above expressions to the ones used in the literature, by comparing them to the expressions derived within the extended Kane model. Contributions arising from the Hamiltonian $\hat{H}_\mathrm{IV}$ are considered to be small and are thus within the extended Kane model neglected for the derivation of the effective mass. Keeping in mind that the states (3.67) - (3.74) are eigenstates of the Hamiltonian

$\hat{H}_0$, the in general infinite-dimensional matrix of invariants $\mathrm{I}_{0;ij}^{15;5}$ consists of only two entries:

$$\mathrm{I}_{0;cv}^{15;5} = \frac{\hbar}{m_0} \langle S|p_x|X\rangle \equiv P, \tag{3.109}$$

and

$$\mathrm{I}_{0;cc'}^{15;5} = \frac{\hbar}{m_0} \langle S|p_x|X'\rangle \equiv P'. \tag{3.110}$$

Apart from the coupling of the s-like states to the p-like states, symmetry permits also a mutual coupling of the p-like states. As pointed out in Ref. [42], the matrix elements of the momentum operator between degenerate states have to vanish. This is easily understood by considering, e.g., $\hbar/m_0 \langle Z|p_x|Y\rangle = -\mathrm{i} \langle Z|[x, \hat{H}_0]|Y\rangle = -\mathrm{i}(E_v - E_v) \langle Z|x|Y\rangle = 0$, implying that intra-band couplings are prohibited. Using (3.46) we finally obtain the last possible invariant:

$$\mathrm{I}_{0;vc'}^{55;5} = \frac{\hbar}{\sqrt{2}m_0} (\langle Z|p_x|Y'\rangle + \langle Y|p_x|Z'\rangle) = \sqrt{2}Q \tag{3.111}$$

As the basis states (3.67) - (3.74) are eigenstates of $\hat{H}_0$, in the expression of the effective mass (3.107), one has to replace the invariants by $\mathcal{I}_{\mathbf{k};cj}^{67;5} \to \mathcal{I}_{\mathbf{k};cj}^{6175;5} = -\sqrt{\frac{2}{3}}\,\mathrm{I}_{0;cj}^{15;5}$, $\mathcal{I}_{\mathbf{k};cj}^{68;5} \to \mathcal{I}_{\mathbf{k};cj}^{6185;5} = \frac{2}{\sqrt{3}}\,\mathrm{I}_{0;cj}^{15;5}$ and the energies by $E_{7;j} \to E_{75;j} = E_j + 1/\sqrt{2}\,\mathcal{I}_{\mathrm{I};jj}^{75\,75;1}$ and $E_{8,j} \to E_{85;j} = E_j + 1/2\,\mathcal{I}_{\mathrm{I};jj}^{85\,85;1}$. For the p-like valence and conduction bands the energies are denoted by $E_{74,v} = -E_0 - \Delta_0$, $E_{84,v} = -E_0$ and $E_{74,c} = E_0' + \Delta_0' - E_0$, $E_{84,c} = E_0' - E_0$ [35, 47] (compare Fig. 3.2). With these definitions, the effective mass within the extended Kane model reads:

$$\frac{m_c^{\mathrm{K}}}{m_0} = \left[1 + \frac{2m_0}{3\hbar^2}\left(\frac{|P|^2}{E_0 + \Delta_0} + \frac{2|P|^2}{E_0} + \frac{|P'|^2}{E_0 - E_0'} + \frac{2|P'|^2}{E_0 - E_0' - \Delta_0'}\right)\right]^{-1}. \tag{3.112}$$

One major difference between the exact effective mass (3.107) and this approximated one is – beside the limitation on 14 states – the point that in extended Kane model, the conduction band is only capable to couple to bands with spatial symmetry Γ^5. Within the expression of the exact effective mass (3.107), bands with Γ^6 symmetry couple to bands with spatial symmetry Γ^2, Γ^3 and Γ^4. The expression of the effective mass (3.107) is thus a generalization to arbitrary bands with Γ^6 symmetry. Note, however, that if the $|\Gamma^6\rangle_c$ conduction band is a "pure" s-like band, the expression

for an approximate effective mass m_c', obtained by second order perturbation theory in the basis (3.48), and the exact one m_c, coincide in all but the energies $E_{7,j}$ and $E_{8,j}$.

As mentioned earlier, by assigning an (experimentally obtained) value to the invariants, one is able to diagonalize the 14×14 matrix of the extended Kane Hamiltonian for each value of $\mathbf{k}$. Table 3.3 lists some of these band structure parameters for commonly used materials. For the Γ^6

Table 3.3.: Band structure parameters for the extended 14×14 Kane model [35, 53, 54]

		GaAs	AlAs	InSb	InAs	AlSb	GaSb	InP
E_0	(eV)	1.519	3.13	0.237	0.418	2.384	0.813	1.424
E_0'	(eV)	4.488	4.540	3.160	4.390	3.5	3.3	4.6
Δ_0	(eV)	0.341	0.300	0.810	0.380	0.673	0.75	0.108
Δ_0'	(eV)	0.171	0.150	0.330	0.240	0.3	0.33	0.50
Δ^-	(eV)	-0.050		-0.244			-0.28	0.22
P	(eV Å)	10.493	8.97	9.641	9.197	8.463	10.1	8.88
P'	(eV Å)	4.780	4.780	6.325	0.873			
Q	(eV Å)	8.165	8.165	0.130	8.331			
C_k	(eV Å)	-0.0034	0.002	-0.0082	-0.0112	0.006		
γ_1		6.85	3.25	37.10	20.40	4.15	13.4	5.08
γ_2		2.10	0.65	16.50	8.30	1.01	4.7	1.60
γ_3		2.90	1.21	17.70	9.10	1.71	6.0	2.10
κ		1.20		15.60	7.60	0.31		
q		0.01		0.39	0.39	0.07		

band in GaAs, the deviation from the parabolic dispersion can be found in Fig. 3.3. Although there are deviations from the pure parabolic behaviour, for $k \lesssim 5 \cdot 10^{-2} \text{Å}^{-1}$ the spatial anisotropy remains relatively weak. This is, however, not the case for holes in the Γ^8 valence band. We will therefore discuss the characteristics of bands with Γ^7 and Γ^8 symmetry, up to second order perturbation theory, in the next part of this section.

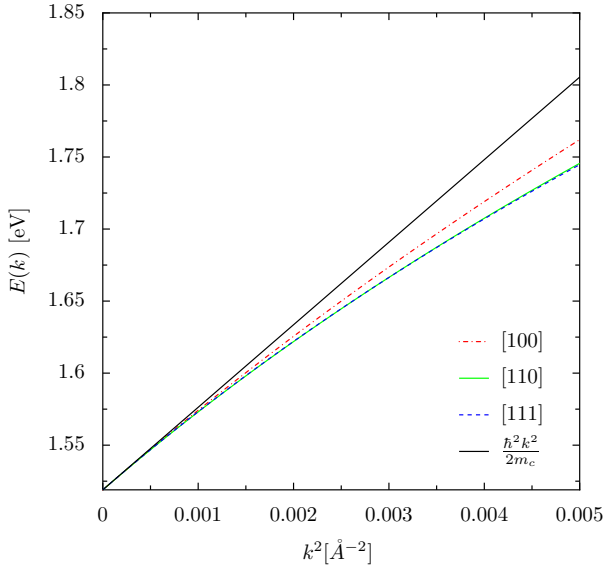

Figure 3.3.: Deviation of the Γ^6 conduction band from parabolic dispersion for various directions in $\mathbf{k}$-space. The calculation is based on the 14×14 Kane model and was carried out for GaAs.

3.4.4. Second order perturbation theory of Γ^7 & Γ^8 bands

We will now transfer the considerations of Sec. 3.3 to bands which transform according to the irreducible representations Γ^7 and Γ^8. The most prominent representatives of such bands are the valence bands [31, 35, 36, 42, 47]. We start with the uppermost valence bands with Γ^8 symmetry. One major difference, compared to Γ^6 bands, is the occurrence of terms linear in $\mathbf{k}$. Since there are two matrices which couple to invariants related to Γ^5 (see Appendix A.9), these terms can appear in two distinct ways. With the help of the matrices M and N (3.93)-(3.102) all invariants needed are readily calculated and the first order effective Hamiltonian of Γ^8 bands is given by:

$$\begin{aligned}\hat{\mathcal{H}}^{\mathbf{k}(1)}_{8;i} &= \mathcal{I}^{88;5}_{\mathbf{k},\mathrm{A};ii}\, k_\gamma \mathrm{X}^{88;5}_{\mathrm{A};\gamma} + \mathcal{I}^{88;5}_{\mathbf{k};\mathrm{B};ii}\, k_\gamma \mathrm{X}^{88;5}_{\mathrm{B};\gamma} \\ &= \frac{\mathcal{I}^{88;5}_{\mathbf{k};\mathrm{A};ii}}{\sqrt{3}} \left(\{J_y, J_z\}\, k_x + \text{c.p.}\right) + \frac{\mathcal{I}^{88;5}_{\mathbf{k};\mathrm{B};ii}}{\sqrt{3}} \left(\left\{J_x, J_y^2 - J_z^2\right\} k_x + \text{c.p.}\right). \end{aligned} \tag{3.113}$$

For the invariants $\mathcal{I}^{88;5}_{\mathbf{k},\mathrm{A};ii}$ and $\mathcal{I}^{88;5}_{\mathbf{k},\mathrm{B};ii}$ the choice of basis (3.64) is of great

importance. In the eigenbasis of $\hat{H}_0$ (3.48) the invariants corresponding to $\mathcal{I}^{88;5}_{\mathbf{k},\mathrm{A};ii}$ are $\mathcal{I}^{8a8a;5}_{\mathbf{k},\mathrm{A};ii}$, which depend solely on the matrix elements of the momentum operator. As argued above, the matrix elements of the momentum operator between degenerate states have to vanish. Hence, this invariant does not exist in the common 14×14 Kane models. Such an approximation is, however, not justified for arbitrary Γ^8 bands. On the other hand the corresponding invariants $\mathcal{I}^{8a8a;5}_{\mathbf{k},\mathrm{B};ii}$ of the second invariant, $\mathcal{I}^{88;5}_{\mathbf{k};\mathrm{B};ii}$, depend only on the matrix elements of the Hamiltonian $\hat{H}_{\mathrm{IV}}$. Similarly to the matrix elements of the momentum operator, the matrix elements $\langle X|\partial V_0/\partial_y|Z\rangle = \mathrm{i}/\hbar\,\langle X|[p_y, \hat{H}_0]|Z\rangle = 0$ (see Ref. [53]) have to vanish. Nevertheless, in the literature [35, 47, 53] the second invariant $\mathcal{I}^{88;5}_{\mathbf{k},\mathrm{A};vv} = 2C_k$ is, contrary to $\mathcal{I}^{88;5}_{\mathbf{k},\mathrm{A};vv} = 0$, assumed to be non-vanishing. In Ref. [53], e.g., C_k is a result of bilinear second order perturbation theory in $\hat{H}_{\mathrm{III}}$ and $\hat{H}_{\mathrm{IV}}$.

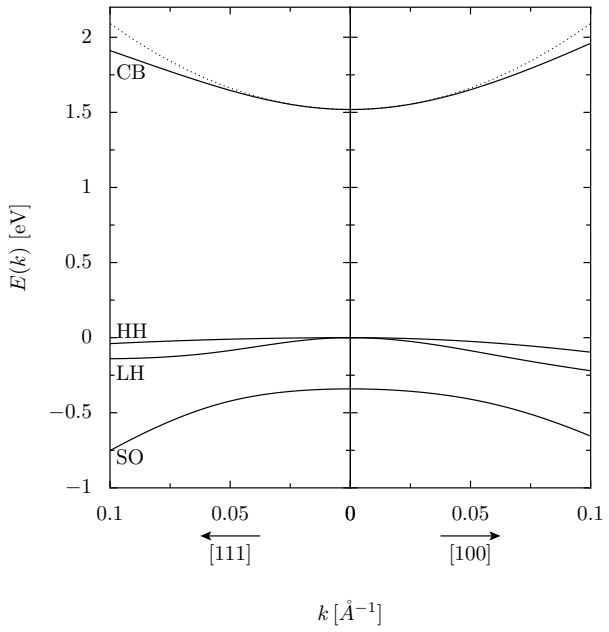

Figure 3.4.: Energy spectrum of GaAs based on the 14×14 extended Kane model in the vicinity of the band gap. The dotted line represents the pure parabolic energy spectrum of the effective mass approximation (see Eq. (3.106)).

Turning now to second order Löwdin perturbation theory, the effective

Hamiltonian for an arbitrary $|\Gamma_i^8\rangle$ band is given by:

$$\begin{aligned}\hat{\mathcal{H}}_{8;i}^{\mathbf{k}(2)} &= \sum_{\substack{\gamma\gamma' \\ \beta \\ j\neq i}} \frac{\mathcal{I}_{\mathbf{k};ij}^{8\beta;5}\mathcal{I}_{\mathbf{k};ji}^{\beta 8;5}}{E_{8;i}-E_{\beta;j}} \otimes \left(\mathcal{K}_{\mathbf{k};\gamma}^{5}\mathcal{K}_{\mathbf{k};\gamma'}^{5}\,\mathrm{X}_{\gamma}^{8\beta;5}\mathrm{X}_{\gamma'}^{\beta 8;5}\right) \\ &= -\frac{\hbar^2}{2m_0}\Bigg[\gamma_1^i\mathbf{k}^2 \\ &\quad -2\gamma_2^i\left(\left(J_x^2-\frac{1}{3}J^2\right)k_x^2+\text{c.p.}\right)\Bigg] \\ &\quad -4\gamma_3^i\left(\{J_y,J_z\}\{k_y,k_z\}+\text{c.p.}\right) \\ &\quad -2\mu_{\mathrm{B}}\left(\kappa^i\,\mathbf{J}\cdot\mathbf{B}+q^i\left(J_x^3B_x+\text{c.p.}\right)\right). \end{aligned} \tag{3.114}$$

The constants $\gamma_1^i, \gamma_2^i, \gamma_3^i, \kappa^i, q^i$ are the generalized Luttinger constants [55] for an arbitrary Γ^8 band with band index i. They are again augmented by contributions from the Hamiltonian $\hat{H}_{\mathrm{IV}}$. Explicitly they read:

$$\gamma_1^i = -1-\frac{m_0}{2\hbar^2}\sum_{j\neq i}\left[\mathcal{A}_{ij}+\mathcal{B}_{ij}+\mathcal{C}_{ij}^{\mathrm{AA}}+\mathcal{C}_{ij}^{\mathrm{BB}}\right], \tag{3.115}$$

$$\gamma_2^i = -\frac{m_0}{4\hbar^2}\sum_{j\neq i}\left[\mathcal{A}_{ij}-\mathcal{B}_{ij}+\mathrm{i}(\mathcal{C}_{ij}^{\mathrm{AB}}-\mathcal{C}_{ij}^{\mathrm{BA}})\right], \tag{3.116}$$

$$\gamma_3^i = -\frac{m_0}{4\hbar^2}\sum_{j\neq i}\left[\mathcal{A}_{ij}+\mathcal{B}_{ij}-\mathcal{C}_{ij}^{\mathrm{BB}}\right], \tag{3.117}$$

$$\kappa^i = -\frac{m_0}{4\hbar^2}\sum_{j\neq i}\left[\mathcal{A}_{ij}-\frac{10}{3}\mathcal{B}_{ij}+\frac{7}{3}\mathcal{C}_{ij}^{\mathrm{AA}}-\frac{7}{6}\mathcal{C}_{ij}^{\mathrm{BB}}+\frac{13}{12}\mathrm{i}(\mathcal{C}_{ij}^{\mathrm{AB}}-\mathcal{C}_{ij}^{\mathrm{BA}})\right], \tag{3.118}$$

$$q^i = -\frac{m_0}{3\hbar}\sum_{j\neq i}\left[\mathcal{B}_{ij}-\mathcal{C}_{ij}^{\mathrm{AA}}+\frac{1}{2}\mathcal{C}_{ij}^{\mathrm{BB}}+\frac{\mathrm{i}}{4}(\mathcal{C}_{ij}^{\mathrm{AB}}-\mathcal{C}_{ij}^{\mathrm{BA}})\right], \tag{3.119}$$

where we have used the abbreviations

$$\mathcal{A}_{ij} = \frac{\mathcal{I}_{\mathbf{k};ij}^{86;5}\mathcal{I}_{\mathbf{k};ji}^{68;5}}{E_{8;i}-E_{6;j}}, \tag{3.120}$$

$$\mathcal{B}_{ij} = \frac{\mathcal{I}_{\mathbf{k};ij}^{87;5}\mathcal{I}_{\mathbf{k};ji}^{78;5}}{E_{8;i}-E_{7;j}}, \tag{3.121}$$

and

$$\mathcal{C}_{ij}^{\mathrm{AB}} = \frac{\mathcal{I}_{\mathbf{k};\mathrm{A};ij}^{88;5}\mathcal{I}_{\mathbf{k};\mathrm{B};ji}^{88;5}}{E_{8,i} - E_{8,j}}. \tag{3.122}$$

In principle, one could think of an additional constant γ_4^i, proportional to the term $\left(\left\{J_x, \left(J_y^2 - J_z^2\right)\right\}\{k_y, k_z\} + \mathrm{c.p.}\right)$. This is, however, not possible for the p-like valence bands due to time-reversal invariance (see Ref. [55]). Moreover, such a constant can not exist for any Γ^8 band, since second order perturbation theory yields:

$$\gamma_4^i = -\frac{m_0}{4\hbar^2}\sum_j \left[\mathcal{C}_{ij}^{\mathrm{AB}} + \mathcal{C}_{ij}^{\mathrm{BA}}\right] = 0. \tag{3.123}$$

This becomes more evidently by choosing, e.g., the phase convention all matrix elements of $\mathcal{I}_{\mathbf{k};\mathrm{A};ij}^{88;5}$ to be real. As a consequence of this choice, all matrix elements of $\mathcal{I}_{\mathbf{k};\mathrm{B};ji}^{88;5}$ are purely imaginary, and $\mathcal{C}_{ij}^{\mathrm{AB}} + \mathcal{C}_{ij}^{\mathrm{BA}} = \mathcal{C}_{ij}^{\mathrm{AB}} + (\mathcal{C}_{ij}^{\mathrm{AB}})^* = 0$.

The first three Luttinger parameters $\gamma_1, \gamma_2, \gamma_3$ are of special interest for the effective mass of these valence bands. In contrast to the Γ^6 like bands, due to the enhanced number of parameters the effective mass is quite anisotropic (compare Fig. 3.5). A diagonalisation of the second order Hamiltonian $\hat{\mathcal{H}}_{8v}^{\mathbf{k}(2)}$ (3.114) yields two distinct effective masses. They are called the mass of the heavy hole (HH) and light hole (LH), respectively. Depending on the crystallographic directions, they read

$$\frac{m_0}{m_{\mathrm{HH(LH)}}} = \gamma_1 \mp \sqrt{6\gamma_3^2 - 2\gamma_2^2 + 6\frac{k_x^4 + k_y^4 + k_z^4}{k^4}(\gamma_2^2 - \gamma_3^2)}. \tag{3.124}$$

After discussing the effective masses of bands with Γ^6 and Γ^8 symmetry, there is only one irreducible representation left. The expression for the effective mass of charge carriers in bands, which transform according to Γ^7 is quite similar to the one with Γ^6 symmetry. Performing again second order Löwdin perturbation theory, we obtain:

$$\frac{\hbar^2}{2m_{SO}} = \frac{\hbar^2}{2m_0} + \frac{1}{2}\sum_{j\neq i}\left(\frac{\mathcal{I}_{\mathbf{k};vj}^{76;5}\mathcal{I}_{\mathbf{k};jv}^{67;5}}{E_{7;v} - E_{6;j}} + \frac{\mathcal{I}_{\mathbf{k};vj}^{78;5}\mathcal{I}_{\mathbf{k};jv}^{87;5}}{E_{7;v} - E_{8;j}}\right). \tag{3.125}$$

In order to estimate the range of validity of the effective Hamiltonians obtained by second order perturbation theory, the parabolic behaviour of the valence bands in the neighbourhood of the band gap is shown in

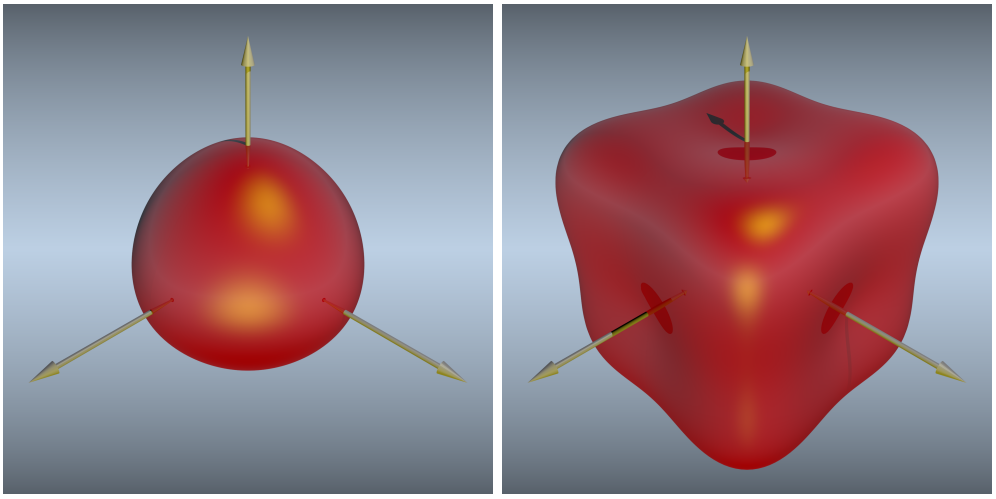

(a) Light hole (LH) (b) Heavy hole (HH)

Figure 3.5.: Surfaces of constant energy in GaAs ($E = -50$ meV) of the Γ^8 valence bands in **k**-space. Whereas the spatial dependence of the energy of the light holes is only weak, the heavy holes deviate noticeable from spherical symmetry.

Fig. 3.6. The deviation from the parabolic behaviour becomes notable for wave vectors of the order of $k \gtrsim 5 \cdot 10^{-3}\text{Å}^{-1}$, especially for the light hole bands.

A summary of second order expressions within the 14×14 Kane model is given in Tab. 3.4.

3.4.5. Dresselhaus term of the conduction band

The appearance of the second order effective Hamiltonian (3.106) is, apart from the effective mass and the g-factor, the same as that of a free electron without spin-orbit coupling. We will now re-introduce spin-orbit-interaction by adding a term obtained within third order perturbation theory. Since the zinc blende structure has no center of inversion – even without magnetic field – there is also a spin-dependent splitting of the conduction band. The lowest order term that leads to such a spin-splitting is called the cubic Dresselhaus term [42]:

$$\begin{aligned}\hat{\mathcal{H}}_c^{\mathrm{D}} = \lambda_{cc}[&k_x \left(k_y^2 - k_z^2\right) \sigma^x \\ &+ k_y \left(k_z^2 - k_x^2\right) \sigma^y + k_z \left(k_x^2 - k_y^2\right) \sigma^z]\end{aligned} \tag{3.126}$$

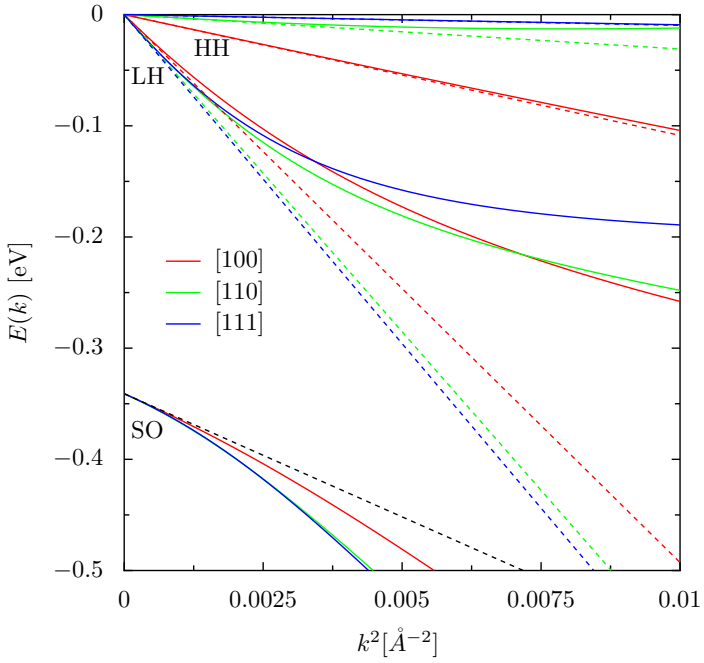

Figure 3.6.: Deviation of the valence bands from parabolic dispersion for various directions in **k**-space. The calculation based on the 14×14 Kane model and was carried out for GaAs. The dashed lines represent the pure parabolic behaviour of the effective mass approximation.

This extra term to the effective Hamiltonian couples the motion of the electrons in the conduction band to their spin. Such a coupling leads to a de-phasing of an initially polarized spin density, i.e., the Dyakonov-Perel' spin relaxation mechanism [9]. Because of the importance for the development of new spintronic devices, the magnitude of all relevant Hamiltonians leading to a spin-splitting has to be known. We therefore start with the calculation of the parameter λ_{ii}. The structure of (3.62) is again very convenient for finding very quickly the right matrix products which are responsible for the cubic Dresselhaus term. They are

$$k_i k_j k_l \mathrm{X}_i^{67;5} \mathrm{X}_j^{78;5} \mathrm{X}_l^{86;5}, \tag{3.127}$$

$$k_i k_j k_l \mathrm{X}_i^{68;5} \mathrm{X}_j^{87;5} \mathrm{X}_l^{76;5}, \tag{3.128}$$

$$k_i k_j k_l \mathrm{X}_i^{68;5} \mathrm{X}_{\mathrm{B};j}^{88;5} \mathrm{X}_l^{86;5}, \tag{3.129}$$

where Einstein's summation convention is implied. Note that for the derivation of these matrix products, no information about the invariants

Γ_c^6	$\frac{m_0}{m_c^{\mathrm{K}}}$	$= 1 + \frac{2m_0}{3\hbar^2}\left(\frac{\lvert P\rvert^2}{E_0+\Delta_0} + \frac{2\lvert P\rvert^2}{E_0} + \frac{\lvert P'\rvert^2}{E_0-E_0'} + \frac{2\lvert P'\rvert^2}{E_0-E_0'-\Delta_0'}\right)$
	g^{K}	$= \frac{2m_0}{3\hbar^2}\left(\frac{\lvert P\rvert^2}{E_0+\Delta_0} - \frac{\lvert P\rvert^2}{E_0} + \frac{\lvert P'\rvert^2}{E_0-E_0'} - \frac{\lvert P'\rvert^2}{E_0-E_0'-\Delta_0'}\right)$
Γ_v^8	γ_1^{K}	$= -1 + \frac{2m_0}{3\hbar^2}\left(\frac{\lvert P\rvert^2}{E_0} + \frac{\lvert Q\rvert^2}{E_0'} + \frac{\lvert Q\rvert^2}{E_0'+\Delta_0'}\right)$
	γ_2^{K}	$= \frac{m_0}{3\hbar^2}\left(\frac{\lvert P\rvert^2}{E_0} - \frac{\lvert Q\rvert^2}{E_0'}\right)$
	γ_3^{K}	$= \frac{m_0}{3\hbar^2}\left(\frac{\lvert P\rvert^2}{E_0} + \frac{\lvert Q\rvert^2}{E_0'}\right)$
	κ^{K}	$= \frac{2m_0}{\hbar^2}\left(\frac{1}{6}\frac{\lvert P\rvert^2}{E_0} - \frac{5}{9}\frac{\lvert Q\rvert^2}{E_0'} + \frac{7}{18}\frac{\lvert Q\rvert^2}{E_0'+\Delta_0'}\right)$
	q^{K}	$= \frac{2m_0}{\hbar^2}\left(\frac{2}{9}\frac{\lvert Q\rvert^2}{E_0'} - \frac{2}{9}\frac{\lvert Q\rvert^2}{E_0'+\Delta_0'}\right)$
Γ_v^7	$\frac{m_0}{m_{\mathrm{SO}}^{\mathrm{K}}}$	$= -1 + \frac{2m_0}{3\hbar^2}\left(\frac{\lvert P\rvert^2}{E_0+\Delta_0} + \frac{2\lvert Q\rvert^2}{\Delta_0+E_0'+\Delta_0'}\right)$
	g^{K}	$= -\frac{2m_0}{3\hbar^2}\left(\frac{\lvert P\rvert^2}{E_0+\Delta_0} - \frac{\lvert Q\rvert^2}{\Delta_0+E_0'+\Delta_0'}\right)$

Table 3.4.: Summary of all expressions derived by second order perturbation theory within the extendend 14×14 Kane model.

was necessary. Moreover, this selection of the relevant matrix products is directly conferred upon the invariants. The material constant of the Dresselhaus term is thus, without cumbersome calculations, readily given by

$$\lambda_{ii} = \frac{1}{2}\sqrt{\frac{3}{2}}\sum_{jll'}\left[\frac{\mathrm{i}\left(\mathcal{I}^{67;5}_{\mathbf{k};ij}\mathcal{I}^{78;5}_{\mathbf{k};jl}\mathcal{I}^{86;5}_{\mathbf{k};li} - \mathcal{I}^{68;5}_{\mathbf{k};il}\mathcal{I}^{87;5}_{\mathbf{k};lj}\mathcal{I}^{76;5}_{\mathbf{k};ji}\right)}{\left(E_{6,i}-E_{7,j}\right)\left(E_{6,i}-E_{8,l}\right)} + \frac{1}{2\sqrt{2}}\frac{\mathcal{I}^{68;5}_{\mathbf{k};il}\mathcal{I}^{88;5}_{\mathbf{k};\mathrm{B};ll'}\mathcal{I}^{86;5}_{\mathbf{k};l'i}}{\left(E_{6,i}-E_{8,l}\right)\left(E_{6,i}-E_{8,l'}\right)}\right], \tag{3.130}$$

where once again the expression holds for arbitrary bands with Γ^6 symmetry.

3.4.6. Influence of strain on the conduction band

As a next step, we include also strain induced effects which lead in addition to the Dresselhaus term to a spin-orbit coupling. As discussed in Sec. 3.1.2, in the presence of linear strain additional strain-dependent terms appear in the Hamiltonian, i.e., $\hat{H} \to \hat{H} + \hat{H}_{\mathrm{V}} + \hat{H}_{\mathrm{VI}} + \hat{H}_{\mathrm{VII}} + \hat{H}_{\mathrm{VIII}}$ (3.26). Since all symmetry operations of the unstrained Hamiltonian still apply, the influence of strain on the energy spectrum $E(\mathbf{k})$ can again be

derived with the help of the methods developed in Sec. 3.3. Note, however, that the additional terms in the Hamiltonian are limited to first order in the strain tensor. Hence, only terms linear in the components of $\boldsymbol{\varepsilon}$ are valid for any effective Hamiltonian obtained by perturbation theory. This point has a profound influence on the selection of needed invariants. For effective Hamiltonians depending solely on the strain tensor only contributions arising from $\hat{H}_{\mathrm{V}}$ and $\hat{H}_{\mathrm{VI}}$ are of relevance. In order to obtain this $\mathbf{k}$-independent effective strain Hamiltonian, the symmetry properties of the operators of these strain dependent Hamiltonians have to be determined. A complete list of the symmetrized operators is given in App. A.1 and their corresponding parameters in App. A.4.

As in the previous sections, we consider again general Γ^6 bands. The special case of the s-like conduction band can then be easily restored from the general case by ignoring the contributions from the spatial Γ^4-like part of the band.

Considering now the symmetry properties of the strain tensor, there are three possible irreducible representations according to which it transforms: $\mathcal{K}^1_{\boldsymbol{\varepsilon}}$, $\mathcal{K}^3_{\boldsymbol{\varepsilon};\gamma}$ and $\mathcal{K}^5_{\boldsymbol{\varepsilon};\gamma}$. See App. A.4 for their definitions. Hence, independent of their spatial symmetry, both for $\hat{H}_{\mathrm{V}}$ and $\hat{H}_{\mathrm{VI}}$ only operators $\mathcal{O}^{\mu}_{l;\gamma}$ with corresponding symmetry are possible. In order to unify the parameters we thus choose analogously to (3.92) a suited set of parameters $\mathrm{K}^{s;\mu}_{\mathrm{VI};\gamma}$ for the spin-dependent Hamiltonian $\hat{H}_{\mathrm{VI}}$. With the definition of the spin-dependent parameters (3.57) and the orthogonality of the matrices X (3.43), we decompose the parameters $\mathrm{K}^{s;\mu}_{\mathrm{VI};\gamma}$ into a set whose associated parameters $\mathcal{K}^{\mu}_{\boldsymbol{\varepsilon};\gamma}$, transform exclusively on one irreducible representation. Considering, for instance, the parameters $\mathrm{K}^{s;4}_{\mathrm{VI};\gamma}$ with Γ^4 symmetry, such a set reads:

$$\mathrm{K}^{s;4}_{\mathrm{VIa};\gamma} = \mathcal{K}^1_{\boldsymbol{\varepsilon}}\, \mathrm{X}^{44;1}_{1;s\gamma}, \tag{3.131}$$

$$\mathrm{K}^{s;4}_{\mathrm{VIb};\gamma} = \mathcal{K}^3_{\boldsymbol{\varepsilon};\lambda}\, \mathrm{X}^{44;3}_{\lambda;s\gamma}, \tag{3.132}$$

$$\mathrm{K}^{s;4}_{\mathrm{VIc};\gamma} = \mathcal{K}^5_{\boldsymbol{\varepsilon};\lambda}\, \mathrm{X}^{44;5}_{\lambda;s\gamma}. \tag{3.133}$$

In first order perturbation theory only operators that transform according to the irreducible representation Γ^1 or Γ^4 are able to contribute to the Γ^6 band. Keeping in mind this limitation, according to App. A.4 only the operators $\hat{\mathrm{O}}^1_{\mathrm{V}}$, $\hat{\mathrm{O}}^4_{\mathrm{VIa};1}$, $\hat{\mathrm{O}}^4_{\mathrm{VIb};1}$ and $\hat{\mathrm{O}}^4_{\mathrm{VIc};1}$ have to be taken into account for first order perturbation theory. With the further restriction that their corresponding operators $\mathcal{O}^{\mu}_{l;\gamma}$ also have to transform according to Γ^1 or Γ^4, the usage of the decomposition (3.131) becomes obvious and from $\hat{H}_{\mathrm{VI}}$, only the operator $\hat{\mathrm{O}}^4_{\mathrm{VIa};1}$ is able to contribute.

With the known symmetry properties of the operators, all spatial invariants are readily calculated with the help of (3.46) and by re-using the matrices $\mathrm{M}^{66;1}$ (3.80) and $\mathrm{N}^{66;14}$ (3.83), the needed invariants $\mathcal{I}^{66;1}_{\boldsymbol{\varepsilon};ij}$ are obtained. Up to first order, the effective Hamiltonian depending solely on the components of the strain tensor is given by:

$$\hat{\mathcal{H}}^{\boldsymbol{\varepsilon}}_i = \mathcal{I}^{66;1}_{\boldsymbol{\varepsilon};ii}\, \mathcal{K}^1_{\boldsymbol{\varepsilon}} = a_i \mathrm{Tr}\boldsymbol{\varepsilon}, \tag{3.134}$$

where Tr stands for the trace. In the following we will neglect the contribution of $\hat{\mathrm{O}}^4_{\mathrm{VIa};1}$, as it is only relevant for Γ^6 bands where states with spatial symmetry Γ^4 dominate. For a pure s-like conduction band, the hydrostatic strain constant a_c then reads:

$$a_c = \left\langle S \left| \frac{\hat{D}_{xx} + \hat{D}_{yy} + \hat{D}_{zz}}{3} \right| S \right\rangle. \tag{3.135}$$

Note that in literature there is a rather large uncertainty in the magnitude of the value of a_c. Reference [54], and references therein, estimate a_c to be in the range $-18.3 \ldots -6.3\,\mathrm{eV}$. Due to the fact that there is also a hydrostatic strain dependence of the valence bands, one source of uncertainty is associated to common experiments which are merely able to measure the strain dependence of the band gap. Nevertheless, we will stick in the following to the advised value of $a_c = -7.2\,\mathrm{eV}$ of Ref. [54].

Let us now turn to effective Hamiltonians which depend linearly on the components of the strain tensor, as well as linearly on $\mathbf{k}$. There are two possible ways for the generation of this type of effective Hamiltonians. One possibility is first order perturbation theory with respect to the Hamiltonians $\hat{H}_{\mathrm{VII}}$ and $\hat{H}_{\mathrm{VIII}}$. The second source of such terms originates from second order perturbation theory including combinations of the Hamiltonians $\hat{H}_{\mathrm{III}}$ and $\hat{H}_{\mathrm{IV}}$ with $\hat{H}_{\mathrm{V}}$ and $\hat{H}_{\mathrm{VI}}$, respectively.

With the three components of $\mathbf{k}$, and the six independent ones of $\boldsymbol{\varepsilon}$, there are a total of 18 different combinations of $k_i\varepsilon_{jl}$. There are thus also 18 independent components for the parameters $\mathcal{K}^{\mu}_{\mathbf{k}\boldsymbol{\varepsilon};\gamma}$. Regarding the direct product of the irreducible representations $\Gamma^5 \otimes (\Gamma^1 \oplus \Gamma^3 \oplus \Gamma^5) = \Gamma^1 \oplus \Gamma^3 \oplus 2\Gamma^4 \oplus 3\Gamma^5$, there is either one combination transforming according to Γ^1 and Γ^3, two according to Γ^4, and three according to Γ^5. A symmetrized set of these parameters is given in App. A.4.

Regarding again the symmetry limitations discussed above, in first order there are no contributions from the Hamiltonian $\hat{H}_{\mathrm{VII}}$ and the first order terms have to arise due to $\hat{H}_{\mathrm{VIII}}$. The operators of $\hat{H}_{\mathrm{VIII}}$ with matching symmetry are $\hat{\mathrm{O}}^1_{\mathrm{VIII}}$, $\hat{\mathrm{O}}^4_{\mathrm{VIIIa}}$, and $\hat{\mathrm{O}}^4_{\mathrm{VIIIb}}$. Considering their associated

parameters, only $\mathrm{K}^{s;4}_{\mathrm{VIIIb};\gamma}$ possesses the term $\mathcal{K}^{1}_{\mathbf{k}\boldsymbol{\varepsilon}}\mathrm{X}^{44;1}_{1;s\gamma}$. Hence, only the corresponding invariants $\tilde{\mathrm{I}}^{ab;4}_{\mathrm{VIIIb}}$ of $\hat{\mathrm{O}}^{4}_{\mathrm{VIIIb}}$ are able to contribute to the invariant $\mathcal{I}^{66,1}_{\boldsymbol{\varepsilon},ij}$, and the effective Hamiltonian for the $|\Gamma^6_i\rangle$ band is given by:

$$\hat{\mathcal{H}}^{\mathbf{k}\boldsymbol{\varepsilon};1}_{i} = \frac{\mathcal{I}^{66;1}_{\mathbf{k}\boldsymbol{\varepsilon};ii}}{\sqrt{2}}(\varepsilon_{yz}k_x + \varepsilon_{zx}k_y + \varepsilon_{xy}k_z). \tag{3.136}$$

Note, however, that this spin-independent Hamiltonian vanishes for s-like bands, i.e., $\hat{\mathcal{H}}^{\mathbf{k}\boldsymbol{\varepsilon};1}_{c} = 0$.

In first order perturbation theory two more effective Hamiltonians are possible, $\hat{\mathcal{H}}^{\mathbf{k}\boldsymbol{\varepsilon}1;4}_{i}$ and $\hat{\mathcal{H}}^{\mathbf{k}\boldsymbol{\varepsilon}2;4}_{i}$. In the first one,

$$\begin{aligned}\hat{\mathcal{H}}^{\mathbf{k}\boldsymbol{\varepsilon}1;4}_{i} = -\mathcal{I}^{66;4}_{\mathbf{k}\boldsymbol{\varepsilon}1,ii}\,[&(\varepsilon_{zz} - \varepsilon_{yy})k_x\sigma^x \\ &+(\varepsilon_{xx} - \varepsilon_{zz})k_y\sigma^y + (\varepsilon_{yy} - \varepsilon_{xx})k_z\sigma^z]\,,\end{aligned} \tag{3.137}$$

which is proportional to the parameters $\mathcal{K}^{4}_{\mathbf{k}\boldsymbol{\varepsilon}1;\gamma}$, the invariants depend solely on the matrix elements of $\hat{\mathrm{O}}^{4}_{\mathrm{VIIIa}}$ and vanish therefore also for s-like bands. The first non-zero effective Hamiltonian for the s-like conduction band is given by:

$$\begin{aligned}\hat{\mathcal{H}}^{\mathbf{k}\boldsymbol{\varepsilon}2;4}_{c} = \mathcal{I}^{66;4}_{\mathbf{k}\boldsymbol{\varepsilon}2;cc}\,[&(\varepsilon_{xy}k_y - \varepsilon_{zx}k_z)\sigma^x \\ &+(\varepsilon_{yz}k_z - \varepsilon_{xy}k_x)\sigma^y + (\varepsilon_{zx}k_x - \varepsilon_{yz}k_y)\sigma^z]\,.\end{aligned} \tag{3.138}$$

Although this term is non-zero for the s-like conduction band, it depends directly on the matrix elements of the first term of the Hamiltonian $\hat{H}_{\mathrm{VIII}}$ which is assumed to be rather small (see, e.g., Ref.[33]). In recent experiments [56–58], however, both effective Hamiltonians $\hat{\mathcal{H}}^{\mathbf{k}\boldsymbol{\varepsilon}1;4}_{c}$, as well as $\hat{\mathcal{H}}^{\mathbf{k}\boldsymbol{\varepsilon}2;4}_{c}$, have been measured. Thus, first order perturbation theory can not explain these results and the effective Hamiltonians have to arise by second order perturbation theory, which couples the invariants $\mathcal{I}^{\alpha\beta;5}_{\mathbf{k}}$ with those of strain dependent Hamiltonians $\mathcal{I}^{\alpha\beta;\mu}_{\boldsymbol{\varepsilon}}$.

We have already determined above the matrices $\mathrm{M}^{67;5}$ (3.93), $\mathrm{M}^{68;5}$ (3.94), $\mathrm{N}^{67;55}$ (3.99) and $\mathrm{N}^{68;55}$ (3.100) needed for the invariants $\mathcal{I}^{67;5}_{\mathbf{k}}$ and $\mathcal{I}^{68;5}_{\mathbf{k}}$. For the invariants of the strain dependent Hamiltonians more matrices M and N are required. Considering the parameters $\mathcal{K}^{5}_{\boldsymbol{\varepsilon};\lambda}$ of the invariants $\mathcal{I}^{67;5}_{\boldsymbol{\varepsilon}}$ and $\mathcal{I}^{68;5}_{\boldsymbol{\varepsilon}}$, according to App. A.4, there are four possible operators able to contribute: $\mathrm{O}^{2}_{\mathrm{VI}}$, $\mathrm{O}^{3}_{\mathrm{VI}}$, $\mathrm{O}^{4}_{\mathrm{VIc}}$ and $\mathrm{O}^{5}_{\mathrm{VIb}}$. Hence, we need the additional matrices

$$\mathrm{N}^{67;52} = \begin{pmatrix} \sqrt{2} & 0 \\ 0 & -\frac{1}{3}\sqrt{\frac{2}{3}} \end{pmatrix}, \quad \mathrm{N}^{67;53} = \begin{pmatrix} 0 & 0 \\ 0 & \frac{4}{3\sqrt{3}} \end{pmatrix}, \tag{3.139}$$

$$\mathrm{N}^{67;54} = \begin{pmatrix} 0 & 0 \\ 0 & \frac{2\sqrt{2}}{3} \end{pmatrix}, \tag{3.140}$$

as well as

$$\mathrm{N}^{68;52} = \begin{pmatrix} 0 & 0 & 0 \\ 0 & 0 & -\frac{4}{3\sqrt{3}} \end{pmatrix}, \quad \mathrm{N}^{68;53} = \begin{pmatrix} -\sqrt{2} & 0 & 0 \\ 0 & -\sqrt{\frac{2}{3}} & -\frac{1}{3}\sqrt{\frac{2}{3}} \end{pmatrix}, \tag{3.141}$$

and

$$\mathrm{N}^{68;54} = \begin{pmatrix} 0 & -\mathrm{i}\frac{\sqrt{2}}{3} & 0 \\ -1 & -\frac{1}{\sqrt{3}} & -\frac{1}{3} \end{pmatrix}. \tag{3.142}$$

For the coupling of bands with Γ^6 symmetry to bands with Γ^8 symmetry there are also invariants of the type $\mathcal{I}_{\boldsymbol{\varepsilon}}^{68;3}$ possible. For a coupling due to $\mathrm{O}_{\mathrm{V}}^3$, we need further the matrices

$$\mathrm{M}^{68;3} = \begin{pmatrix} \sqrt{2} & 0 & 0 \\ 0 & -\sqrt{\frac{2}{3}} & \sqrt{\frac{2}{3}} \end{pmatrix}, \tag{3.143}$$

and with a similar reasoning as above the matrices

$$\mathrm{N}^{68;34} = \begin{pmatrix} 0 & \sqrt{2} & 0 \\ -1 & -\frac{\mathrm{i}}{\sqrt{3}} & \mathrm{i} \end{pmatrix}, \quad \mathrm{N}^{68;35} = \begin{pmatrix} 0 & 0 & -\sqrt{2} \\ -1 & \mathrm{i} & -\frac{\mathrm{i}}{\sqrt{3}} \end{pmatrix}, \tag{3.144}$$

due to the coupling to $\mathrm{O}_{\mathrm{VIb}}^4$ and $\mathrm{O}_{\mathrm{VIa}}^5$.

With all these matrices we are finally able to calculate the invariants $\mathcal{I}_{\boldsymbol{\varepsilon}}^{67;4}$, $\mathcal{I}_{\boldsymbol{\varepsilon}}^{68;3}$ and $\mathcal{I}_{\boldsymbol{\varepsilon}}^{68;5}$. In second order perturbation we obtain again two effective Hamiltonians of the type (3.137) and (3.138):

$$\begin{aligned} \hat{\mathcal{H}}_i^{\mathbf{k}\boldsymbol{\varepsilon}1;4} = D_{ii} \,[&(\varepsilon_{zz} - \varepsilon_{yy})k_x\sigma^x \\ &+(\varepsilon_{xx} - \varepsilon_{zz})k_y\sigma^y + (\varepsilon_{yy} - \varepsilon_{xx})k_z\sigma^z]\,, \end{aligned} \tag{3.145}$$

and

$$\begin{aligned} \hat{\mathcal{H}}_i^{\mathbf{k}\boldsymbol{\varepsilon}2;4} = \frac{C_{ii}}{2} \,[&(\varepsilon_{xy}k_y - \varepsilon_{zx}k_z)\sigma^x \\ &+(\varepsilon_{yz}k_z - \varepsilon_{xy}k_x)\sigma^y + (\varepsilon_{zx}k_x - \varepsilon_{yz}k_y)\sigma^z]\,, \end{aligned} \tag{3.146}$$

where we defined the coupling parameters D_{ii} and C_{ii} analogously to Ref. [56–58].

The second order contribution to D_{ii} arises from the coupling between the invariants $\mathcal{I}^{68;3}_{\boldsymbol{\varepsilon};ij}$, with those of $\mathcal{I}^{68;5}_{\mathbf{k};ij}$. The material constant D_{ii}, again generalized for arbitrary Γ^6 bands, then reads:

$$D_{ii} = -\mathcal{I}^{66;4}_{\mathbf{k}\boldsymbol{\varepsilon}1;ii} + \frac{1}{2\sqrt{2}} \sum_j \frac{\mathcal{I}^{68;5}_{\mathbf{k};ij}\mathcal{I}^{86;3}_{\boldsymbol{\varepsilon};ji} + \mathcal{I}^{68;3}_{\boldsymbol{\varepsilon};ij}\mathcal{I}^{86;5}_{\mathbf{k};ji}}{E_{6;i} - E_{8;j}}. \tag{3.147}$$

The coupling of the invariants $\mathcal{I}^{6\beta;5}_{\boldsymbol{\varepsilon};ij}$ with the invariants $\mathcal{I}^{6\beta;5}_{\mathbf{k};ij}$ leads, analogous to the derivation of the effective g-factor, eventually to the second generalized constant:

$$\begin{aligned} C_{3,ii} = 2\mathcal{I}^{66;4}_{\mathbf{k}\boldsymbol{\varepsilon}2;ii} + \mathrm{i} \sum_j \Bigg(& \frac{\mathcal{I}^{67;5}_{\mathbf{k};ij}\mathcal{I}^{76;5}_{\boldsymbol{\varepsilon};ji} - \mathcal{I}^{67;5}_{\boldsymbol{\varepsilon};ij}\mathcal{I}^{76;5}_{\mathbf{k};ji}}{E_{6;i} - E_{7;j}} \\ & - \frac{1}{2} \frac{\mathcal{I}^{68;5}_{\mathbf{k};ij}\mathcal{I}^{86;5}_{\boldsymbol{\varepsilon};ji} - \mathcal{I}^{68;5}_{\boldsymbol{\varepsilon};ij}\mathcal{I}^{86;5}_{\mathbf{k};ji}}{E_{6;i} - E_{8;j}} \Bigg) \end{aligned} \tag{3.148}$$

From the general expression (3.147) for arbitrary bands, the material constant $D = D_{cc}$ of the s-like conduction band can again be obtained by considering only the invariants which couple to bands with spatial Γ^1 symmetry. The only invariant that fulfils this requirement, and is able to couple to the invariants of $\mathcal{I}^{68;5}_{\mathbf{k};cj}$ is $\mathcal{I}^{68,3}_{\boldsymbol{\varepsilon},cj} = -\sqrt{2}\tilde{\mathrm{I}}^{15;5}_{\mathrm{VIa};cj}$. This invariant depends, however, directly on the first term of $\hat{H}_{\mathrm{VI}}$ (3.28). In previous calculations of Ref. [33, 34, 59], this term is neglected. Nevertheless the experiments of Ref. [56–58, 60] contradict the assumption that this term is small and can be ignored. In the following we will stick to Ref. [56] and assume for the conduction band a value of $D = 6.6 \cdot 10^{-12}\, e\mathrm{Vm}$, whereas for the constant $C_3 = C_{3,cc}$ we take the value of Ref. [61], $C_3 = 8.1 \cdot 10^{-10}\, e\mathrm{Vm}$.

3.5. Electrons in two-dimensional systems

So far, all our considerations to effective Hamiltonians were related to three-dimensional bulk materials, where we exploited the symmetry of the crystal to derive effective Hamiltonians. Furthermore, we focused only on the operators acting on the Bloch functions $u_{n0\sigma}$ (3.3) and regarded $\mathbf{k}$ as a parameter. As $\mathbf{k}$ is also an operator acting on the envelope functions (see Sec. 3.1.1), for spatial inhomogeneous external potentials some care is needed since $\mathbf{r}$ of the external potential $V(\mathbf{r})$ is also an operator, and $\mathbf{k}$ and $\mathbf{r}$ do not commute. An external potential is, however, not the only possibility to incorporate a spatial inhomogeneity.

With the help of molecular beam epitaxy, a thin layer of, e.g., GaAs can be grown between a material with larger band gap, say AlGaAs. This results in a spatial dependence of the band edge energies (see Fig. 3.7). If the difference between these band gaps is sufficiently large, the carriers, in particular the electrons of the conduction band, are trapped within this thin layer and form a quasi two-dimensional quantum system. Such a thin layer is therefore called quantum well (QW).

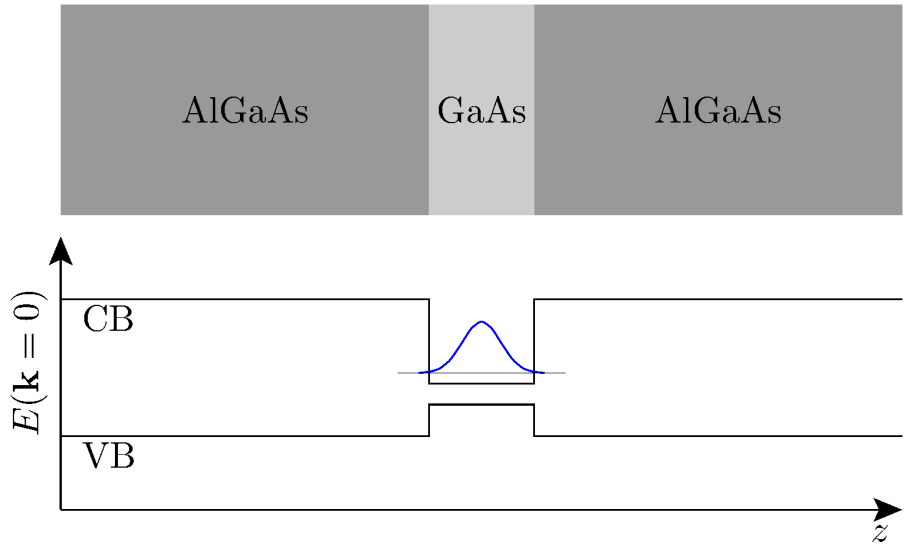

Figure 3.7.: Sketch of a quantum well. The band edge energies $E_n(=\mathbf{0})$ of the conduction and the valence band depend on the z-coordinate in a quantum well.

Discontinuous parameters are not included in the envelope function approximation which assumes a spatially homogeneous material. The transition from one material to another has a direct influence on the Bloch functions $u_{n0\sigma}(\mathbf{r})$, which incorporate all material specific quantities within the $\mathbf{k}\cdot\mathbf{p}$ theory. Nevertheless, the thickness of typical quantum wells is in the range of $\sim 15-50$ nm and consists therefore of about $\sim 30-100$ atomic layers. Thus, by neglecting surface effects, one can still assume that the Bloch functions $u_{n0\sigma}$ in the quantum well remain unchanged compared to the ones of the bulk material. The envelope function approximation is then still justified and the discontinuity at the interfaces is taken into account by an external potential $V(z)$ (Fig. 3.7).

The step-like change of the potential at the interface has to be regarded by boundary conditions. In the following, we will consider only

2D systems where the depth of the quantum well of the conduction band $E_{\text{Barrier}}(0) - E_{\text{QW}}(0)$ is much larger than the energies of the electrons. Hence we approximate the potential $V(z)$ by a QW with infinitely deep barriers. We assume furthermore that the energy $E \approx \hbar^2 \langle k_z^2 \rangle / (2m_c) = (\hbar^2 \pi / d_{\text{eff}})^2 / (2m_c)$ of the ground state of the QW, with effective thickness d_{eff}, is much smaller than the fundamental band gap E_0, however, still larger than all in-plane contributions to the energy of the electrons. Hence, higher states are not excited and the quantum well remains in the ground state. The results from three-dimensional bulk materials derived in the previous sections then still apply, and all quantities such as the effective mass are unchanged. In this simple system we can easily obtain the two-dimensional effective Hamiltonian from the three dimensional one, by replacing

$$k_z^2 \longrightarrow \langle k_z^2 \rangle = \left(\frac{\pi}{d_{\text{eff}}} \right)^2 , \tag{3.149}$$

and

$$k_z^n \longrightarrow \langle k_z^n \rangle = 0, \tag{3.150}$$

for all odd numbers n. Note that all previous results of the zinc blende structure have been derived in the coordinate system $\hat{e}_x \parallel [100], \hat{e}_y \parallel [010]$ and $\hat{e}_z \parallel [001]$. For quantum wells in planes distinct from the (001)-plane, one therefore has to rotate the z-axis to be perpendicular to the plane before carrying out the replacements (3.149) and (3.150).

	(001)QW	(110)QW	(111)QW
$x-$axis	$[110]$	$[001]$	$[11\bar{2}]$
$y-$axis	$[\bar{1}10]$	$[1\bar{1}0]$	$[\bar{1}10]$
$z-$axis	$[001]$	$[110]$	$[111]$

Table 3.5.: Table of commonly used coordinate systems for (001), (110) and (111) quantum wells [22, 27, 62–64] (see Table 3.5.

Therefore, the effective Dresselhaus Hamiltonian depends strongly on the growth direction of the quantum well. For often used quantum wells and their corresponding coordinate systems (see Tab. 3.5) the approxi-

mated effective Dresselhaus Hamiltonians in a 2D quantum system read:

$$H^D_{(001)} = \beta\hbar(k_y\sigma^x + k_x\sigma^y), \tag{3.151}$$

$$H^D_{(110)} = -\frac{1}{2}\beta\hbar k_y\sigma^z, \tag{3.152}$$

$$H^D_{(111)} = \frac{2}{\sqrt{3}}\beta\hbar(k_y\sigma^x - k_x\sigma^y), \tag{3.153}$$

where we utilized the abbreviation $\beta \equiv \lambda_{cc}(\pi/d_{\text{eff}})^2/\hbar$, known as Dresselhaus parameter. In this approximation only terms linear in $\mathbf{k}$ are possible. Qualitatively similar terms could have been also derived by considering the corresponding two-dimensional symmetry group of the plane (D_{2d}, e.g., for a symmetric (001) QW), instead of the three-dimensional symmetry group T_d of the tetrahedron. Nevertheless, for the quantum wells considered here, such an approach leads to different coupling constants, i.e., β, D, C_3. Hence, in order to obtain the correct ones, the three-dimensional symmetry group T_d has to be taken into account.

The strong dependence on the growth direction of the quantum well also influences the two additional effective Hamiltonians (3.145), and (3.146) which cause a spin-splitting of the conduction band by including strain. Their corresponding two-dimensional expressions can be derived in the same way as we obtained the various Dresselhaus terms above. In this work we will discuss only the two-dimensional electron gas of a (001) quantum well. From Chap. 2 we already know that in this (001) plane, surface acoustic waves are most efficiently excited in [110] and [$\bar{1}$10] direction, respectively. We will thus stick to the coordinate system of Tab. 3.5, i.e., $\hat{e}_x \parallel [110]$. The strain dependent Hamiltonians of the quantum well are then

$$H^{\mathbf{k}\boldsymbol{\varepsilon}1} = -D\left[\frac{2\varepsilon_{zz} - \varepsilon_{xx} - \varepsilon_{yy}}{2}(k_y\sigma^x + k_x\sigma^y) + \varepsilon_{xy}(k_x\sigma^x + k_y\sigma^y)\right], \tag{3.154}$$

and

$$H^{\mathbf{k}\boldsymbol{\varepsilon}2} = \frac{C_3}{2}\left[\frac{\varepsilon_{xx} - \varepsilon_{yy}}{2}(k_y\sigma^x - k_x\sigma^y) - (k_x\varepsilon_{yz} + k_y\varepsilon_{zx})\sigma^z\right]. \tag{3.155}$$

Note that in a quantum well the Dresselhaus Hamiltonian, together with (3.154) and (3.155), are all feasible effective Hamiltonians of the bulk that depend linearly on the momentum operator $\mathbf{k}$ and possibly strain.

Nevertheless, due to the confinement of the electrons into the two-dimensional system of the QW, there exists a further effective Hamiltonian causing a spin-splitting of the conduction band. This effective Hamiltonian

$$H_{ii}^{R} = r_{ii}\mathbf{k} \times \boldsymbol{\mathcal{E}} \cdot \boldsymbol{\sigma} \tag{3.156}$$

is called Rashba term. So far, we have only discussed quantum wells whose barriers consist of the same material. Changing, e.g., the amount x of aluminium in $Al_xGa_{1-x}As$, the fundamental band gap is also changed. Due to such an asymmetric setup the electrons in the well are susceptible to an effective asymmetric potential $V(z)$ in the quantum well (see Fig. 3.8). Alternatively to changing the material of the barriers, one could also

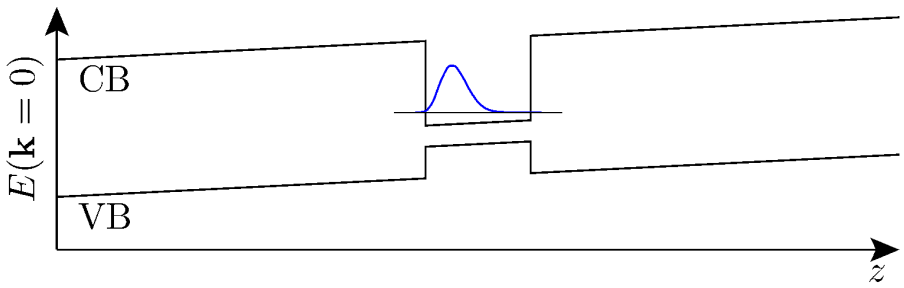

Figure 3.8.: Sketch of a quantum well in an asymmetric potential.

have achieved the same effect by applying an external electric field. As the Dresselhaus spin-orbit coupling has its origin in the lack of inversion symmetry of the crystal, it is often called bulk inversion asymmetry (BIA). In contrast, the Rashba term can only arise due to an asymmetric potential of the surrounding structure and is thus called structure inversion asymmetry (SIA).

The components of the operator $\mathbf{k}$ do not commute with this potential (see (3.13)). Nevertheless, Löwdin perturbation theory is also able to cope with non-commuting parameters and the external potential can be treated as an additional perturbation.

Since $V(z)$ has no off-diagonal matrix elements, the first contribution arises within third order perturbation theory (see App. B). Using again the invariant matrices we derived above, the material constant r_{ii} of the Rashba term reads:

$$r_{ii} = -\frac{e}{2}\sum_{j}\left(\frac{\mathcal{I}_{\mathbf{k};ij}^{67;5}\mathcal{I}_{\mathbf{k};ji}^{76;5}}{(E_{6;i}-E_{7;j})^2} - \frac{1}{2}\frac{\mathcal{I}_{\mathbf{k};ij}^{68;5}\mathcal{I}_{\mathbf{k};ji}^{86;5}}{(E_{6;i}-E_{8;j})^2}\right). \tag{3.157}$$

For the Γ^6 conduction band within the 14×14 Kane model it can be approximated by:

$$\begin{aligned} r_{cc}^K =& \frac{e|P|^2}{3}\left(\frac{1}{E_0^2} - \frac{1}{(E_0+\Delta_0)^2}\right) \\ & - \frac{e|P'|^2}{3}\left(\frac{1}{(E_0-E_0')^2} - \frac{1}{(E_0-E_0'-\Delta_0')^2}\right) \end{aligned} \tag{3.158}$$

Inserting the parameters of Tab. 3.3, for GaAs we obtain a value of $r_{cc}^K = 5.2\, e\mathring{A}^2$.

Since the Rashba term is independent of the symmetries of the bulk material and is subjected only to the structure of the system, the form of the Rashba Hamiltonian remains the same for all growth directions of the quantum well. Moreover, keeping the convention of $\hat{e}_z$ to be parallel to the growth direction, the carriers are exposed to an effective electric field $\langle \mathcal{E}_z \rangle$, perpendicular to the quantum well. Note that in order to be consistent with the Ehrenfest theorem, which implies $\langle \mathcal{E}_z \rangle = 0$ for a bound state, the effective field arises mainly by the asymmetry of the potential of the valence band [65]. The Hamiltonian of the Rashba spin-orbit interaction then reads:

$$H^R = \alpha\hbar\left(k_y\sigma^x - k_x\sigma^y\right), \tag{3.159}$$

where $\alpha = r_{cc}\langle \mathcal{E}_z \rangle / \hbar$ combines the material-specific constant r_{cc} with the structure dependent effective electric field.

Analogously to the structure inversion asymmetry, the out-of-plane component of the induced piezoelectric field E_z leads (2.56) to an additional contribution to the Rashba spin-orbit interaction:

$$H_{\mathrm{SAW}}^R = r_{cc}E_z\left(k_y\sigma^x - k_x\sigma^y\right). \tag{3.160}$$

In contrast to the Rashba term (3.159) this term depends, however, on the strength of the SAW.

4. Quasiclassical transport theory

The effective Hamiltonians discussed in Chap. 3 are able to describe electrons and holes in a perfect crystal structure with external electromagnetic fields as well as in a strained crystal environment. We were particularly interested in the distinct spin-orbit interaction mechanisms, which arise due to strain or piezoelectric fields generated by a SAW in a two-dimensional surrounding. We therefore considered such a specific kind of spatio-temporal deformation and its accompanying piezoelectric field in detail in Chap. 2.

The major advantage of the description of electrons and holes by effective Hamiltonians is their similarity to Hamiltonians of free particles in external fields. Within the $\mathbf{k}\cdot\mathbf{p}$ theory the complete influence of the crystal potential $V_0(\mathbf{r})$ on the charge carriers is absorbed in parameters like the effective mass (3.107) or the Dresselhaus constant (3.130). Moreover, due to the envelope function approximation, the operator $\hbar\mathbf{k}$ of the effective Hamiltonians takes over the role of the momentum operator. Since in the following there is no danger of confusion with the operator $\mathbf{p}$ of the $\mathbf{k}\cdot\mathbf{p}$ theory, we will rename $\hbar\mathbf{k}$ to $\mathbf{p}$ throughout this chapter.

So far we considered only single electrons. Our focus, however, will be on experimental situations with a large number of charge carriers. A quantum statistical description is therefore inevitable. In the two-dimensional quantum well systems we have in mind, the motion of the carriers as well as their spin dynamics is governed by a space and time-dependent surface acoustic wave. Hence, the statistical mechanics of the system we are dealing with is out of equilibrium. To cope with this task, we will therefore introduce in the following the basic concepts of a quasiclassical transport theory. Specifically, within the real-time formulation, the Keldysh technique [66] is capable of dealing with non-equilibrium situations.

In practice, due to imperfections of the lattice such as impurity atoms, vacancies due to missing atoms, etc., the assumption of a perfect crystal structure is hardly sustainable. Within quasiclassical transport theory such imperfections can furthermore be taken into account by an additional

random potential $V_{\text{imp}}(\mathbf{r})$.

In this rather technical chapter we will mainly follow the lines of [67–70]. For more details we recommend the interested reader to the quite extensive literature (see, e.g., [71–82]).

4.1. Many-particle systems

The systems we have in mind are two-dimensional disordered electron gases in a quantum well under an external perturbation of a SAW. Hence, we will consider only electrons in the Γ_c^6 conduction band and drop henceforth all previously introduced band indices. As we argued in Sec. 3.5, in two-dimensional systems the Dresselhaus Hamiltonian $\hat{H}^D$ depends only linearly on the momentum. This linear dependency is shared by the Rashba Hamiltonian $\hat{H}^R$, as well as the Hamiltonians $\hat{H}^{\mathtt{k}\boldsymbol{\varepsilon}1}$ and $\hat{H}^{\mathtt{k}\boldsymbol{\varepsilon}2}$ of the strain-dependent spin-orbit coupling. The Hamiltonian can thus be rewritten as

$$\hat{H} = \frac{\mathbf{p}^2}{2m} - e\Phi(\mathbf{r},t) + \hat{H}_{\text{s.o.}} + \hat{H}^{(i)}, \tag{4.1}$$

where m denotes the effective mass of the electron in the conduction band, and $\Phi(\mathbf{r},t)$ the piezoelectric potential (2.45) generated by a SAW. $\hat{H}^{(i)}$ stands for a general Hamiltonian representing possible interactions. Although the concepts of quasiclassical transport theory are very powerful and capable to describe interactions of electrons with electrons, impurities or phonons, here, we will only consider in detail the interaction with impurities. The Hamiltonian of the spin-orbit interaction can be expressed as

$$\hat{H}_{\text{s.o.}} = \frac{p_i \mathcal{A}_i^a(\mathbf{r},t)\sigma^a}{2m}, \tag{4.2}$$

where the $SU(2)$ vector potential $\boldsymbol{\mathcal{A}}(\mathbf{r},t)$ incorporates all parameters of the spin-orbit Hamiltonians involved. For the Rashba spin-orbit coupling (3.159), for example, the non-vanishing components of the $SU(2)$ vector potential read $(\mathcal{A}^R)_y^x = -(\mathcal{A}^R)_x^y = 2m\alpha$.

Let us now consider a system of N electrons. The single-particle Hamiltonians then act on each electron independently $\hat{H}_1 \otimes \hat{H}_2 \otimes \ldots \otimes \hat{H}_N$ and the N-particle state space is spanned by the tensor product of N single particle states. Using for example states in spatial representation, an orthonormal basis in the N-particle state space reads:

$$|\mathbf{r}_{P_1}\rangle \otimes |\mathbf{r}_{P_2}\rangle \otimes \cdots \otimes |\mathbf{r}_{P_N}\rangle\,. \tag{4.3}$$

Since the particles in our system – say electrons – are an assembly of indistinguishable fermions, only states which are antisymmetric with respect to interchanging two of them are possible. Denoting ζ_P the number of transitions necessary for the permutation P, a completely antisymmetrized N-particle states reads:

$$|\mathbf{r}_1 \wedge \mathbf{r}_2 \wedge \ldots \wedge \mathbf{r}_N\rangle \equiv \frac{1}{\sqrt{N!}} \sum_P (-1)^{\zeta_P} |\mathbf{r}_{P_1}\rangle \otimes |\mathbf{r}_{P_2}\rangle \otimes \cdots \otimes |\mathbf{r}_{P_N}\rangle . \quad (4.4)$$

A convenient tool for the quantum statistics of identical particles is the quantum field theory, hence we introduce the fermion creation field operator

$$\Psi^\dagger(\mathbf{r}) |\mathbf{r}_1 \wedge \mathbf{r}_2 \wedge \ldots \wedge \mathbf{r}_N\rangle \equiv |\mathbf{r} \wedge \mathbf{r}_1 \wedge \mathbf{r}_2 \wedge \ldots \wedge \mathbf{r}_N\rangle , \quad (4.5)$$

which creates an additional fermion and augments the antisymmetrized N-particle state by the state $|\mathbf{r}\rangle$. Analogously, the annihilation field operator

$$\Psi(\mathbf{r}) |\mathbf{r}_1 \wedge \mathbf{r}_2 \wedge \ldots \wedge \mathbf{r}_N\rangle \equiv \sum_{n=1}^{N} (-1)^{n-1} \langle \mathbf{r}|\mathbf{r}_n\rangle |\mathbf{r}_1 \wedge \ldots (\text{no } \mathbf{r}_n) \ldots \wedge \mathbf{r}_N\rangle \quad (4.6)$$

removes a fermion from the N-particle state $|\mathbf{r}\rangle$, if it is occupied by any of them. Otherwise the zero vector $|0\rangle$ is obtained. As a consequence of these definitions, the fundamental anti-commutation relations

$$\Psi(\mathbf{r})\Psi^\dagger(\mathbf{r}') + \Psi^\dagger(\mathbf{r}')\Psi(\mathbf{r}) \equiv \{\Psi(\mathbf{r}), \Psi^\dagger(\mathbf{r}')\} = \delta(\mathbf{r} - \mathbf{r}') \quad (4.7)$$

and

$$\{\Psi(\mathbf{r}), \Psi(\mathbf{r}')\} = \{\Psi^\dagger(\mathbf{r}), \Psi^\dagger(\mathbf{r}')\} = 0 \quad (4.8)$$

follow. Moreover, by a consecutive application of the creation field operator on the vacuum state, one finds the antisymmetrized N-particle state

$$\Psi^\dagger(\mathbf{r}_1)\Psi^\dagger(\mathbf{r}_2) \cdots \Psi^\dagger(\mathbf{r}_N) |0\rangle = |\mathbf{r}_1 \wedge \mathbf{r}_2 \wedge \ldots \wedge \mathbf{r}_N\rangle . \quad (4.9)$$

Beyond the creation and annihilation of fermions, the field operators can also be employed for the representation of operators in the many-particle space. This becomes apparent by considering an arbitrary one-particle operator in spatial representation:

$$\hat{F}^{(1)} = \int \mathrm{d}\mathbf{r} \int \mathrm{d}\mathbf{r}' \, \langle \mathbf{r}|\hat{F}^{(1)}|\mathbf{r}'\rangle |\mathbf{r}\rangle \langle \mathbf{r}'| . \quad (4.10)$$

In the words of quantum field theory, the one-particle operator removes the particle in the state $\langle \mathbf{r}'|$, and recreates one in the state $|\mathbf{r}\rangle$. Hence, in the N-particle space the corresponding operator $\hat{F}$ is given by:

$$\hat{\mathcal{F}}^{(1)} = \int \mathrm{d}\mathbf{r} \int \mathrm{d}\mathbf{r}' \, \langle \mathbf{r}|\hat{F}^{(1)}|\mathbf{r}'\rangle \, \Psi^\dagger(\mathbf{r})\Psi(\mathbf{r}'). \tag{4.11}$$

The index (1) indicates that such an operator, although it operates on the N-particle state space, is still a single-particle operator which acts on each electron independently. We also introduced the notation of calligraphic symbols for operators in the many-body basis ($\hat{F} \leftrightarrow \hat{\mathcal{F}}$). For an interaction between particles, a two-body operator is needed. For an instantaneous interaction with a potential $V^{(2)}(\mathbf{r}, \mathbf{r}')$ it is represented by the two particle operator

$$\hat{\mathcal{V}}^{(2)} = \frac{1}{2} \int \mathrm{d}\mathbf{r} \int \mathrm{d}\mathbf{r}' \Psi^\dagger(\mathbf{r})\Psi^\dagger(\mathbf{r}')V^{(2)}(\mathbf{r}, \mathbf{r}')\Psi(\mathbf{r}')\Psi(\mathbf{r}). \tag{4.12}$$

Before we turn to the dynamics of operators, we introduce the statistical operator in the canonical ensemble

$$\rho = \frac{\mathrm{e}^{-\beta\hat{\mathcal{H}}}}{\mathrm{Tr}\left[\mathrm{e}^{-\beta\hat{\mathcal{H}}}\right]}, \tag{4.13}$$

where Tr denotes the trace in the multi-particle space and $\beta = 1/k_B T$ (k_B is the Boltzmann constant). With the help of the statistical operator, one obtains observables of a temperature dependent system by averaging according to

$$\langle \mathcal{O} \rangle = \mathrm{Tr}\left[\rho\mathcal{O}\right] = \frac{\mathrm{Tr}\left[\mathrm{e}^{-\beta\hat{\mathcal{H}}}\mathcal{O}\right]}{\mathrm{Tr}\left[\mathrm{e}^{-\beta\hat{\mathcal{H}}}\right]}. \tag{4.14}$$

In systems, where the number of particles is not fixed, the grand canonical ensemble is more convenient and one has to replace $\hat{\mathcal{H}} \to \hat{\mathcal{H}} - \mu N$. The single-particle energies are then measured relative to their chemical potential μ.

Let us now turn to the dynamics of our system. Having time-dependent perturbation theory in mind, needed for the description of the non-equilibrium system under consideration, we subdivide the single-particle part of the Hamiltonian (4.1) into two parts – a time-dependent and a time-independent

one. Using (4.11), the first one is the Hamiltonian of a free particle together with Rashba and Dresselhaus spin-orbit interaction:

$$\begin{aligned}\hat{\mathcal{H}}_0 &= \int \mathrm{d}\mathbf{r}\Psi^\dagger(\mathbf{r})\left[-\frac{\hbar^2}{2m}\Delta - \mathrm{i}\frac{\hbar(\mathcal{A}^{R+D})_i^a\sigma^a}{2m}\nabla\right]\Psi(\mathbf{r}) \\ &\equiv \int \mathrm{d}\mathbf{r}\Psi^\dagger(\mathbf{r})h_0(\mathbf{r})\Psi(\mathbf{r}).\end{aligned} \tag{4.15}$$

The second one carries time-dependent spin-orbit interactions as well as the potential generated by the SAW:

$$\begin{aligned}\hat{\mathcal{H}}'(t) &= \int \mathrm{d}\mathbf{r}\Psi^\dagger(\mathbf{r})\left[-\mathrm{i}\frac{\hbar(\mathcal{A}^{\boldsymbol{\varepsilon}})_i^a(\mathbf{r},t)\sigma^a}{2m}\nabla - e\Phi(\mathbf{r},t)\right]\Psi(\mathbf{r}) \\ &\equiv \int \mathrm{d}\mathbf{r}\Psi^\dagger(\mathbf{r})h'(\mathbf{r},t)\Psi(\mathbf{r}).\end{aligned} \tag{4.16}$$

We further assume that the SAW is turned on at a time t_0 ($\hat{\mathcal{H}}'(t<t_0)=0$). The complete Hamiltonian is then the sum of $\hat{\mathcal{H}}(t)=\hat{\mathcal{H}}_0+\hat{\mathcal{H}}'(t)+\hat{\mathcal{H}}^{(i)}(t)$.

These separations open now the way to a very convenient formulation of perturbation theory, the closed time path formalism. We start with the time-dependence of an arbitrary operator $\mathcal{O}$, which in the Heisenberg picture reads

$$\mathcal{O}_{\hat{\mathcal{H}}}(t) = \mathcal{U}^\dagger_{\hat{\mathcal{H}}}(t,t_0)\mathcal{O}(t_0)\mathcal{U}_{\hat{\mathcal{H}}}(t,t_0), \tag{4.17}$$

with

$$\mathcal{U}_{\hat{\mathcal{H}}}(t,t_0) \equiv T\left\{\exp\left(-\frac{\mathrm{i}}{\hbar}\int_{t_0}^{t}\mathrm{d}t'\,\hat{\mathcal{H}}(t')\right)\right\}, \tag{4.18}$$

where we introduced the usual time ordering

$$T\{A(t_1)B(t_2)\} = \begin{cases} A(t_1)B(t_2) & \text{for} \quad t_1 > t_2 \\ B(t_2)A(t_1) & \text{for} \quad t_2 > t_1 \end{cases} \tag{4.19}$$

Due to the properties of time ordering, the unitary operator $\mathcal{U}_{\hat{H}}(t,t_0)$ can be factorized into

$$\mathcal{U}_{\hat{\mathcal{H}}}(t,t_0) = \mathcal{U}_{\hat{\mathcal{H}}_0}(t,t_0)\mathcal{S}'(t,t_0)\mathcal{S}^{(i)}(t,t_0), \tag{4.20}$$

where

$$\mathcal{U}_{\hat{\mathcal{H}}_0}(t,t_0) = \mathrm{e}^{-\frac{\mathrm{i}}{\hbar}\hat{\mathcal{H}}_0(t-t_0)} \tag{4.21}$$

$$\mathcal{S}'(t,t_0) = T\left\{\exp\left(-\frac{\mathrm{i}}{\hbar}\int_{t_0}^{t}\mathrm{d}t'\,\hat{\mathcal{H}}'_{\hat{H}_0}(t')\right)\right\} \tag{4.22}$$

$$\mathcal{S}^{(i)}(t,t_0) = T\left\{\exp\left(-\frac{\mathrm{i}}{\hbar}\int_{t_0}^{t}\mathrm{d}t'\,\hat{\mathcal{H}}^{(i)}_{\hat{H}_0}(t')\right)\right\}. \tag{4.23}$$

Hence, the time-dependence be rewritten as

$$\begin{aligned}\mathcal{O}_{\hat{\mathcal{H}}}(t) &= {\mathcal{S}^{(i)}}^{\dagger}(t,t_0){\mathcal{S}'}^{\dagger}(t,t_0)\mathcal{O}_{\hat{\mathcal{H}}_0}(t)\mathcal{S}'(t,t_0)\mathcal{S}^{(i)}(t,t_0)\\ &= T_c\left\{\mathrm{e}^{-\frac{\mathrm{i}}{\hbar}\int_c \mathrm{d}\tau\,(\hat{\mathcal{H}}'_{\hat{H}_0}(\tau)+\hat{\mathcal{H}}^{(i)}_{\hat{\mathcal{H}}_0}(\tau))}\mathcal{O}_{\hat{\mathcal{H}}_0}(t)\right\},\end{aligned} \tag{4.24}$$

where the contour ordering symbol T_c orders operators along the closed time path contour c depicted in Fig. 4.1. Similarly to the usual time ordering, T_c orders operators with earlier contour time τ to the right. The contour runs on the real axis from t_0 to t and back again.

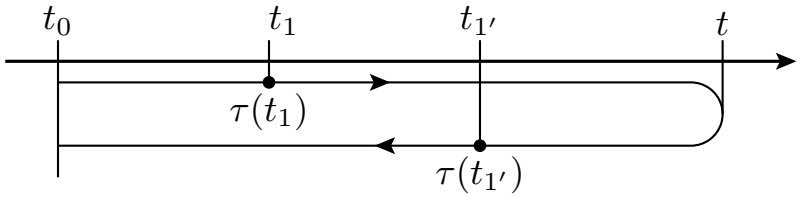

Figure 4.1.: Closed time contour c

Remembering the definitions of the Hamiltonians (4.15) and (4.16), an expansion of the exponential function of (4.24) evidently generates a string of time-dependent field operators. We are thus led to study the behaviour of the field operators under contour ordering, which leads us to the definition of the closed time path Green's function in the next section.

4.2. Green's functions and Keldysh formalism

Before we define the contour-ordered Green's function we start with some remarks concerning products of contour-ordered operators. The Green's functions we will consider later on, consist of a product of a field creation

and a field annihilation operator. From (4.24), their time-dependence is simply given by the contour-ordered expression

$$\Psi_{\hat{\mathcal{H}}}(\mathbf{r}_1,t_1) = T_{c_1}\left\{\mathrm{e}^{-\frac{\mathrm{i}}{\hbar}\int_{c_1}\mathrm{d}\tau\,(\hat{\mathcal{H}}'_{\hat{\mathcal{H}}_0}(\tau)+\hat{\mathcal{H}}^{(i)}_{\hat{\mathcal{H}}_0}(\tau))}\Psi_{\hat{\mathcal{H}}_0}(\mathbf{r}_1,t_1)\right\}, \tag{4.25}$$

$$\Psi^\dagger_{\hat{\mathcal{H}}}(\mathbf{r}_{1'},t_{1'}) = T_{c_2}\left\{\mathrm{e}^{-\frac{\mathrm{i}}{\hbar}\int_{c_2}\mathrm{d}\tau\,(\hat{\mathcal{H}}'_{\hat{\mathcal{H}}_0}(\tau)+\hat{\mathcal{H}}^{(i)}_{\hat{\mathcal{H}}_0}(\tau))}\Psi^\dagger_{\hat{\mathcal{H}}_0}(\mathbf{r}_{1'},t_{1'})\right\}, \tag{4.26}$$

where both contours start at t_0. Their turning point is, however, at different times t_1 and $t_{1'}$. As indicated in Fig. 4.2, the first contour c_1 can be joined with the second c_2 into a new contour with starting point still at t_0 and a returning point at the maximum of $\{t_1,t_{1'}\}$. The product of the time-dependent field operators is thus

$$\Psi_{\hat{\mathcal{H}}}(1)\Psi^\dagger_{\hat{\mathcal{H}}}(1') = T_{c_1+c_2}\left\{\mathrm{e}^{-\frac{\mathrm{i}}{\hbar}\int_{c_1+c_2}\mathrm{d}\tau\,(\hat{\mathcal{H}}'_{\hat{\mathcal{H}}_0}(\tau)+\hat{\mathcal{H}}^{(i)}_{\hat{\mathcal{H}}_0}(\tau))}\Psi_{\hat{\mathcal{H}}_0}(1)\Psi^\dagger_{\hat{\mathcal{H}}_0}(1')\right\}, \tag{4.27}$$

where we introduced the abbreviation $1=(\mathbf{r}_1,t_1)$.

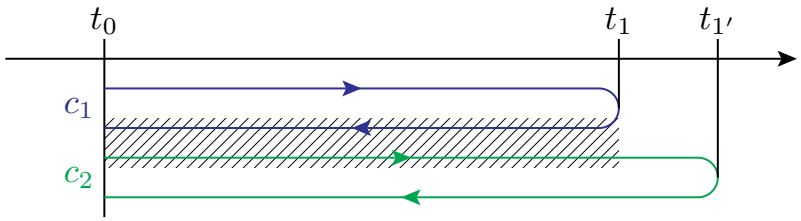

Figure 4.2.: Overlapping parts of the contour cancel each other.

Now we are able to define the contour-ordered Green's function

$$G(1,1') = -\mathrm{i}\frac{\mathrm{Tr}\left[\mathrm{e}^{-\beta\hat{\mathcal{H}}}T_c\left\{\mathrm{e}^{-\frac{\mathrm{i}}{\hbar}\int_c\mathrm{d}\tau\,(\hat{\mathcal{H}}'_{\hat{\mathcal{H}}_0}(\tau)+\hat{\mathcal{H}}^{(i)}_{\hat{\mathcal{H}}_0}(\tau))}\Psi_{\hat{\mathcal{H}}_0}(1)\Psi^\dagger_{\hat{\mathcal{H}}_0}(1')\right\}\right]}{\mathrm{Tr}\left[\mathrm{e}^{-\beta\hat{\mathcal{H}}}\right]}, \tag{4.28}$$

which correlates the creation of a particle at the coordinates $1'$ and the annihilation at 1. Here, the contour $c=c_1+c_2$ is the combination of the contours discussed above. This Green's function will prove a powerful tool for the perturbation theory. Nevertheless, before we start discussing the usage of the Green's function within the non-equilibrium theory, we need to transform it to a more suitable form. Equivalent to the factorization of (4.20) we can express the Boltzmann factor as

$$\mathrm{e}^{-\beta\hat{\mathcal{H}}} = \mathrm{e}^{-\beta\hat{\mathcal{H}}_0}T_{c_a}\left\{\mathrm{e}^{-\frac{\mathrm{i}}{\hbar}\int_{t_0}^{t_0-\mathrm{i}\beta}\mathrm{d}\tau\,\hat{\mathcal{H}}^{(i)}_{\hat{\mathcal{H}}_0}(\tau)}\right\}, \tag{4.29}$$

where T_{c_a} orders along the path from t_0 down into the lower complex plane to $t_0 - \mathrm{i}\beta$. Note that the external perturbation $\hat{\mathcal{H}}'(t)$ vanishes for $t \leq t_0$ and the Green's function can be written as

$$G(1,1') = -\mathrm{i}\frac{\mathrm{Tr}\left[\mathrm{e}^{-\beta\hat{\mathcal{H}}_0}T_{c_i}\left\{\mathrm{e}^{-\frac{\mathrm{i}}{\hbar}\int_{c_i}\mathrm{d}\tau\,\hat{\mathcal{H}}^{(i)}_{\hat{\mathcal{H}}_0}(\tau)}\mathrm{e}^{-\frac{\mathrm{i}}{\hbar}\int_{c}\mathrm{d}\tau\,\hat{\mathcal{H}}'_{\hat{\mathcal{H}}_0}(\tau)}\Psi_{\hat{\mathcal{H}}_0}(1)\Psi^{\dagger}_{\hat{\mathcal{H}}_0}(1')\right\}\right]}{\mathrm{Tr}\left[\mathrm{e}^{-\beta\hat{\mathcal{H}}_0}T_{c_i}\left\{\mathrm{e}^{-\frac{\mathrm{i}}{\hbar}\int_{c_i}\mathrm{d}\tau\,\hat{\mathcal{H}}^{(i)}_{\hat{\mathcal{H}}_0}(\tau)}\mathrm{e}^{-\frac{\mathrm{i}}{\hbar}\int_{c}\mathrm{d}\tau\,\hat{\mathcal{H}}'_{\hat{\mathcal{H}}_0}(\tau)}\right\}\right]}, \tag{4.30}$$

where the contour $c_i = c + c_a$ is depicted in Fig. 4.3. Again, since under contour ordering operators commute, T_{c_i} takes care of the correct order of operators. In the denominator we also exploited the fact that on a closed contour $T_c\{\mathcal{S}'\mathcal{S}^{(i)}\} = 1$.

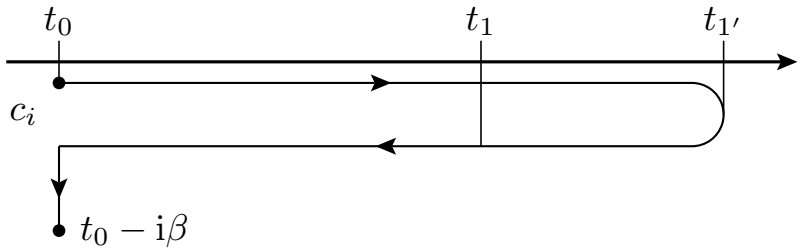

Figure 4.3.: Closed time contour c_i, where the downward part corresponds to evolution in the imaginary time intervall $[0,-\mathrm{i}\beta]$

At the appendix contour part c_a, there is by definition no interaction with the external perturbation – the SAW. In the following we will not be interested in transient phenomena. Hence, we assume that due to interactions between particles and impurities, all initial correlations are washed out within the collision time scale, long before the external perturbation starts. In such a case, the c_a part of the contour vanishes and we can take effectively $t_0 \to -\infty$. If, additionally, we expand the return path of the contour to $+\infty$, we obtain the Schwinger-Keldysh closed time path [74] shown in Fig. 4.4. It runs from $t = -\infty$ to $t = +\infty$ and returns then back to $t = -\infty$. Eventually, we obtain the contour-ordered closed time

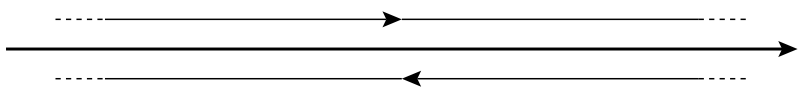

Figure 4.4.: Schwinger-Keldysh closed time path C.

path Green's function

$$G_C(1,1') = -\mathrm{i}\mathrm{Tr}\left[\rho_0 T_C\left\{\mathrm{e}^{-\frac{\mathrm{i}}{\hbar}\int_C \mathrm{d}\tau\,(\hat{\mathcal{H}}'_{\hat{\mathcal{H}}_0}(\tau)+\hat{\mathcal{H}}^{(i)}_{\hat{\mathcal{H}}_0}(\tau))}\Psi_{\hat{\mathcal{H}}_0}(1)\Psi^\dagger_{\hat{\mathcal{H}}_0}(1')\right\}\right]$$
$$= -\mathrm{i}\left\langle T_C\left\{\mathrm{e}^{-\frac{\mathrm{i}}{\hbar}\int_C \mathrm{d}\tau\,(\hat{\mathcal{H}}'_{\hat{\mathcal{H}}_0}(\tau)+\hat{\mathcal{H}}^{(i)}_{\hat{\mathcal{H}}_0}(\tau))}\Psi_{\hat{\mathcal{H}}_0}(1)\Psi^\dagger_{\hat{\mathcal{H}}_0}(1')\right\}\right\rangle, \quad (4.31)$$

where we used (4.14) together with the statistical density operator:

$$\rho_0 = \frac{\mathrm{e}^{-\beta\hat{\mathcal{H}}_0}}{\mathrm{Tr}\left[\mathrm{e}^{-\beta\hat{\mathcal{H}}_0}\right]} \quad (4.32)$$

.

Since ρ_0 is quadratic in the field operators, Wick's theorem can be utilized. It states that expressions of the type

$$\langle T_C\left\{O(1)O(2)O(3)\ldots O(2n-2)O(2n-1)O(2n)\right\}\rangle \quad (4.33)$$

can be decomposed into a sum over all possible pairwise products

$$\langle T_C\left\{O(1)O(2)O(3)\ldots O(2n-2)O(2n-1)O(2n)\right\}\rangle \quad (4.34)$$
$$= \sum_{\text{a.p.p.}}\prod_{i\neq j}(-1)^{\zeta_P}\left\langle T_C\left\{O(i)O(j)\right\}\right\rangle. \quad (4.35)$$

The usefulness of Wick's theorem becomes more obvious by considering, for example, particles coupled to an external field such as $\hat{\mathcal{H}}'_{\hat{\mathcal{H}}_0}$, which is quadratic in the field operators, while ignoring any interaction of the particles ($\hat{\mathcal{H}}^{(i)}_{\hat{\mathcal{H}}_0} = 0$). In such a situation the Green's function is given by

$$G_0(1,1') = -\mathrm{i}\left\langle T_C\left\{\mathrm{e}^{-\frac{\mathrm{i}}{\hbar}\int_C \mathrm{d}2\,h'(2)\Psi^\dagger_{\hat{\mathcal{H}}_0}(2)\Psi_{\hat{\mathcal{H}}_0}(2)}\Psi_{\hat{\mathcal{H}}_0}(1)\Psi^\dagger_{\hat{\mathcal{H}}_0}(1')\right\}\right\rangle. \quad (4.36)$$

Expanding the exponential function yields in zeroth order the free contour-ordered Green's function:

$$G_0^{(0)}(1,1') = -\mathrm{i}\left\langle T_C\left\{\Psi_{\hat{\mathcal{H}}_0}(1)\Psi^\dagger_{\hat{\mathcal{H}}_0}(1')\right\}\right\rangle. \quad (4.37)$$

This expression, however, is exactly of the form of the products appearing in Wick's theorem. The accomplishment of Wick's theorem is evidently that higher order terms derived by an expansion of the exponential function, can be decomposed into products of the free contour-ordered Green's function. The first order contribution can thus be expressed by

$$G_0^{(1)}(1,1') = \int_C \mathrm{d}2\,G_0^{(0)}(1,2)h'(2)G_0^{(0)}(2,1'), \quad (4.38)$$

and higher order terms accordingly.

Let us now introduce a very useful representation of the contour-ordered Greens's function by mapping it onto a 2×2-dimensional matrix $\hat{G}_{ij}(1,1')$. In this so called Keldysh space, the time t_1 of the matrix element $\hat{G}_{ij}(1,1')$ resides on the part i, and t_1' on the part j of the Schwinger-Keldysh closed time path C. Here the first part of the contour, which runs from $t=-\infty$ to $t=+\infty$, is labelled as 1 and the return path as 2. Explicitly, the matrix elements of $\hat{G}(1,1')$ read

$$\hat{G}_{11}(1,1') = -\mathrm{i}\,\langle T\left\{\Psi_{\hat{\mathcal{H}}}(1)\Psi^{\dagger}_{\hat{\mathcal{H}}}(1')\right\}\rangle\,, \tag{4.39}$$

$$\hat{G}_{12}(1,1') \equiv G^{<}(1,1') = \mathrm{i}\,\langle\Psi^{\dagger}_{\hat{\mathcal{H}}}(1')\Psi_{\hat{\mathcal{H}}}(1)\rangle\,, \tag{4.40}$$

$$\hat{G}_{21}(1,1') \equiv G^{>}(1,1') = -\mathrm{i}\,\langle\Psi_{\hat{\mathcal{H}}}(1)\Psi^{\dagger}_{\hat{\mathcal{H}}}(1')\rangle\,, \tag{4.41}$$

$$\hat{G}_{22}(1,1') = -\mathrm{i}\,\langle\tilde{T}\left\{\Psi_{\hat{\mathcal{H}}}(1)\Psi^{\dagger}_{\hat{\mathcal{H}}}(1')\right\}\rangle\,, \tag{4.42}$$

where $\tilde{T}$ denotes the anti-time-ordering operator.

Returning to the first order expression (4.38), the ij-component of the corresponding first order term of the real-time matrix Green's function is

$$\hat{G}^{(1)}_{ij}(1,1') = \sum_{kk'}\int \mathrm{d}2\,\hat{G}^{(0)}_{ik}(1,2)\hat{h}'_{kk'}(2)\hat{G}^{(0)}_{k'j}(2,1'), \tag{4.43}$$

where we introduced the matrix representation of the function

$$\hat{h}'_{ij}(1) = h'(1)\sigma^{z}_{ij}. \tag{4.44}$$

Thus in Keldysh space, the first order expression is obtained by a matrix product together with an integration. This leads us to the definition of the symbol "$\otimes$" (not to be mistaken with the same symbol, we used for the Kronecker product in, e.g., (3.47)), which combines the matrix product together with the internal integration. The first order matrix equation thus becomes:

$$\hat{G}^{(1)} = \hat{G}^{(0)}\otimes\hat{h}'\hat{G}^{(0)} = \hat{G}^{(0)}\hat{h}'\otimes\hat{G}^{(0)} \tag{4.45}$$

Since not all matrix elements of the Green's function are independent of each other, Larkin and Ovchinnikov [83] introduced a more convenient representation

$$\check{G} \equiv \frac{1}{2}(1-\mathrm{i}\sigma^{y})\sigma^{z}\hat{G}(1+\mathrm{i}\sigma^{y}) = \begin{pmatrix} G^{R} & G^{K} \\ 0 & G^{A}\end{pmatrix}, \tag{4.46}$$

with the retarded, advanced and Keldysh component of the Green's function:

$$G^R(1,1') = \hat{G}_{11}(1,1') - \hat{G}_{12}(1,1') = \hat{G}_{21}(1,1') - \hat{G}_{22}(1,1'), \tag{4.47}$$

$$G^A(1,1') = \hat{G}_{11}(1,1') - \hat{G}_{21}(1,1') = \hat{G}_{12}(1,1') - \hat{G}_{22}(1,1'), \tag{4.48}$$

$$G^K(1,1') = \hat{G}_{21}(1,1') + \hat{G}_{12}(1,1') = \hat{G}_{11}(1,1') + \hat{G}_{22}(1,1'). \tag{4.49}$$

Especially the Keldysh Green's function G^K will be of great importance later on, since it carries the statistical information about the energy occupation of the system. Note that a major advantage of such a triangular representation is the fact that it keeps this triangular structure under matrix multiplications.

We will now introduce Feynman diagrams as a powerful tool for the derivation of the Green's function, where here again we stick to the case of vanishing interactions $\hat{\mathcal{H}}^{(i)} = 0$ (4.36). In such a diagrammatic representation, the free Green's function $\check{G}_0^{(0)}$ is symbolized by

$$\check{G}_0^{(0)}(1,1') \equiv$$ 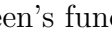 , (4.50)

and the first order contribution (4.45) by

$$\check{G}_0^{(1)}(1,1') \equiv$$ 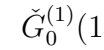 , (4.51)

where the interaction with the external perturbation h' is represented by the cross sign. The full Green's function $\check{G}_0$ can then be written in the diagrammatic representation according to

$$\check{G}_0(1,1') \equiv$$

$$=$$ 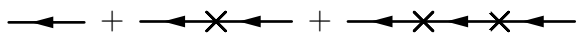

$$+$$ 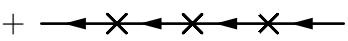

$$+ \ldots \tag{4.52}$$

From this infinite sum of diagrams, the Dyson equation for the trivial case of coupling to a scalar potential is easily obtained:

 (4.53)

or explicitly in the matrix representation ($\check{h}'(1) = h'(1)\sigma^0$)

$$\check{G}_0 = \check{G}_0^{(0)} + \check{G}_0^{(0)} \otimes \check{h}'\check{G}_0 = \check{G}_0^{(0)} + \check{G}_0\check{h}' \otimes \check{G}_0^{(0)}. \tag{4.54}$$

At this point, we take a closer look on the temporal derivative of the Green's functions. Using the von Neumann equation together with the commutator rules of the field operators, one can easily show that

$$\left[\mathrm{i}\hbar\frac{\partial}{\partial t_1} - h_0(1)\right]\check{G}_0^{(0)}(1,1') = \hbar\delta(1-1')\mathbb{1}, \tag{4.55}$$

or by using (4.54)

$$\left[\mathrm{i}\hbar\frac{\partial}{\partial t_1} - h_0(1) - h'(1)\right]\check{G}_0(1,1') = \hbar\delta(1-1')\mathbb{1}. \tag{4.56}$$

This justifies the definition of the inverse matrix Green's function :

$$\check{G}_0^{-1}(1,1') \equiv \left[\mathrm{i}\hbar\frac{\partial}{\partial t_1} - \frac{\left(-\mathrm{i}\hbar\nabla_1 + \boldsymbol{\mathcal{A}}^a(1)\sigma^a/2\right)^2}{2m} + e\Phi(1)\right]\delta(1-1')\mathbb{1}. \tag{4.57}$$

for non-interacting particles. Note that the artificial separation of $\boldsymbol{\mathcal{A}}$ into a time-dependent and a time-independent part is thus lifted and the two Hamiltonians (4.15) and (4.16) are recombined. In the Green's function (4.57), $\boldsymbol{\mathcal{A}}$ resembles a vector potential known from electrodynamics. Actually, we will delve into this analogy in the next section. Yet, we want to remark that in the expression above we neglected the term $\sim \boldsymbol{\mathcal{A}}^2\sigma^0$, since on the one hand, it has no influence on the dynamics of the spins, and on the other hand it is much smaller than the SAW potential $e\Phi$.

Furthermore, as the inverse matrix Green's function obviously commutes with the Green's function, the commutator relation

$$\left[\check{G}_0^{-1} \overset{\otimes}{,} \check{G}_0\right] = 0, \tag{4.58}$$

follows.

We will now focus on the interaction of electrons with a random impurity potential. For more details see e.g. [67]. We assume for the sake of simplicity an ensemble of N_i identical impurities at the location $\mathbf{r}_i$

$$\hat{\mathcal{H}}^{(i)}(\mathbf{r}) = \int \mathrm{d}\mathbf{r} \sum_{i=1}^{N_i} \Psi^\dagger(\mathbf{r}) V_{\mathrm{imp}}(\mathbf{r} - \mathbf{r}_i)\Psi(\mathbf{r}). \tag{4.59}$$

In a large system with volume V one can suppose that the impurities are evenly distributed, and the properties of the system are completely determined in terms of the mean impurity concentration $n_i = N_i/V$. This implies, however, that only quantities, which are averaged over all possible impurity positions are relevant, and we introduce therefore the impurity average over an arbitrary quantity $F(\mathbf{r}_1, \mathbf{r}_2, \ldots, \mathbf{r}_N)$

$$\langle F \rangle_{\text{imp}} = \int \prod_{i=1}^{N} \frac{\mathrm{d}\mathbf{r}_i}{V} F(\mathbf{r}_1, \mathbf{r}_2, \ldots, \mathbf{r}_N), \tag{4.60}$$

which depends on the position of the impurities.

Similarly to the first order expression (4.51) above, we introduce the first order diagram for the interaction with the random impurity potential

$$\check{G}^{(1)}(1,1') = \tag{4.61}$$

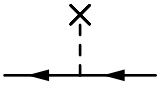

However, the impurity average $\langle \check{G}^{(1)} \rangle_{\text{imp}}$ over this first order contribution yields merely a constant, which can be simply renormalized away by a redefinition of the reference for measuring energy. The first non-trivial term occurs within second order perturbation theory

$$\check{G}^{(2)}(1,1') = \tag{4.62}$$

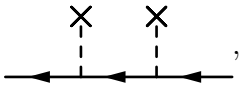

where due to the impurity averaging one has to differentiate between the case of an interaction with two different impurities or an interaction with one impurity twice. In the first case of two distinct impurities the average yields again only a constant, which can analogously to the above reasons simply be renormalized away. The second case of scattering at one impurity twice corresponds to the diagram

$$\langle \check{G}^{(2)} \rangle_{\text{imp}} (1,1') = \tag{4.63}$$

where the stochastic correlation due to the averaging process is associated with

$$\langle V(\mathbf{r}) V(\mathbf{r}') \rangle_{\text{imp}} = n_i \int \mathrm{d}\mathbf{r}''\, V_{\text{imp}}(\mathbf{r} - \mathbf{r}'') V_{\text{imp}}(\mathbf{r}' - \mathbf{r}''). \tag{4.64}$$

As in the following all the terms of the Green's function will be impurity averaged, we will drop the brackets $\langle \rangle_{\text{imp}}$ for simplicity.

In higher order contributions of the above expansion, scattering at a single impurity more than twice is possible, e.g.:

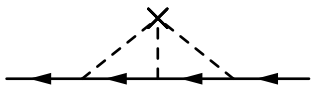

(4.65)

However, in the system we have in mind, such multiple scattering terms can be neglected. (Born approximation [67]). This corresponds to the assumption that the mean free path of the electrons between two scattering events is huge compared to the Fermi wavelength and the ratio $\hbar/p_f l$ is therefore small. The prescription for the derivation of an arbitrary order of the impurity averaged Green's function is then clear: tie pairwise together all potential crosses in every possible way. There are thus, e.g., three possible diagrams for the fourth order contribution:

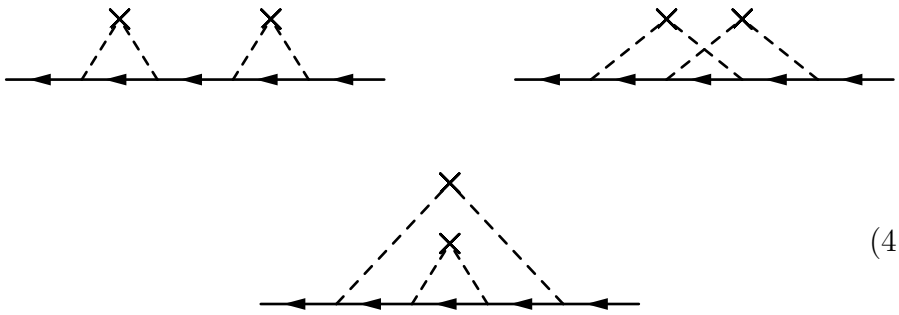

(4.66)

We continue this diagrammatic approach for the derivation of the Dyson equation by introducing the self-energy. The self-energy consists of all diagrams that cannot be separated by cutting an internal particle line. For example, in the three diagrams above the first one is separable, whereas the second and the third are irreducible diagrams. The self-energy $\check{\Sigma}(1,1')$ is then defined as the sum over all irreducible diagrams with amputated external legs:

$\check{\Sigma}(1,1') \equiv$ 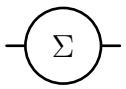

$=$ 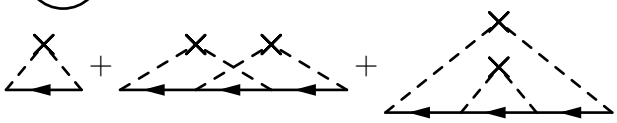 $+ \ldots$ (4.67)

With this definition, the full Green's function can be constructed by summing up all diagrams, which reduce to irreducible diagrams by cutting a

line once, twice and so on, or in the diagrammatic language

$\check{G}(1,1') =$

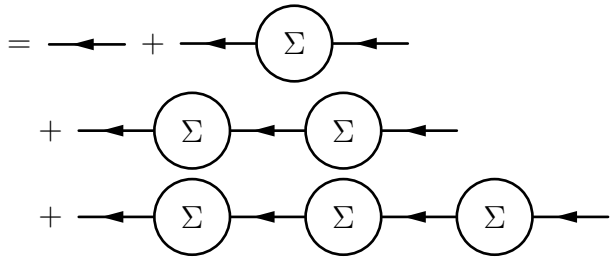

(4.68)

Equivalently to the case of non-interacting particles (4.52), this expansion results in the Dyson equation

(4.69)

which includes now also interactions with impurities. In the matrix Green's function notation the Dyson equation reads:

$$\check{G} = \check{G}_0 + \check{G}_0 \otimes \check{\Sigma} \otimes \check{G} = \check{G}_0 + \check{G} \otimes \check{\Sigma} \otimes \check{G}_0. \tag{4.70}$$

By multiplying this equation with the inverse matrix Green's function (4.57) one can derive the left-right-subtracted Dyson equation

$$-\mathrm{i}\left[\check{G}_0^{-1}(1,2) \circledast \check{G}(2,1')\right] = -\mathrm{i}\left[\check{\Sigma}(1,2) \circledast \check{G}(2,1')\right]. \tag{4.71}$$

So far, the representation of the self-energy is a functional of the free matrix Green's function $\check{G}_0$. For further calculations this dependence is not expedient and we introduce a further approximation, the non-crossing approximation (see e.g [67]). As its name implies we neglect, similar to the Born approximation ($\hbar/p_f l \ll 1$) terms in the self-energy with crossing impurity lines (e.g. the second term of the expansion in (4.67)). The self-consistent self-energy in Born approximation can then be written as

$\check{\Sigma}(1,1') =$

(4.72)

where the impurities are correlated by the full matrix Green's function. In the following we will assume the following impurity correlation (4.64)

$$\langle V(\mathbf{r})V(\mathbf{r}')\rangle_{\mathrm{imp}} = n_i v_0^2 \delta(\mathbf{r}-\mathbf{r}'), \tag{4.73}$$

which is associated with an impurity potential $V_{\text{imp}}(\mathbf{p}) \approx v_0$ that varies slowly in momentum space. Under this condition, the self-energy is given by:

$$\check{\Sigma}(1,1') = \langle V(\mathbf{r}_1)\check{G}(1,1')V(\mathbf{r}_{1'})\rangle_{\text{imp}} = n_i v_0^2 \delta(\mathbf{r}_1 - \mathbf{r}_{1'})\check{G}(1,1'). \tag{4.74}$$

With this self-energy, together with the above discussed Keldysh formalism we will obtain in the next section a Boltzmann like equation, which also takes spin-orbit interaction into account.

4.3. Generalized Boltzmann equation and diffusive limit

The Dyson equation (4.70), we derived so far, is a rather technical expression. By solving it, one would obtain a solution for the Green's function, which depends on two distinct space-times $(1,1')$ and is fully capable to describe the complete dynamics of the system. However, for our purposes it contains too much information. More precisely, we are interested in the spatio-temporal dynamics of the charge and spin density. The charge density is given by equal time and space coordinates

$$\rho(\mathbf{r},t) = \sum_\sigma \langle \Psi^\dagger_{\hat{\mathcal{H}}}(1)\Psi_{\hat{\mathcal{H}}}(1)\rangle = -\mathrm{i}\sum_\sigma G^<(1,1), \tag{4.75}$$

and the charge current density without external magnetic field by

$$\mathbf{j}(1) = \frac{e\hbar}{2m}\sum_\sigma (\nabla_1 - \nabla_{1'})G^<(\mathbf{r},t,\mathbf{r}',t')_{|\mathbf{r}_1=\mathbf{r}_{1'}}. \tag{4.76}$$

In order to extract the macroscopic quantities from the matrix Green's function, we introduce the Wigner coordinates,

$$\begin{aligned} \mathbf{R} &= \frac{\mathbf{r}_1 + \mathbf{r}_{1'}}{2}, \quad T = \frac{t_1 + t_{1'}}{2}, \\ \mathbf{r} &= \frac{\mathbf{r}_1 - \mathbf{r}_{1'}}{2}, \quad t = \frac{t_1 - t_{1'}}{2}, \end{aligned} \tag{4.77}$$

which transform the system to center-of-mass and relative coordinates, respectively. Obviously, the variables $x = (\mathbf{r},t)$ describe microscopic and $X = (\mathbf{R},T)$ macroscopic quantities. The external perturbations generated by a SAW, e.g., depend solely on the center-of-mass variables X. Moreover, in equilibrium, meaning without a SAW, the system is spatially and

temporally translational invariant and thus independent of X. As a next step, we neglect for the moment the spin-orbit interaction ($\boldsymbol{\mathcal{A}} = 0$) and consider the Fourier transformation of the functions of the Dyson equation with respect to the relative coordinates

$$\check{G}(X,p) \equiv \int \mathrm{d}x\, \mathrm{e}^{-\frac{\mathrm{i}}{\hbar}px} \check{G}(X,x), \tag{4.78}$$

and with the abbreviations

$$p = (E, \mathbf{p}), \quad px = -Et + \mathbf{p}\cdot\mathbf{r}. \tag{4.79}$$

Furthermore, we introduce the distribution function

$$f(X,\mathbf{p}) \equiv \frac{1}{2}\left[1 + \int \frac{\mathrm{d}E}{2\pi\mathrm{i}} G^K(X,p)\right], \tag{4.80}$$

from which the above defined two-dimensional charge and current densities are obtained by

$$\rho(X) = \sum_\sigma \int \frac{\mathrm{d}\mathbf{p}}{(2\pi\hbar)^2} f(X,\mathbf{p}) \tag{4.81}$$

and

$$\mathbf{j}(X) = \sum_\sigma \int \frac{\mathrm{d}\mathbf{p}}{(2\pi\hbar)^2} \frac{\mathbf{p}}{m} f(X,\mathbf{p}). \tag{4.82}$$

The convenience of the transformation to mixed coordinates then becomes evident, by considering expressions of the type $A(1,2)\otimes B(2,1')$. Such convolutions, which appear in the Dyson equation, can be written in the mixed representation as [71]

$$(A\otimes B)(X,p) = \mathrm{e}^{\mathrm{i}\frac{\hbar}{2}(\partial_X^A\partial_p^B - \partial_X^B\partial_p^A)} A(X,p)B(X,p), \tag{4.83}$$

with

$$\partial_X^A = (-\partial_T, \nabla_{\mathbf{R}}), \qquad \partial_p^A = (-\partial_E, \nabla_{\mathbf{p}}), \tag{4.84}$$

and

$$\partial_X^A\partial_p^B = -\frac{\partial^A}{\partial T}\frac{\partial^B}{\partial E} + \nabla_{\mathbf{R}}^A\cdot\nabla_{\mathbf{p}}^B. \tag{4.85}$$

The superscript denotes the object on which the derivative operates. The wave length and frequency of the surface acoustic waves considered here is of the order of $\sim 5\,\mu$m and $\sim 500\,$MHz, respectively. Compared to the microscopic quantities which are determined by the Fermi momentum and Fermi energy, the external length and time scale is huge and hence,

$\hbar\partial_X\partial_p \ll 1$. As a consequence, for our purposes, it is sufficient to expand the exponential function in (4.83) up to first order. This procedure is known as the gradient expansion.

Let us now consider the spectral weight function

$$A(X,p) \equiv \mathrm{i}\left(G^R(X,p) - G^A(X,p)\right), \tag{4.86}$$

whose equation of motion is obtained by subtracting the diagonal elements of the left-right-subtracted Dyson equation (4.71):

$$\left[G_0^{-1} - \frac{1}{2}(\Sigma^R + \Sigma^A) \overset{\otimes}{,} A\right] - \left[\mathrm{i}(\Sigma^R - \Sigma^A) \overset{\otimes}{,} \frac{1}{2}(G^R + G^A)\right] = 0. \tag{4.87}$$

Applying the gradient expansion to this equation generates, in first order, a differential equation which is solved by

$$A(X,p) = \frac{\mathrm{i}(\Sigma^R - \Sigma^A)}{\left(E - \xi_{\mathbf{p}} - V(x) - \frac{1}{2}(\Sigma^R + \Sigma^A)\right)^2 + \left(\frac{\mathrm{i}(\Sigma^R - \Sigma^A)}{2}\right)^2}, \tag{4.88}$$

with $\xi_{\mathbf{p}} = \mathbf{p}^2/2m$. We will stick to the case of small impurity concentrations n_i, where the self-energy is small. The spectral weight function is then a sharply peaked function and can by approximated by

$$A(X,p) \approx 2\pi\delta(E - \xi_{\mathbf{p}} - V(X)). \tag{4.89}$$

This approximation, which in the absence of any interactions is of course exact, is the so-called quasi-particle approximation.

Note that, for example, in the case of strong electron-phonon interaction, the assumption of a sharply peaked spectral weight density in terms of the energy E is no longer valid and one has to rely on a different approach. Although $A(X,p)$ in such a case of strong electron-phonon interaction is no longer peaked in the variable E, it is still a peaked function of the momentum and thus $\xi_{\mathbf{p}}$ [84, 85]. Analogously to the quasi-particle approximation, with the help of this so-called quasi-classical approximation one obtains an equation similar to the Boltzmann equation; the Eilenberger equation [86].

We will now take advantage of the simple form of the spectral weight function in the quasi-particle approximation to derive an expression for the impurity scattering, which depends on the distribution function $f(X,\mathbf{p})$. The gradient expansion of the Keldysh component of the right-hand-side

of the Dyson equation (4.71) yields in leading order:

$$-\mathrm{i}\left[\check{\Sigma} \overset{\otimes}{,} \check{G}\right]^K (X,p) \approx -\mathrm{i}G^K(X,p)\left(\Sigma^R(X,p) - \Sigma^A(X,p)\right) + \Sigma^K(X,p)A(X,p). \tag{4.90}$$

For a constant impurity potential in momentum space, the self-energy within the Born approximation can according to (4.74) be written as

$$\check{\Sigma}(X,p) = n_i v_0^2 \int \frac{\mathrm{d}\mathbf{p}'}{(2\pi\hbar)^2} \check{G}(X,p'). \tag{4.91}$$

Using this expression together with the definition of the distribution function (4.80) and the spectral weight function (4.89) in (4.90), one obtains the electron-impurity collision integral:

$$I_{\mathrm{imp}}[f] = -\frac{2\pi n_i v_0^2}{\hbar} \int \frac{\mathrm{d}\mathbf{p}'}{(2\pi\hbar)^2} \delta(\xi_{\mathbf{p}} - \xi_{\mathbf{p}'})(f(X,\mathbf{p}) - f(X,\mathbf{p}')). \tag{4.92}$$

For the two-dimensional electron gas we have in mind, one can simplify this integral by taking advantage of the identity

$$\int \frac{\mathrm{d}\mathbf{p}'}{(2\pi\hbar)^2} = N_0 \int_0^\infty \mathrm{d}\xi_{\mathbf{p}} \int_0^{2\pi} \frac{\mathrm{d}\varphi}{2\pi}, \tag{4.93}$$

where $N_0 = m/(2\pi\hbar)^2$ denotes the density of states per spin and area, and φ is the angle of the momentum $\mathbf{p}$ in polar coordinates. The collision integral takes therefore the form

$$I_{\mathrm{imp}}[f] = -\frac{1}{\tau}\left(f - \langle f \rangle\right), \tag{4.94}$$

where we encounter the impurity scattering rate $\tau^{-1} = N_0 2\pi n_i v_0^2/\hbar$, which is associated with the average time between two scattering events. The brackets $\langle \ldots \rangle = \int \mathrm{d}\varphi/2\pi \ldots$ indicate the angular average.

We will now turn to the left-hand-side of the Dyson equation (4.71) to derive the Boltzmann equation. In leading order of the gradient expansion one finds:

$$-\mathrm{i}\left[G_0^{-1} \overset{\otimes}{,} \check{G}\right] \approx \partial_E G_0^{-1} \partial_T \check{G} - \partial_T G_0^{-1} \partial_E \check{G} - \nabla_{\mathbf{p}} G_0^{-1} \cdot \nabla_{\mathbf{R}} \check{G} + \nabla_{\mathbf{R}} G_0^{-1} \cdot \nabla_{\mathbf{p}} \check{G}. \tag{4.95}$$

If we still neglect the influence of spin-orbit coupling ($\boldsymbol{\mathcal{A}} = 0$) and consider instead an electromagnetic vector potential $\mathbf{A}(X)$, the free inverse Green's function reads:

$$G_0^{-1}(X,p) = E - \frac{\left(\mathbf{p} + e\mathbf{A}(X)\right)^2}{2m} + e\Phi(X) \tag{4.96}$$

At this point, however, some care is required. With the procedure discussed so far, one would obtain an expression for the distribution function that is not gauge invariant. In order to circumvent this problem, one "shifts" in the Fourier transformation (4.78) the momentum towards the kinematic momentum $\mathbf{p} \to \mathbf{p}^* = \mathbf{p} + e\mathbf{A}(X)$:

$$\check{G}(X,p) \equiv \int \mathrm{d}x\, \mathrm{e}^{-\frac{\mathrm{i}}{\hbar}(p+eA(X))x} \check{G}(X,x). \tag{4.97}$$

A gradient expansion analogous to (4.95) then leads together with the corresponding distribution function to the $U(1)$ gauge-invariant Boltzmann equation

$$\left(\partial_T + \frac{\mathbf{p}^*}{m} \cdot \nabla_{\mathbf{R}} + \mathbf{F} \cdot \nabla_{\mathbf{p}^*}\right) f(X,\mathbf{p}) = I_{\mathrm{imp}}[f], \tag{4.98}$$

with the Lorentz force

$$\mathbf{F} = -e\left(\mathbf{E} + \frac{\mathbf{p}^*}{m} \times \mathbf{B}\right). \tag{4.99}$$

We return now to our actual goal, a Boltzmann-like equation including the effects of spin-orbit coupling. The purpose of writing in the free Green's function (4.57) the spin-orbit interaction similarly to an electromagnetic vector potential, was to obtain a $SU(2)$ gauge-invariant expression in analogy to the procedure above. The simple concept of a "shift" is, however, not applicable in the presence of the non-Abelian $SU(2)$ vector field $\boldsymbol{\mathcal{A}}^a(X)\sigma^a/2$. Nevertheless, as in the case of an electromagnetic field, the gauge-invariance is restored by the inclusion of a factor $\exp[-\mathrm{i}eA(X)x]$ in (4.97), as pointed out in Ref. [68], a similar approach can be pursued with the help of the transformation

$$\left[G_0^{-1}(1,1') \circledS \check{G}(1',2)\right] \to \mathcal{U}_\Gamma(X,1)\left[G_0^{-1}(1,1') \circledS \check{G}(1',2)\right]\mathcal{U}_{\Gamma'}(2,X). \tag{4.100}$$

The Wilson line [87] is the exponential of the line integral of the gauge potential

$$\mathcal{U}_\Gamma(2,1) = \mathcal{P}\mathrm{e}^{-\mathrm{i}\int \mathrm{d}y \mathcal{A}(y)}, \tag{4.101}$$

where the symbol $\mathcal{P}$ denotes path ordering along the curve Γ from 1 to 2. Since it is evaluated in terms of the small relative coordinates x, the curve Γ is in the following always chosen to be a straight line. We are thus led to the definition of a locally covariant Green's function

$$\check{\widetilde{G}}(1,2) \equiv \mathcal{U}_\Gamma(X,1)\check{G}(1,2)\mathcal{U}_\Gamma(2,X) \tag{4.102}$$

and its associated distribution function

$$f(X,\mathbf{p}) \equiv \frac{1}{2}\left[1 + \int \frac{\mathrm{d}E}{2\pi\mathrm{i}}\widetilde{G}^K(X,p)\right]. \tag{4.103}$$

The inverse free Green's function in the presence of spin-orbit interaction (compare (4.57)) and without external magnetic field reads:

$$G_0^{-1}(X,p) = E - \frac{\left(\mathbf{p} + \boldsymbol{\mathcal{A}}^a(X)\sigma^a/2\right)^2}{2m} + e\Phi(X). \tag{4.104}$$

With the assumption of a weak spin-orbit interaction compared to the Fermi energy, a gradient expansion of the locally covariant left-hand-side of the Dyson equation (4.100), and a subsequent energy integration, then results in a Boltzmann-like equation ($f = f(X,\mathbf{p})$):

$$\partial_T f + \frac{\mathbf{p}}{m}\cdot\widetilde{\nabla}_{\mathbf{R}} f + \frac{1}{2}\{\boldsymbol{\mathcal{F}}, \nabla_{\mathbf{p}} f\} = -\frac{1}{\tau}\left(f - \langle f\rangle\right). \tag{4.105}$$

Note that by introducing the covariant derivative

$$\widetilde{\nabla}_{\mathbf{R}} = \nabla_{\mathbf{R}} + \frac{\mathrm{i}}{\hbar}[\boldsymbol{\mathcal{A}}, \ldots], \tag{4.106}$$

together with the generalized Lorentz-force

$$\boldsymbol{\mathcal{F}} = -e\mathbf{E} - \left(\boldsymbol{\mathcal{E}} + \frac{\mathbf{p}}{m}\times\boldsymbol{\mathcal{B}}\right), \tag{4.107}$$

this expression has a very similar form compared to the Boltzmann equation (4.98). In the absence of a classical magnetic field, the components of the generalized electromagnetic field read:

$$\mathbf{E} = -\nabla\Phi, \tag{4.108}$$

$$\mathcal{E}_i^a = -\partial_T \mathcal{A}_i^a, \tag{4.109}$$

$$\mathcal{B}_i^a = \frac{1}{2}\epsilon_{ijk}\mathbb{F}_{jk}^a, \tag{4.110}$$

$$\mathbb{F}_{jk}^a = \partial_{x_j}\mathcal{A}_k^a - \partial_{x_k}\mathcal{A}_j^a + \mathrm{i}[\mathcal{A}_j, \mathcal{A}_k]^a. \tag{4.111}$$

Note that the generalized distribution function

$$f = f^0\sigma^0 + f^x\sigma^x + f^y\sigma^y + f^z\sigma^z, \tag{4.112}$$

combines the charge and the spin distribution of the system

$$\rho = \rho^0\sigma^0 + \rho^x\sigma^x + \rho^y\sigma^y + \rho^z\sigma^z, \tag{4.113}$$

and accordingly the charge and spin currents and is thus effectively a two-dimensional matrix. The zeroth component σ^0 of the Pauli matrices denotes the identity matrix. The corresponding charge ($\mu = 0$) and spin densities ($\mu = x, y, z$)

$$\rho^\mu(X) = \frac{1}{2}\int \frac{\mathrm{d}\mathbf{p}}{(2\pi\hbar)^2}\mathrm{Tr}\{f(X,\mathbf{p})\cdot\sigma^\mu\} \tag{4.114}$$

or charge and spin currents

$$\mathbf{j}^\mu(X) = \frac{1}{2}\int \frac{\mathrm{d}\mathbf{p}}{(2\pi\hbar)^2}\frac{\mathbf{p}}{m}\mathrm{Tr}\{f(X,\mathbf{p})\cdot\sigma^\mu\} \tag{4.115}$$

are obtained in an analogous way as in (4.81) and (4.82). Moreover, the spin-dependency of the generalized distribution function, explains the commutator term in the generalized derivative (4.106), which additionally to the spatial derivative, describes spin precession around the spin-orbit field.

In order to transform the Boltzmann equation into a more tractable form, we rely on the further assumption that the time between two collisions due to impurity scattering events, is much lesser than the temporal change of all external influences. This implies in our case that the frequency of the SAW has to be much shorter than the scattering rate, i.e., $\omega_{\mathrm{SAW}}\tau \ll 1$. We assume furthermore that the wavelength λ_{SAW} of the SAW is much larger than the length of the mean free path $l = p\tau/m \ll \lambda_{\mathrm{SAW}}$. Note, however, that although we assume small scattering times, the Fermi energy is still assumed to be the largest energy, i.e., $E_F \gg \hbar/\tau$. In other words, only few electrons around the Fermi energy are excited, and we may assume for the angular averaged distribution functions

$$\langle f^\mu(X,\mathbf{p})\rangle \approx \frac{1}{N_0}\delta(\xi_{\mathbf{p}} - E_F)\rho^\mu(X). \tag{4.116}$$

The external SAW-fields are then incapable to drive the system far from the local equilibrium – the Fermi distribution – and the ansatz to expand the distribution function

$$f(X,\mathbf{p}) \approx \langle f(X,p)\rangle + \mathbf{e}_{\mathbf{p}}\cdot\delta\mathbf{f}(X,p), \tag{4.117}$$

in spherical harmonics in momentum space is justified, where $\mathbf{e_p} = (\cos\varphi, \sin\varphi)$ denotes the unit vector in $\mathbf{p} = p\,\mathbf{e_p}$ direction [72, 88–90]. Following this approach, one can also separate the Boltzmann equation into a spherical symmetric part by taking the angular average

$$\partial_T \langle f \rangle + \frac{p}{m} \widetilde{\nabla}_{\mathbf{R}} \cdot \delta\mathbf{f} - \frac{1}{4p} \left\{ e\mathbf{E} + \boldsymbol{\mathcal{E}}, \delta\mathbf{f} + \frac{\partial \delta\mathbf{f}}{\partial p}, \right\} = 0 \tag{4.118}$$

and a "p-wave" part

$$\mathbf{e_p} \cdot \left(\partial_T \delta\mathbf{f} + \frac{1}{\tau}\delta\mathbf{f} + \frac{p}{m}\widetilde{\nabla}_{\mathbf{R}} \langle f \rangle - \frac{1}{2} \left\{ e\mathbf{E} + \boldsymbol{\mathcal{E}}, \frac{\partial \langle f \rangle}{\partial p} \right\} \right) = 0. \tag{4.119}$$

By the assumption of small scattering times, the second equation

$$\delta\mathbf{f} = -\tau \frac{p}{m} \widetilde{\nabla}_{\mathbf{R}} \langle f \rangle + \frac{\tau}{2} \left\{ e\mathbf{E} + \boldsymbol{\mathcal{E}}, \frac{\partial \langle f \rangle}{\partial p} \right\}, \tag{4.120}$$

inserted in the first one yields an equation, which depends exclusively on the averaged distribution function. Substituted in the expression for the spin densities (4.114) and regarding (4.116) one finally obtains the "continuity" equation

$$\frac{\partial \rho}{\partial t} + \widetilde{\nabla} \cdot \mathbf{j} = 0, \tag{4.121}$$

with the current density

$$\mathbf{j} = -D\widetilde{\nabla}\rho + \frac{\mu}{e} \{ e\mathbf{E} + \boldsymbol{\mathcal{E}}, \rho \}, \tag{4.122}$$

which depends solely on the center-of-mass coordinates. Here, we introduced the diffusion constant

$$D = \frac{1}{2} v_F^2 \tau, \tag{4.123}$$

where $v_F = p_F/m$ denotes the Fermi velocity and the mobility of the electrons is $\mu = e\tau/n$ [89].

We quoted the phrase "continuity" equation, since as we will discuss later, only the number of particles is conserved. Due to spin-precession, which is incorporated in the generalized derivative, an initial polarisation of the electron gas effectively vanishes within the relaxation time. The relaxation rate is, however, influenced by the external fields of the surface acoustic wave. We will discuss this point in detail in the next chapter.

5. Charge and spin dynamics under the influence of a SAW

In the first chapter we discussed the various possible microscopic sources of spin-orbit interaction. The lack of a center of inversion in the tetragonal structure of GaAs is the origin of the bulk inversion asymmetry (BIA) induced Dresselhaus spin-orbit interaction (3.151). Furthermore, in a two-dimensional quantum well there is an another possible type of spin-orbit coupling, the Rashba spin-orbit interaction. Whereas the Dresselhaus term is a consequence of the properties of the material under consideration, the Rashba term (3.159) has its origin in a possible structure inversion asymmetry (SIA) of the quantum well. These two sources of spin-orbit interaction are present independently of an external perturbation. Additional possible spin-orbit couplings come into play if the medium is deformed by a surface acoustic wave. Although the strain induced spin-orbit interactions $\hat{H}^{\mathbf{k}\boldsymbol{\varepsilon}1}$ (3.154) and $\hat{H}^{\mathbf{k}\boldsymbol{\varepsilon}2}$ (3.155) are valid only for a constant linear strain, we quietly assumed in Chap. 4 a spatiotemporal $\boldsymbol{\varepsilon}(\mathbf{r}, t)$ strain as a source of spin-orbit interaction. This assumption was, however, well justified as the relevant length scale of the electrons, the microscopic mean free path, is very small compared to the macroscopic wavelength of the SAW. As we have pointed out in the second chapter, the Rayleigh-type surface acoustic wave consists, in addition to the deformation of the material, of a piezoelectric field with components in propagation direction and perpendicular to the surface. The perpendicular part of the piezoelectric field induces then a further, SAW dependent contribution to the Rashba spin-orbit interaction $\hat{H}^{R}_{\mathrm{SAW}}$ (3.160).

All in all, in this chapter we have therefore to deal with five distinct sources of spin-orbit interaction:

Dresselhaus Hamiltonian	$\hat{H}^D$	SAW independent
Rashba Hamiltonian	$\hat{H}^R$	SAW independent
Strain induced Hamiltonians	$\hat{H}^{\mathbf{k}\varepsilon 1}$, $\hat{H}^{\mathbf{k}\varepsilon 2}$	SAW dependent
SAW induced Rashba Hamiltonian	$\hat{H}^R_{\mathrm{SAW}}$	SAW dependent

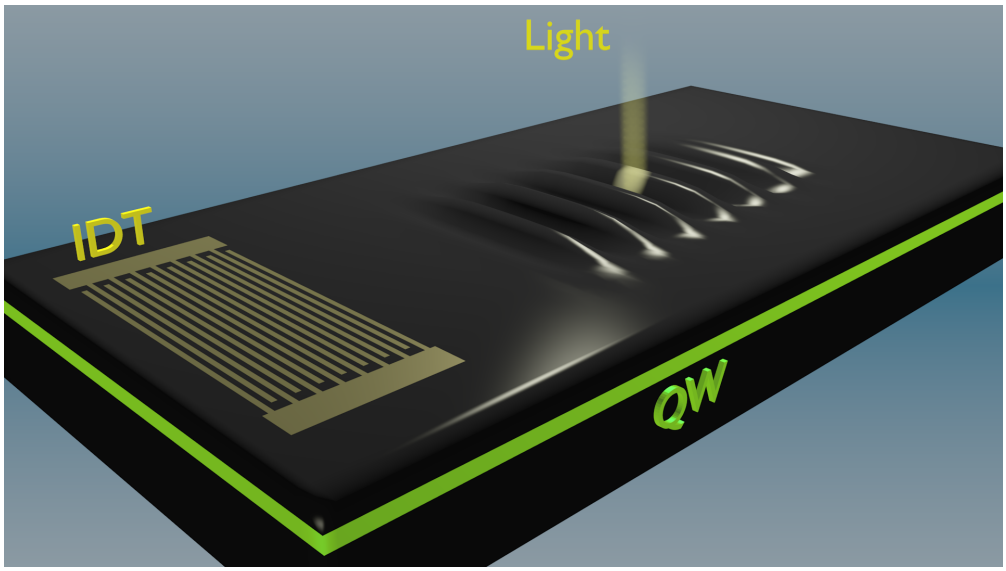

Figure 5.1.: Sketch of a typical experimental setup: Within a quantum well (QW), a two-dimensional electron gas is generated by a laser beam. Subsequently, this carrier density is modulated by a SAW, which is generated by the interdigital transducer (IDT).

Over the last decades, the manipulation of a two-dimensional electron gas by a SAW was often demonstrated experimentally as well as treated theoretically [21–28, 62, 91–117]. Hence, we consider here a typical arrangement used in many experiments and discussed frequently in literature. As depicted in 5.1, an interdigital transducer (IDT) generates a SAW that subsequently propagates over the surface. In a depth of about $\sim 100\,\mathrm{nm}$ a quantum well is located. At room temperature and below, owing to the energy gap of $\sim 1.5\,\mathrm{eV}$, between the valence and the con-

duction band (compare 3.4) there are hardly any carriers in the conduction band due to thermal excitation. A local carrier density $\rho^0(\mathbf{r})$ in the conduction band is thus generated by a laser with a typical diameter of several micrometers. In addition, this excitation naturally generates a corresponding local hole density $h(\mathbf{r})$ in the valence band. In this environment of negatively charged electrons, together with the positively charged holes, supplementary to their later discussed dynamics, further prominent processes are present.

Due to their opposite charge, electrons and holes are – like a hydrogen atom – able to form neutrally charged, atom-like structures, so-called excitons. The generation of excitons can be expressed within a simple model by the product density, $R(\mathbf{r}) = c\,\rho^0(\mathbf{r})h(\mathbf{r})$, with a generation constant of $c \sim 0.1 - 10\,\mathrm{cm}^2/\mathrm{s}$ [99, 118, 119]. As a counteracting process, excitons can be ionized by electric fields as well as by thermal excitations [120]. A further important mechanism is the recombination of electrons and holes under emission of photons. Such a process can occur either by direct recombination, or by radiative decay. Typical radiative lifetimes of excitons are in the range of $0.1 - 1\,\mathrm{ns}$ [99].

Apart from the interaction of the charge carriers, the SAW is able to spatially modulate the valence and conduction band in two ways: The first modulation called type-I, is primarily caused by the hydrostatic strain dependent effective Hamiltonian (3.134), where under compression the band gap expands. The second (type-II) modulation of the valence and conduction band is related to the piezoelectric potential Φ_{SAW} of the SAW. Since the electric in-plane field affects both, electrons and holes, the modulation spatially shifts the conduction band minima and valence band maxima, contrary to the type-I modulation, in the same way. The band gap energy is therefore constant under a type-II modulation. As indicated in Fig. 5.2, the different types of modulation have a pronounced effect on the charge carrier dynamics. Since the electrons tend to move to the potential minima of the conduction band, and the holes to the maxima of the valence band, respectively, due to type-I modulation electrons and holes accumulate at the same phase point of the SAW, whereas the type-II modulation effectively separates them by approximately half a wave length.

In order to determine the dominating modulation we estimate the energy of the piezoelectric potential $\mathrm{e}\Phi_{\mathrm{SAW}}$ (2.45) and of the effective Hamiltonian $\hat{\mathcal{H}}_c^{\varepsilon}$ (3.134) of the hydrostatic strain: Whereas the piezoelectric potential $\mathrm{e}\Phi_{\mathrm{SAW}} \sim \mathcal{C}\,[\mathrm{eV}]$ depends only on the strength of the SAW, $\mathcal{C}$, the energy shift due to hydrostatic strain $E_{\mathrm{hyd}} \sim 3.5 \cdot 10^{-3}\mathcal{C}k\,[\mathrm{eV}\mu\mathrm{m}]$, is also proportional to the wave vector k (see derivation of Eq. (2.57)). For wave

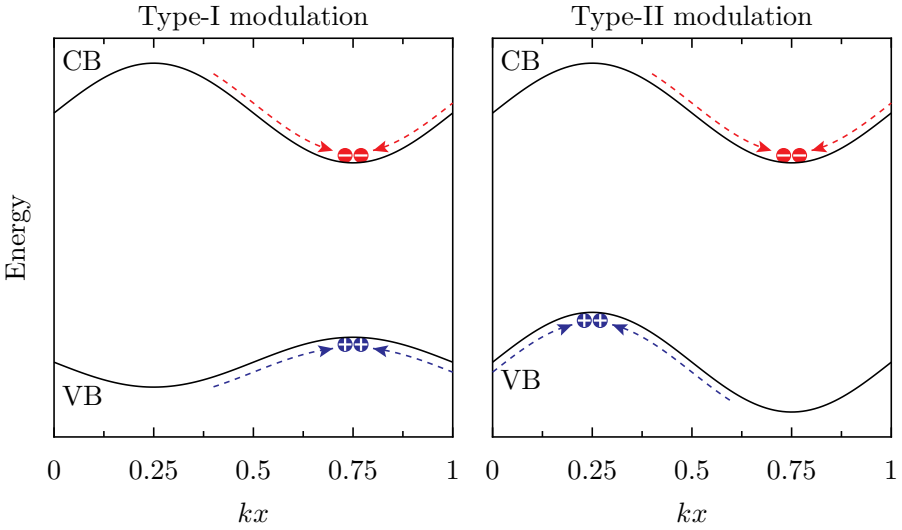

Figure 5.2.: Sketch of the modulation of the valence and conduction band. The type-I modulation has its origin in the band shift of the bands due to hydrostatic strain, whereas the type-II modulation is caused by the piezoelectric potential Φ_{SAW}.

lengths $\sim \mu$m discussed here, the type-II modulation is therefore about a factor 100 stronger than the type-I modulation, and will therefore be neglected in the following.

Due to on the tendency of electrons and holes to accumulate at distinct phase points we neglect in this chapter their mutual interaction. Moreover, the spatial isolation of the electrons and holes also suppresses a further, usually important, source of spin-relaxation, the Bir-Aronov-Pikus spin-relaxation mechanism [7], which depends directly on the interaction of electrons and holes.

Note that the results and the presentation of this section are partly adapted from Ref. [121].

5.1. Charge Dynamics

In this section we examine the influence of a SAW on the charge density where we encounter two distinct regimes, depending on the strength of the SAW (compare also Ref. [121]). The proper understanding of the spatio-temporal distribution of the carriers is essential for the description of the

spin dynamics. We therefore start with the drift-diffusion equation of the electrons, obtained from (4.121), where we neglect spin-charge coupling. According to (4.113), the charge carrier distribution is associated to the identity matrix. As a consequence, the commutator term in the covariant derivative (4.106) vanishes, and one obtains a drift-diffusion equation for an electron under the influence of an external electric field

$$\frac{\partial \rho^0}{\partial t} + \nabla \cdot (\mu \mathbf{E} \rho^0) - D \nabla^2 \rho^0 = 0. \tag{5.1}$$

Since we are considering a two-dimensional electron gas, the charge carriers can only be accelerated by the in-plane component of the electric field generated by the SAW. Keeping the convention established in Chap. 2, we assume a SAW propagating in $\mathbf{e}_x$-direction. The in-plane component of the piezoelectric field of the SAW can according to (2.56) be written as

$$\mathbf{E}(\mathbf{r}) = E\, \mathbf{e}_x \cos\left(kx - \omega t\right), \tag{5.2}$$

where in this chapter, analogously to the notation of Chap. 2, k, ω and v denote the wave vector, the frequency and the velocity of the SAW, respectively. Note that according to (2.56) and (2.57), the amplitude E of the electric field corresponds to the strength of the SAW, and influences therefore also the amplitude of the components of the strain tensor $\boldsymbol{\varepsilon}$.

Since there is no drift ($E_y = 0$) of the carriers perpendicular to the direction of the SAW, the solution of the drift-diffusion equation (5.1) factorizes, $\rho^0(\mathbf{r}, t) = NX(x, t)Y(y, t)$, where the constant

$$N = \int \mathrm{d}\mathbf{r} \rho^0(\mathbf{r}) \tag{5.3}$$

is given by the number of carriers in the two-dimensional quantum well plane. The motion of the carriers in y-direction is determined by the solution of the diffusion equation,

$$Y(y, t) = \frac{1}{\sqrt{4\pi D t}} \int_{-\infty}^{\infty} \mathrm{d}y' \exp\left[-\frac{(y - y')^2}{4Dt}\right] Y(y', 0). \tag{5.4}$$

For the motion in x-direction, we have to discriminate whether the dynamics of the carriers is governed by the drift term or the diffusion term, respectively. Assuming an initial spatial variation of the density on the length scale of the wavelength λ of the SAW, a simple estimation shows that if the driving electric field of the SAW is weak, $\mu E \ll Dk$, the dynamics in SAW direction is dictated by diffusion and $X(x, t)$ is similar

to $Y(y,t)$. Since in this limit of weak surface acoustic waves the dynamics of the carriers is rather unspectacular, in the following we are always interested in the case $\mu E \gg Dk$. In typical non-degenerate semiconductors the Einstein relation $D = \mu k_B T/e$ can be employed to estimate the diffusion constant [99, 122–125], implying that the condition $Dk \ll \mu E$ becomes independent of the mobility, namely reduces to $k_B T \ll eE/k$. As the magnitude of a typical piezoelectric field generated by a SAW is of the order of $\sim$ keV/cm [28] (compare also e.g. (2.56)), even at room temperature, the drift term dominates over the diffusion term. Hence, to start with, we neglect diffusion and the drift diffusion equation (5.1) reduces to a first order differential equation with solution

$$X(x,t) = \frac{v - \mu E \cos\left[k\,\xi(x,t)\right]}{v - \mu E \cos\left(kx - \omega t\right)} X\left(\xi(x,t), 0\right), \tag{5.5}$$

where

$$\xi(x,t) = \frac{2}{k} \arctan\left\{ \sqrt{\frac{v-\mu E}{v+\mu E}} \tan\left[\arctan\left(\sqrt{\frac{v+\mu E}{v-\mu E}} \tan\left(\frac{kx-\omega t}{2} \right) \right) + \frac{\sqrt{v^2 - (\mu E)^2}}{2v}\,\omega t \right] \right\}. \tag{5.6}$$

Note that $\xi(x, t=0) = x$.

Some care is needed because of the periodicity of $\tan\left[(kx - \omega t)/2\right]$, since for an arbitrary initial condition one has to choose the right branch in order to obtain the solution with the correct initial distribution. One can circumvent this difficulty by choosing an initial condition with all carriers located within one period. In Fig. 5.3 we therefore assumed a Gaussian initial distribution with a standard deviation of $\lambda/10$ and thus much smaller than the wavelength. Apparently, the solution of $X(x,t)$ (5.5) depends strongly on the ratio $\mu E/v$. For $\mu E < v$, the carriers are not fast enough to follow the SAW, yet they flow from one minimum to the next, with the average velocity

$$\overline{v} = v - \sqrt{v^2 - (\mu E)^2},\ \mu E < v. \tag{5.7}$$

The situation is quite different for $\mu E > v$, when the charge carriers are fast enough to follow the SAW, i.e. they are "surfing". This means that they are subjected to a stationary potential in a reference frame moving with the SAW, and at the point $x_0 = \arccos\left(v/\mu E\right)/k$ in this frame they

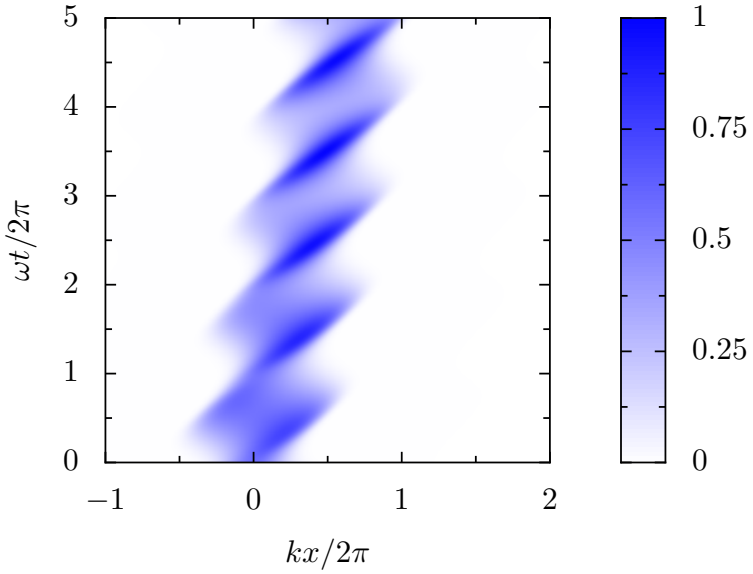

Figure 5.3.: Motion of the charge carriers $X(x,t)$ in x-direction with $\mu E/v = 0.5$. Figure adapted from Ref. [121].

move with its velocity. Since the potential is periodic, there is such a point in every period. Independently of the initial distribution $X(x,0)$, the carriers flow towards the point x_0 corresponding to their period, until they reach a stationary distribution. Thus, for $\mu E > v$ the solution (5.5) converges to $X(x,t) \sim \delta(k(x-x_0) - \omega t)$, and the carrier density $X(x,t)$ is concentrated in an infinitely small wire parallel to the wave front. The assumption of a spatial extension of the carrier density of the order of the wavelength is then no longer justified. This implies that the diffusion term cannot be neglected any further. Switching to the reference frame of the moving SAW, the charge density distribution becomes stationary, and the drift term is cancelled by the diffusion term. Since the charge current vanishes in the moving frame,

$$X(x,t) = \exp\left[\frac{\mu E \sin(kx - \omega t) - v(kx - \omega t)}{Dk}\right], \tag{5.8}$$

which is sharply peaked at $kx - \omega t = kx_0$, is a solution of (5.1). Hence for $|kx - \omega t - kx_0| \ll 1$, $X(x,t)$ can be approximated by a Gaussian distribution,

$$X(x,t) \approx \frac{e^{-\frac{(kx-\omega t-kx_0)^2}{2\sigma^2}}}{\sqrt{2\pi}\sigma}, \tag{5.9}$$

with standard deviation

$$\sigma = \sqrt{Dk/\sqrt{(\mu E)^2 - v^2}}. \tag{5.10}$$

Note that the exact solution (5.8) of the continuity equation (5.1) does not depend on the sign of μ. In other words, this solution describes the dynamics of electrons as well as that of holes, provided both are in the surfing regime, i.e., $\mu_\mathrm{e} E$, $\mu_\mathrm{h} E > v$. In this case, the distance between the two pockets of carriers is

$$\Delta x_0 = \frac{\arccos\left(v/\mu_\mathrm{h} E\right) - \arccos\left(v/\mu_\mathrm{e} E\right)}{k} \tag{5.11}$$

and therefore confirms the assumption of spatially separated electron and hole densities.

We will exploit the fact that in the "surfing" regime the charge carriers are concentrated in narrow wires in the following discussion of the spin dynamics. In particular, such a confinement is able to enhance the spin-lifetime.

5.2. Spin dynamics due to Rashba & Dresselhaus spin-orbit interaction

As indicated by the title of this section, we neglect for the moment the spin-orbit interaction caused by the SAW. The remaining spin-orbit interaction is then given by the Rashba and the Dresselhaus Hamiltonians (3.159) and (3.151), respectively. The non-vanishing components of the $SU(2)$ vector potential $\boldsymbol{\mathcal{A}} = \boldsymbol{\mathcal{A}}^x \sigma^x + \boldsymbol{\mathcal{A}}^y \sigma^y + \boldsymbol{\mathcal{A}}^z \sigma^z$ (compare (4.2)) are therefore given by

$$(\mathcal{A})_y^x = 2m(\beta + \alpha) \equiv \hbar m \alpha_+, \tag{5.12}$$

$$(\mathcal{A})_x^y = 2m(\beta - \alpha) \equiv \hbar m \alpha_-. \tag{5.13}$$

For the discussion of the spin dynamics we come back to the "continuity" equation (4.121), where we already inserted the current (4.122) and used the definition of the covariant derivative (4.106).

$$\frac{\partial \rho}{\partial t} + \nabla \cdot (\mu \mathbf{E} \rho) - D\nabla^2 \rho = \frac{\mathrm{i}}{\hbar} \left[\boldsymbol{\mathcal{A}}, 2D\nabla\rho - \mu \mathbf{E} \rho\right] - \frac{D}{\hbar^2} \left[\boldsymbol{\mathcal{A}}, [\boldsymbol{\mathcal{A}}, \rho]\right] \tag{5.14}$$

For the charge component ρ^0, which is proportional to the identity matrix, we immediately retrieve the equation of motion for the charge carriers

(5.1). As already mentioned in the previous chapter, the quotes in the phrase "continuity" equation become apparent by considering the right-hand-side of the above equation. The first term, linear in $\boldsymbol{\mathcal{A}}$, describes a precession of the spins, whereas the second term, quadratic in the $SU(2)$ vector potential, is responsible for the relaxation of the spin density. Using the commutator relation $[\sigma^a, \sigma^b] = 2\mathrm{i}\epsilon_{abc}\sigma^c$ with the Levi-Civita symbol ϵ_{abc}, we obtain the Bloch equations for the components of the spin density $(a = x, y, z)$

$$\partial_t \rho^a + \mu \nabla \cdot \mathbf{E} \rho^a - D\nabla^2 \rho^a = -\frac{2}{\hbar}\, \epsilon_{abc}\, \boldsymbol{\mathcal{A}}^b \cdot (2D\nabla - \mu \mathbf{E})\rho^c - \Gamma^{ab}\rho^b, \quad (5.15)$$

where we defined the spin relaxation matrix

$$\Gamma^{ab} = 4\frac{D}{\hbar^2}\left(\sum_i \boldsymbol{\mathcal{A}}^i \cdot \boldsymbol{\mathcal{A}}^i \delta_{ab} - \boldsymbol{\mathcal{A}}^a \cdot \boldsymbol{\mathcal{A}}^b\right). \quad (5.16)$$

As the diffusion constant D (4.123) is proportional to the scattering time τ, the spin lifetime increases with decreasing scattering time. Remembering the effective Dresselhaus and Rashba spin-orbit Hamiltonians (3.151) and (3.159), this behaviour can be quite easily understood. Between two scattering events, an electron moves linearly and its spin precesses around the internal effective "magnetic field" $\mathbf{b} = \mathbf{p} \cdot \boldsymbol{\mathcal{A}}^a/2m$. As we assume weak spin-orbit coupling $\mathbf{b} \ll \hbar/\tau$ compared to the scattering rate, the precession angle $\sim |\mathbf{b}|\tau$ between two scattering events is small. After each scattering event, the electron changes its direction of motion and therefore also the direction of the internal "magnetic field" $\mathbf{b}$. Thus, the random motion of the electrons is directly transferred to the spin dynamics, which therefore also resembles a diffusion process. The spin relaxation due to the random motion of the charge carriers is known as the Dyakonov-Perel relaxation mechanism [9, 126].

For a homogeneous spin distribution and without a SAW, one can immediately determine the spin lifetimes from the eigenvalues of the inverse spin relaxation matrix Γ^{-1}. In our situation of Rashba and Dresselhaus spin-orbit interaction within a (001)-quantum well the relaxation matrix is, for our choice of coordinates, diagonal and its eigenvalues are:

$$\Gamma_x = 4Dm^2\alpha_-^2 \quad (5.17)$$

$$\Gamma_y = 4Dm^2\alpha_+^2 \quad (5.18)$$

$$\Gamma_z = 4Dm^2(\alpha_-^2 + \alpha_+^2). \quad (5.19)$$

Depending on the sign and magnitude of the Rashba constant α, for the first and the second equation there is in principle the special case of $\beta = \alpha$ or $\beta = -\alpha$ and hence $\Gamma^{xx} = 0$ or $\Gamma^{yy} = 0$, respectively. Such a case of a vanishing relaxation rate implies an infinite spin lifetime. Although this limit, known as persistent spin helix, can be realized in experiments [127, 128], we here consider the more general case $|\alpha| \neq \beta$.

5.2.1. Homogeneous initial conditions

The spin dynamics depends strongly on the initial conditions. In this subsection we consider an experimental setup where a short laser pulse homogeneously polarizes the complete surface. In the surfing regime electrons and holes are strongly localized and effectively spatially separated, see Eq. (5.11), and are transported—along with their spins—across the sample. The description of the spin dynamics is considerably simplified by switching to a reference frame co-moving with the SAW, $x \to x - vt - x_0$. A change to such a reference frame leads to an additional term in the continuity equation which acts like an additional internal magnetic field,

$$\partial_t \rho + \widetilde{\nabla}\mathbf{j} + \mathrm{i}[\mathbf{v}\boldsymbol{\mathcal{A}}, \rho] = 0. \tag{5.20}$$

A further simplification can be achieved by applying the following $SU(2)$ gauge transformation:

$$\boldsymbol{\mathcal{A}} \to U^\dagger \boldsymbol{\mathcal{A}} U + iU^\dagger \nabla U,\ U = \exp\left(\mathrm{i}x\mathcal{A}_x\right). \tag{5.21}$$

In this gauge, the covariant derivative $\tilde{\partial}_x \to \partial_x$ is diagonal in spin space but leads to an x-dependent vector potential $\mathcal{A}_y(x)$. However, since the charge carriers are Gaussian-distributed at the origin in the co-moving system with $\sigma \ll 1/2m\alpha_-$, one can neglect the x-dependence of the vector potential, hence $\mathcal{A}_y(x) \approx \mathcal{A}_y(0)$.

The time-dependence of the spin density in the presence of the SAW is governed by an effective relaxation matrix γ, whose (complex) eigenvalues are given by

$$\gamma_{x,z} = 2Dm^2\alpha_+^2 \pm 2\,\mathrm{i}\sqrt{v^2m^2\alpha_-^2 - D^2m^4\alpha_+^4}, \tag{5.22}$$

$$\gamma_y = 4Dm^2\alpha_+^2. \tag{5.23}$$

Since all carriers move with the same velocity v, the real part of these eigenvalues is related to the spin decay length,

$$L_s = \frac{v}{\Re(\gamma)}, \tag{5.24}$$

whereas the imaginary part determines the spatial precession length [1],

$$\lambda = \frac{2\pi v}{\Im(\gamma)}. \tag{5.25}$$

For a SAW moving in y-direction we proceed in the same way. The carriers are then concentrated in a small wire parallel to the x-axis. In this case one finds

$$\gamma_x = 4Dm^2\alpha_-^2, \tag{5.26}$$

$$\gamma_{y,z} = 2Dm^2\alpha_-^2 \pm 2\,\mathrm{i}\sqrt{v^2m^2\alpha_+^2 - D^2m^4\alpha_-^4} \tag{5.27}$$

which is obtained from Eqs. (5.22) and (5.23) by interchanging x and y as well as $+$ and $-$.

Comparing the real parts with Eqs. (5.17) and (5.18), one finds a maximal enhancement of the spin lifetime by a factor of $2(\alpha_-/\alpha_+)^2$ for the x direction, and $2(\alpha_+/\alpha_-)^2$ for the y direction ("motional narrowing"). Note that the real parts of $\gamma_{x/z}$ and $\gamma_{y/z}$ are by a factor of two smaller than their perpendicular counterparts, γ_y and γ_x, respectively. These perpendicular counterparts, describing the relaxation of spins parallel to the SAW wave front, are not affected by the SAW in the simple case of a homogeneous spin density.

Specifically, we have calculated numerically the x-spin density for a SAW travelling in x-direction and for different E values. For simplicity, we set $\alpha_+ = \alpha_-$, which in the surfing regime implies a spin lifetime increase by a factor of two. Not being interested in the spatial variation of the spin density, we consider the spin polarization $P_s = |\mathbf{P}_s|$, by integrating the spin density over the whole surface. From the Bloch equations (5.15) one sees that, without a SAW, the spin polarization decays exponentially with the spin scattering rate (5.17). Hence we define the average spin lifetime by

$$\langle\tau\rangle = \frac{\int_0^\infty tP_s\,\mathrm{d}t}{\int_0^\infty P_s\,\mathrm{d}t}. \tag{5.28}$$

For the numerical analysis, we started at $t = 0$ with a Gaussian distribution with a standard deviation $\sigma \gg 1/2m\alpha_-$, polarized in x direction and in z direction, respectively. The spin lifetime as a function of the ratio $\mu E/v$ is shown in Fig. 5.4, where the expectation value $\langle\tau\rangle$ is normalized to the corresponding spin lifetime $\tau_0 = \Gamma_x^{-1}$ without SAW, cf. Eq. (5.17). As one approaches the surfing regime $\mu E > v$ the spin lifetime converges to the expected value $2(\alpha_-/\alpha_+)^2$.

[1] The additional factor 2π corrects the typographical error of Ref. [121]

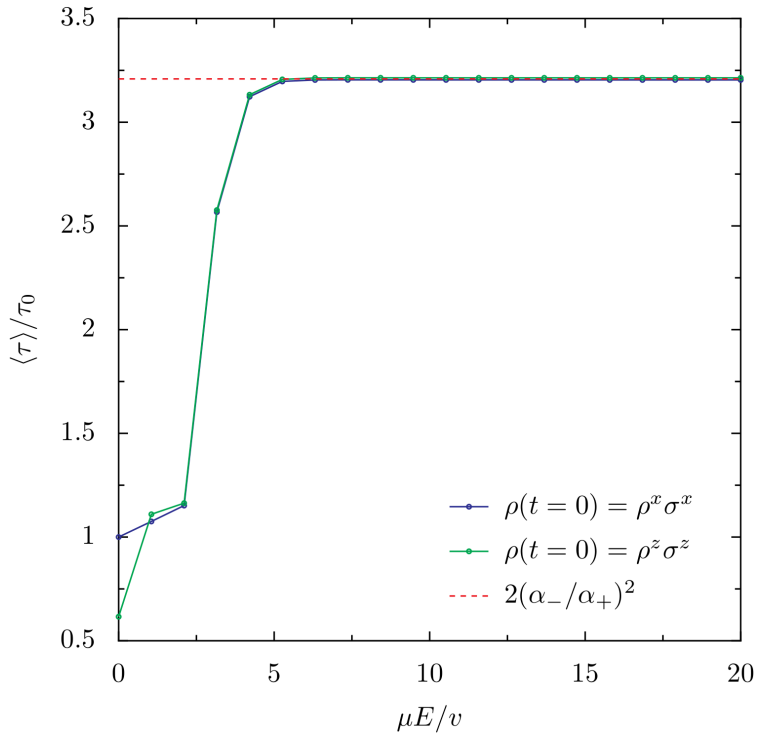

Figure 5.4.: Numerical results for the increase of the spin lifetime $\langle\tau\rangle$ due to a SAW. The spin lifetime is normalized by $\tau_0 = \Gamma_x^{-1}$, cf. Eq. (5.17).

5.2.2. Inhomogeneous initial conditions

So far we have discussed the spin dynamics of an initially homogeneous spin distribution, for which case there is no spin current parallel to the SAW wave front. However this assumption is not justified in experiments where the initial spin distribution is created by, say, a focused laser beam. Again, without loss of generality, we consider a SAW moving in x-direction.

While for the homogeneous case the spins are precessing only around the axis parallel to the SAW wave front, now there will be diffusion along the wave front, and hence they will also rotate around the SAW propagation direction. As a consequence, the spins along the narrow moving wire will not have the same orientation. In order to deal with this additional precession we employ the following ansatz for the spin density:

$$\rho^a = \rho^0(r, \varphi, t)\, \eta^a(\varphi, t), \tag{5.29}$$

where $r = 2m\sqrt{\alpha_-^2 x^2 + \alpha_+^2 y^2}$ denotes the renormalized (dimensionless) radius, and $\varphi = \arctan[\alpha_+ y/(\alpha_- x)]$. The carrier density in the surfing regime, $\rho^0(r, \varphi, t)$, was already determined in Sec. 5.1, with $X(x,t)$ given in (5.8); according to Eq. (5.4) the carrier density along the y-axis for a Gaussian initial distribution with standard deviation y_0 reads

$$Y(y,t) = \frac{1}{\sqrt{2\pi(2Dt + y_0^2)}} \exp\left[-\frac{y^2}{2(2Dt + y_0^2)}\right]. \tag{5.30}$$

Instead of switching to the SAW co-moving reference frame as in the homogeneous case, we stay in the laboratory frame but perform again a gauge transformation,

$$\boldsymbol{\mathcal{A}} \to U^\dagger \boldsymbol{\mathcal{A}} U + iU^\dagger \nabla U,\ U = \exp\left[\mathrm{i}(x - x_0 - vt)\mathcal{A}_x\right], \tag{5.31}$$

since as above all relevant spin dynamics takes place in a small wire parallel to the SAW wave front. With the ansatz (5.29), and by neglecting terms $\mathcal{O}(r^{-1})$, the continuity equation (4.121) reads

$$\partial_t \eta - \mathrm{i}\,\frac{v}{\cos\varphi}\left[\mathcal{A}_x(\varphi), \eta\right] + D\left[\mathcal{A}_y, [\mathcal{A}_y, \eta]\right] = 0, \tag{5.32}$$

where $\mathcal{A}_x(\varphi) = \exp\left(-\mathrm{i}\frac{\varphi}{2}\sigma^z\right)\mathcal{A}_x \exp\left(\mathrm{i}\frac{\varphi}{2}\sigma^z\right)$ is the vector potential rotated around the z-axis. The second term in Eq. (5.32) leads to spin precession around the φ-dependent vector potential $\mathcal{A}_x(\varphi)$, whereas the third term is responsible for the relaxation of the spin components perpendicular to the x-axis. The Bloch equations now read

$$\partial_t \eta^a = -\gamma(\varphi)^{ab}\eta^b, \tag{5.33}$$

with the φ-dependent effective relaxation matrix

$$\gamma(\varphi) = \begin{pmatrix} 0 & 0 & 2mv\alpha_- \\ 0 & 4Dm^2\alpha_+^2 & 2mv\alpha_- \tan\varphi \\ -2mv\alpha_- & -2mv\alpha_- \tan\varphi & 4Dm^2\alpha_+^2 \end{pmatrix}. \tag{5.34}$$

Assuming that the temporal resolution is not high enough to measure the time-dependence of the spin density directly (see, e.g., Ref. [111]), we characterize the additional rotation of the spins due to the diffusion parallel to the SAW wave front by the time-integrated spin density: note that all spins are confined within a narrow wire, and the spin density

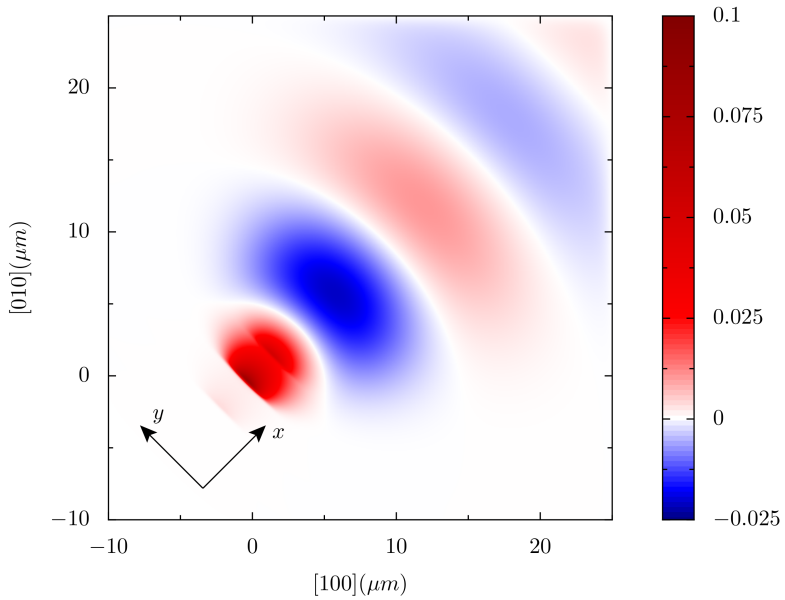

Figure 5.5.: Time-integrated spin density, $\overline{s}^z$, for a SAW moving in [110] direction. Figure adapted from Ref. [121].

vanishes everywhere but for $x - x_0 \approx vt$. For the time-integrated spin density we therefore obtain

$$\overline{s}^a = \int_0^\infty \rho^a \, \mathrm{d}t \simeq a_0 Y\left(y, (x - x_0)/v\right) \eta^a\left(r, \varphi\right). \tag{5.35}$$

The results presented in Figs. 5.5 and 5.6 were obtained by calculating numerically the time-dependence of the spin density ρ^z, assuming at $t = 0$ a Gaussian distribution with standard deviation of 1 μm. Specifically, Figs. 5.5 and 5.6 show the time-integrated spin density for a SAW moving in x- and y-direction, respectively. We have chosen parameters comparable to the experimental ones[111], namely $2m\alpha/\hbar = 0.02\,\mu\mathrm{m}^{-1}$, $2m\beta/\hbar = 0.17\,\mu\mathrm{m}^{-1}$, $D = 30\,\mathrm{cm}^2/\mathrm{s}$, and $v = 2.9 \times 10^5\,\mathrm{cm/s}$. The elliptical shape of the time-integrated spin density, which is a consequence of the φ-dependence of $\mathcal{A}_x(\varphi)$, is clearly visible in both figures, in remarkable agreement with the observed behaviour [111].

The time-integrated s^z takes a very simple form along certain directions. For example, along the x-direction for $y = 0$ (recall that our coordinate choice means $\hat{\mathbf{x}} \parallel [110]$, $\hat{\mathbf{y}} \parallel [\bar{1}10]$) we find

$$\overline{s}^z = a_0 \frac{\exp\left(-(x - x_0)/L_{s,110}\right)}{\sqrt{y_0^2 + 2D(x - x_0)/v}} \cos\left[\frac{2\pi(x - x_0)}{\lambda_{110}}\right], \tag{5.36}$$

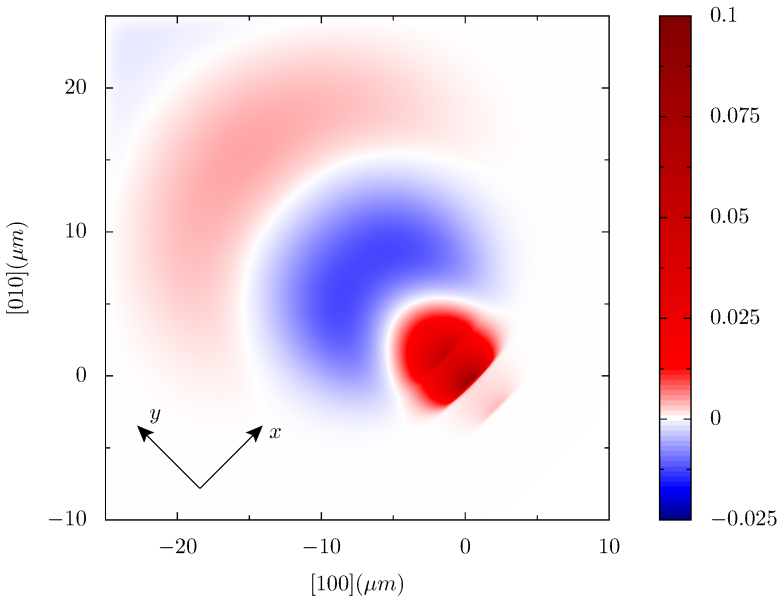

Figure 5.6.: Time-integrated spin density, $\overline{s}^z$, for a SAW moving in $[\bar{1}10]$ direction. Figure adapted from Ref. [121].

where

$$L_{s,110} = \frac{v}{2Dm^2\alpha_+^2},\ \lambda_{110} = \frac{\pi v}{\sqrt{v^2m^2\alpha_-^2 - D^2m^4\alpha_+^4}}; \tag{5.37}$$

this is plotted in Fig. 5.7, upper panel (solid black line). The constant a_0 is fixed by fitting the numerical data, as discussed below. For a SAW propagating in y direction (for $x = 0$), one finds a similar expression, with the substitutions $x, L_{s,110}, \lambda_{110} \to y, L_{s,\bar{1}10}, \lambda_{\bar{1}10}$:

$$L_{s,\bar{1}10} = \frac{v}{2Dm^2\alpha_-^2},\ \lambda_{\bar{1}10} = \frac{\pi v}{\sqrt{v^2m^2\alpha_+^2 - D^2m^4\alpha_-^4}}, \tag{5.38}$$

compare Fig. 5.7, lower panel (solid black line). In both propagation directions the numerical and analytical data are in good agreement for $x,\ y \gtrsim 3\,\mu$m. The reason for the deviation near the origin is that for the chosen parameters, the standard deviation 1 μm of the initial Gaussian is only marginally smaller than the SAW wavelength $2\pi/k = 2.55\,\mu$m, leading to two small wires instead of one. This causes the peak for $x,\ y$ close to this value. The spin dynamics is, however, the same in both wires. We emphasize that the dependence of the spin precession length on the direction of motion of the SAW is in very good agreement with the experimental observations [111] .

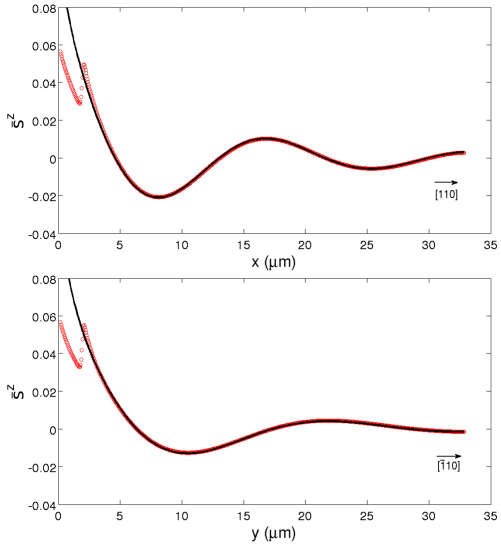

Figure 5.7.: Time-integrated spin density, $\overline{s}^z$, along the [110] and [$\bar{1}$10] directions. The red circles represent the numerical solution of Eq. (4.121). The black solid line shows the analytical expression (5.36). Figure adapted from Ref. [121].

5.3. Spin dynamics including SAW-induced spin-orbit interaction

As discussed in the previous section, the confinement of the charge carriers in narrow wires causes a propagation direction dependent increase of the spin lifetime. Considering, for example, a SAW propagating in [110] direction, we found in the limit of $\mu E/v \gg 1$ an enhancement of the spin-lifetime by a factor of ~ 3.2 (compare Fig. 5.7). Nevertheless, an increase of the strength of the SAW implies also a gain of relevance of the SAW dependent spin-orbit interactions $\hat{H}^{\mathbf{k}\boldsymbol{\varepsilon}1}$, $\hat{H}^{\mathbf{k}\boldsymbol{\varepsilon}2}$ and $\hat{H}^{R}_{\mathrm{SAW}}$. In Chap. 2 the strength of the SAW was characterized by the dimensionless constant $\mathcal{C}$ (see, e.g., (2.56)). Assuming a mobility of $\mu = 10^4\,\mathrm{cm^2V^{-1}s^{-1}}$ [20, 99], we are able to choose for the dimensionless constant $\mathcal{C} = \mu E/v$.

In Chap. 2 we calculated for a SAW, propagating in $x \parallel [110]$ direction, the components of the strain tensor $\boldsymbol{\varepsilon}$ (2.57). Inserting these components into the strain dependent spin-orbit Hamiltonians $\hat{H}^{\mathbf{k}\boldsymbol{\varepsilon}1}$ (3.154) and $\hat{H}^{\mathbf{k}\boldsymbol{\varepsilon}2}$ (3.155) (remind the transition from the wave vector $\hbar\mathbf{k} \to \mathbf{p}$ of Chap. 4)

we obtain

$$\hat{H}^{\mathbf{k}\epsilon 1} = \frac{D}{\hbar} 43 \cdot 10^{-7} \mathcal{C} \sin(kx - \omega t)(p_y \sigma^x + p_x \sigma^y), \tag{5.39}$$

and

$$\hat{H}^{\mathbf{k}\epsilon 2} = \frac{C_3}{2\hbar} \cdot 10^{-7} \mathcal{C} \Big[12 \sin(kx - \omega t)(p_y \sigma^x - p_x \sigma^y) \\ -2.0 \cos(kx - \omega t) p_y \sigma^z \Big]. \tag{5.40}$$

Here, the coupling constant D should not be confounded with the diffusion constant!

With the component of the piezoelectric field, E_z, perpendicular to the surface (2.56), the SAW dependent Rashba term $\hat{H}^R_{\mathrm{SAW}}$ reads:

$$\hat{H}^R_{\mathrm{SAW}} = r_{cc} \cdot 3.4 \, \frac{\mathrm{kV}}{\mathrm{m}} \mathcal{C} \sin(kx - \omega t)(p_y \sigma^x - p_x \sigma^y). \tag{5.41}$$

Within the geometry of a (001) quantum well, apparently, the first SAW dependent Hamiltonian $\hat{H}^{\mathbf{k}\epsilon 1}$ acts similar to the Dresselhaus term, whereas $\hat{H}^{\mathbf{k}\epsilon 2}$ describes a Rashba-like spin-orbit Hamiltonian with an additional term proportional to σ^z. This motivates the following definitions of effective SAW dependent Rashba and Dresselhaus constants:

$$\alpha_{\mathrm{S}} = 6.0 \frac{C_3}{\hbar} \cdot 10^{-7} + 3.4 r_{cc} \, \frac{\mathrm{kV}}{\mathrm{m}} = 9.6 \cdot 10^{-1} \frac{\mathrm{m}}{\mathrm{s}}, \tag{5.42}$$

$$\beta_{\mathrm{S}} = 43 \frac{D}{\hbar} \cdot 10^{-7} = 2.2 \cdot 10^{-2} \frac{\mathrm{m}}{\mathrm{s}}. \tag{5.43}$$

The additional constant

$$\frac{C_3}{\hbar} \cdot 10^{-7} = 1.2 \cdot 10^{-1} \frac{\mathrm{m}}{\mathrm{s}}, \tag{5.44}$$

describes a coupling to σ^z.

Comparing α_{S} with β_{S}, the SAW-induced spin-orbit interaction is obviously more of the type of Rashba spin orbit interaction.

To summarize all involved spin-orbit interactions, we express the $SU(2)$ vector potential $\boldsymbol{\mathcal{A}} = \boldsymbol{\mathcal{A}}^D + \boldsymbol{\mathcal{A}}^R + \boldsymbol{\mathcal{A}}^D_{\mathrm{S}} + \boldsymbol{\mathcal{A}}^R_{\mathrm{S}} + \boldsymbol{\mathcal{A}}^\delta_{\mathrm{S}}$ as a set of matrices:

$$\boldsymbol{\mathcal{A}}^D + \boldsymbol{\mathcal{A}}^R = \hbar m \begin{pmatrix} 0 & \alpha_- & 0 \\ \alpha_+ & 0 & 0 \end{pmatrix}, \tag{5.45}$$

$$\boldsymbol{\mathcal{A}}_{\mathrm{S}}^{D}(x,t)+\boldsymbol{\mathcal{A}}_{\mathrm{S}}^{R}(x,t)=\hbar m\begin{pmatrix}0 & \alpha_{\mathrm{S}-} & 0\\ \alpha_{\mathrm{S}+} & 0 & 0\end{pmatrix}\mathcal{C}\sin(kx-\omega t), \tag{5.46}$$

and

$$\boldsymbol{\mathcal{A}}_{\mathrm{S}}^{\delta}(x,t)=\hbar m\begin{pmatrix}0 & 0 & 0\\ 0 & 0 & \delta_{\mathrm{S}}\end{pmatrix}\mathcal{C}\cos(kx-\omega t). \tag{5.47}$$

The constants, $\alpha_{\mathrm{S}\pm}=\beta_{\mathrm{S}}\pm\alpha_{\mathrm{S}}$, and, $\delta=10^{-7}C_3/2\hbar^2$, are defined analogously to $\alpha_{\pm}$. Comparing the constants $\alpha_{\mathrm{S}\pm}$ and δ with the constants of the Rashba and Dresselhaus spin-orbit interaction used in the section above, $\alpha=18\,\mathrm{m/s}$, and, $\beta=150\,\mathrm{m/s}$, for a weak SAW $\mathcal{C}<1$ the additional SAW-induced spin-orbit interactions are negligible. Hence, we will consider in the following only the high-field regime $\mathcal{C}\gg 1$.

A notable simplification was achieved in Subsec. 5.2.1 for homogeneous initial conditions by switching to the co-moving reference frame combined with the SU gauge transformation (5.21). The significant advantage of this gauge transformation was the diagonal structure of the covariant derivation $\tilde{\partial}_x=\partial_x$ in spin space. For a position-dependent $SU(2)$ vector potential this is in general, however, no longer the case and spatial derivatives of the vector potential have to be taken into account.

Nevertheless, as in the co-moving reference frame the charge carriers are concentrated in narrow wires at $x=0$, the spins are only susceptible to the vector potential in the vicinity of the origin. For a width of the wire of the order σ (5.10), much smaller than the wavelength λ, we can therefore approximate the vector potential by $\boldsymbol{\mathcal{A}}(x)\approx\boldsymbol{\mathcal{A}}(0)$. Hence, in analogy to (5.21), we can still apply to the gauge transformation

$$\boldsymbol{\mathcal{A}}\to U^{\dagger}\boldsymbol{\mathcal{A}}U+iU^{\dagger}\nabla U,\ U=\exp\left(\mathrm{i}x\mathcal{A}_x(0)\right), \tag{5.48}$$

and neglect the spatial change of spin-orbit interaction.

With $x_0=\arccos(1/\mathcal{C})$ (see Sec. 5.1) we obtain for the $SU(2)$ vector potentials (5.46) and (5.47) in the co-moving frame:

$$\boldsymbol{\mathcal{A}}_{\mathrm{S}}^{D}(0)+\boldsymbol{\mathcal{A}}_{\mathrm{S}}^{R}(0)=\sqrt{\mathcal{C}^2-1}\hbar m\begin{pmatrix}0 & \alpha_{\mathrm{S}-} & 0\\ \alpha_{\mathrm{S}+} & 0 & 0\end{pmatrix}, \tag{5.49}$$

and

$$\boldsymbol{\mathcal{A}}_{\mathrm{S}}^{\delta}(0)=\hbar m\begin{pmatrix}0 & 0 & 0\\ 0 & 0 & \delta_{\mathrm{S}}\end{pmatrix}. \tag{5.50}$$

For a homogeneous initial spin distribution the procedure introduced in Sec. 5.2.1 remains the same, and we obtain analogously to (5.22) and

(5.23) the effective relaxation matrix:

$$\gamma_{x,z} = 2Dm^2\left[\tilde{\alpha}_+^2(\mathcal{C}) + \delta^2\right] \pm 2\mathrm{i}\sqrt{v^2m^2\tilde{\alpha}_-^2(\mathcal{C}) - D^2m^4\left[\tilde{\alpha}_+^2(\mathcal{C}) + \delta^2\right]^2}, \tag{5.51}$$

$$\gamma_y = 4Dm^2\tilde{\alpha}_+^2(\mathcal{C}), \tag{5.52}$$

where we used the abbreviations

$$\tilde{\alpha}_\pm(\mathcal{C}) = \alpha_\pm + \alpha_{\mathrm{S}\pm}\sqrt{\mathcal{C}^2 - 1}. \tag{5.53}$$

The spin lifetime, which is again related to the inverse of the real part

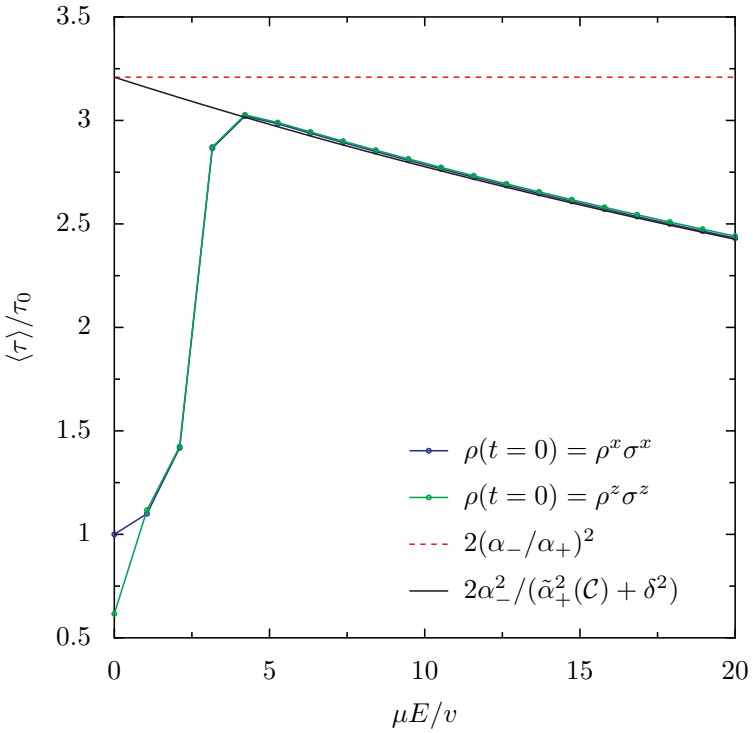

Figure 5.8.: Numerical results for the increase of the spin lifetime $\langle\tau\rangle$ due to a SAW, while taking additional spin-orbit interactions (s.o.i.) due to the SAW into account. For the calculation we assumed initially x- and z-polarized spin densities with Gaussian distribution, respectively. The spin lifetime is normalized by $\tau_0 = \Gamma_x^{-1}$, cf. Eq. (5.17).

of the effective relaxation rates (5.51), depends therefore on the strength

of the SAW. In the limit of strong SAW-strength $\mathcal{C} \gg 1$, the average spin lifetime of an, e.g., initially x-polarized spin density becomes:

$$\tau_x = \frac{1}{2Dm^2\left[\tilde{\alpha}_+^2(\mathcal{C}) + \delta^2\right]} \tag{5.54}$$

Thus, after an initial increase, the spin lifetime declines for $\mathcal{C} \gg 1$ due to the additional $\mathcal{C}$-dependent spin-orbit interactions induced by the SAW. As the width of the wire σ (5.10) depends on $\mathcal{C}$, as well as on D, the condition $\sigma \ll \lambda$ for the approximation (5.54) is influenced also by the diffusion constant. For $D = 15\,\mathrm{cm}^2/\mathrm{s}$, e.g., the maximum of the average spin lifetime is reached for $\mathcal{C} \approx 5$ (see Fig. 5.8).

For the transition of the relaxation rates (5.51) to the rates of a SAW propagating in y-direction some care is needed. Whereas (5.27) was easily derived by a replacement of + by -, now the different phase relation between the components of the displacement $\mathbf{u}(y,t)$ and the piezoelectric field $\mathbf{E}(y,t)$ have to be regarded. According to (2.48), the value of e of the piezoelectric tensor changes its sign for a SAW propagating in $[\bar{1}10]$-direction. As all other quantities remain the same, we are able to re-use the solution for the piezoelectric field $\mathbf{E} \to \mathbf{E}$ (2.56), and the strain tensor (2.57) by replacing $\boldsymbol{\varepsilon} \to -\boldsymbol{\varepsilon}$. This change of the sign can easily be included in the above expressions (5.51) and (5.51) and by switching the sign of the coupling constants $\alpha_{\mathrm{S}\pm} \to -\alpha_{\mathrm{S}\pm}$.

Hence, in addition to the replacement of the indices, $+ \leftrightarrow -$, of $\alpha_\pm$ and $\alpha_{\mathrm{S}\pm}$, for a SAW propagating in y-direction, Eq. (5.53) has to be modified by

$$\tilde{\beta}_\pm(\mathcal{C}) = \alpha_\pm - \alpha_{\mathrm{S}\pm}\sqrt{\mathcal{C}^2 - 1}, \tag{5.55}$$

and the lifetime of the spins is given by:

$$\tau_y = \frac{1}{2Dm^2\left[\tilde{\beta}_-^2(\mathcal{C}) + \delta^2\right]}. \tag{5.56}$$

Regarding the above values for α_{S} and β_{S}, the Rashba-like term of the strain contribution dominates and $\alpha_{\mathrm{S}+} \approx -\alpha_{\mathrm{S}-} \approx \alpha_{\mathrm{S}}$, or equivalently $\tilde{\alpha}_\pm(\mathcal{C}) \approx \tilde{\beta}_\pm(\mathcal{C}) \approx \alpha_\pm + \alpha_{\mathrm{S}}\sqrt{\mathcal{C}^2 - 1}$. Therefore, for a SAW propagating in y-direction, the additional SAW-induced spin-orbit contributions (5.46) and (5.47) also lead to a reduction of the spin lifetime with increasing acoustic power $\mathcal{C}$.

6. Conclusion and outlook

For the development of new spintronic devices, a fundamental understanding of charge as well as spin dynamics is of great importance. In this work we investigated the influence of surface acoustic waves on the two-dimensional electron gas of a quantum well, where SAWs prove to be a powerful and versatile concept for the control and manipulation of the spin degrees of freedom. One of the most important aspects in the search for future spintronic devices represents the desired prolongation of the spin lifetime. The main focus of this work was therefore to study the influence of a SAW on the spin relaxation rate. As an important result, we found a strong dependence of the spin lifetime on:

- the growth direction of the quantum well,
- the propagation direction of the SAW,
- initial conditions of the spin polarization,
- the acoustic power of the SAW.

The origin of the spatial anisotropy of the relaxation rate lies in the properties of the underlying material. After a basic introduction of surface acoustic waves in Chap. 2, we therefore studied in Chap. 3 the various sources of spin-orbit couplings in semiconductors of zinc blende structure. For this purpose, we utilized the $\mathbf{k} \cdot \mathbf{p}$ theory in conjunction with the theory of invariants to obtain effective Hamiltonians. Specifically for the derivation of strain dependent spin-orbit interactions the formulation in terms of symmetrized quantities proved to be advantageous.

Subsequently, we introduced the basic concepts of quasiclassical quantum transport theory in Chap. 4. The Green's functions within the Keldysh formalism turned out to be especially suited to transfer the microscopic description of electrons and spins by effective Hamiltonians to a mesoscopic characterization by charge and spin densities.

With the help of these densities we finally discussed in Chap. 5 the influence of a SAW on the relaxation rate of a spin density within a (001)

quantum well. For the theoretical description of the spin dynamics, we assumed an initially polarized spin density generated by a short laser pulse. The temporal evolution of the spin density turned out to be strongly influenced by the initial conditions. We therefore compared an initially homogeneously polarized spin density to the one generated by a laser pulse with diameter of the order of the SAW wavelength. For $\mu E/v \gg 1$ the charge carriers are concentrated in narrow wires. The increase of the spin lifetime can thus be related to the motional narrowing effect, which effectively hampers the Dyakonov-Perel spin-relaxation mechanism. The analytical results as well as the numerical calculations for GaAs agree excellently with the measured results of Ref. [111].

As a last point, we investigated the interplay between the spin lifetime enhancement due to the motional narrowing effect, and the influence of additional SAW-induced sources of spin-orbit interaction on the relaxation rate. It turned out that for SAW propagating in [110]-direction, as well as in $[\bar{1}10]$-direction, the additional spin-orbit couplings enhance the relaxation rate, and thus the spin lifetime decreases with rising acoustic power of the SAW.

In this work, we focused on quantum wells in the (001) plane. Nevertheless, with the detailed microscopic discussions of Chap. 3, other growth directions can be treated analogously. For a quantum well grown in [110]-direction, e.g., the Dresselhaus term consists only of an out-of-plane component (see Eq. (3.152)). Interestingly, a SAW propagating in the $[1\bar{1}0]$-direction of this geometry becomes independent of the Dresselhaus parameter β (see Ref. [121] for details). A comprehensive treatment of all possible growth directions supporting the propagation of a SAW represents therefore an interesting field for future research. Especially the question whether the additional SAW-induced spin-orbit interactions, contrary to the case of the (001) plane, are able to enhance the spin lifetime in other growth directions, is of interest as it would enable a tunable relaxation rate.

Furthermore, the application of two intersecting SAWs for the modulation of a two-dimensional spin density [100, 101, 103, 111] represents an interesting concept. Similar to the one-dimensional moving wires of a single SAW, two orthogonal SAW beams lead in the crossing zone to dynamic quantum dots (DQD). Utilizing again the Boltzmann-like equation (4.105), the charge distribution of these DQD can be described by the product $\rho^0(\mathbf{r},t) = X(x,t)X(y,t)$ of the solutions of (5.8). With transformations similar to (5.48), in this case for strongly located charge carriers, both components of the vector potential can be gauged away. Hence, even

taking into account the additional SAW-induced contributions, the relaxation rate vanishes and the spin lifetime formally is enhanced to infinity.

On the other hand, according to experiment [111], there is – although strongly enhanced – still a finite spin lifetime. Possible reasons could be:

- The influence of additional spin-relaxation mechanisms, e.g., Elliot-Yafet relaxation [29, 30] has to be taken into account.
- The solution $\rho^0(\mathbf{r}, t) = X(x, t)X(y, t)$ for charge carriers implies the possibility of an arbitrarily sharp localized carrier density. In practice this is, however, not possible due to the repelling Coulomb force. The inclusion of the additional electric Coulomb-field in the Boltzmann equation leads therefore to an effective charge carrier distribution with diameter $\tilde{\sigma} > \sigma$. Depending on the number of electrons within one DQD, the assumption of a strongly peaked charge carrier density may no longer be justified and therefore also the gauge transformation (5.48).

The underlying mechanism of the experimentally observed spin relaxation is thus still an open question to be answered in future research.

A. Symmetrized matrices, operators and parameters

In this appendix we present a complete list of symmetrized operators, parameters and matrices which we used in Chap. 3. Note that the Hamiltonian $\hat{H}_{\mathrm{II}} = \hbar^2\mathbf{k}^2/2m_0$, compare Eq. (3.18), is proportional to identity and its operator, $\hat{\mathrm{O}}_{\mathrm{II}}$, is thus not listed below.

A.1. Decomposition of operators

Table A.1.: Symmetrized operators

$\hat{H}_{\mathrm{I}}$	
Γ^4	$\hat{\mathrm{O}}^4_{\mathrm{I};1} = \frac{\sqrt{3}\hbar^2}{4m_0^2c^2}\mathbf{e}_x \cdot (\nabla V_0) \times \mathbf{p}$
$\hat{H}_{\mathrm{III}}$	
Γ^5	$\hat{\mathrm{O}}^5_{\mathrm{III};1} = \frac{\hbar}{m_0}p_x$
$\hat{H}_{\mathrm{IV}}$	
Γ^5	$\hat{\mathrm{O}}^5_{\mathrm{IV};1} = \frac{\sqrt{2}\hbar^2}{4m_0^2c^2}\partial_x V_0$

Table A.2.: Symmetrized operators (continued)

$\hat{H}_{\mathrm{V}}$	
Γ^1	$\hat{\mathrm{O}}^1_{\mathrm{V}} = \frac{1}{3}(\hat{D}_{xx} + \hat{D}_{yy} + \hat{D}_{zz})$
Γ^3	$\hat{\mathrm{O}}^3_{\mathrm{V};1} = \frac{1}{\sqrt{6}}(2\hat{D}_{zz} - \hat{D}_{xx} - \hat{D}_{yy})$
Γ^5	$\hat{\mathrm{O}}^5_{\mathrm{V};1} = 2\hat{D}_{yz}$
$\hat{H}_{\mathrm{VI}}$	
Γ^2	$\hat{\mathrm{O}}^2_{\mathrm{VI}} = \frac{\hbar}{6m_0^2c^2}(\partial_y V_{yz} p_z - \partial_z V_{yz} p_y + \mathrm{c.p.})$
Γ^3	$\hat{\mathrm{O}}^3_{\mathrm{VI};1} = -\frac{\hbar}{2\sqrt{3}m_0^2c^2}(\nabla V_{yz} \times \mathbf{p} \cdot \hat{e}_x - \nabla V_{zx} \times \mathbf{p} \cdot \hat{e}_y)$
Γ^4	$\hat{\mathrm{O}}^4_{\mathrm{VIa};1} = \frac{\hbar}{4\sqrt{3}m_0^2c^2}\nabla(V_{xx} + V_{yy} + V_{zz} - 2V_0) \times \mathbf{p} \cdot \hat{e}_x$ $\hat{\mathrm{O}}^4_{\mathrm{VIb};1} = \frac{\hbar}{8m_0^2c^2}\nabla(2V_0 + 2V_{xx} - V_{yy} - V_{zz}) \times \mathbf{p} \cdot \hat{e}_x$ $\hat{\mathrm{O}}^4_{\mathrm{VIc};1} = \frac{\sqrt{2}\hbar}{4m_0^2c^2}(\nabla V_0 \times \mathbf{p} \cdot \hat{e}_x + \nabla V_{xy} \times \mathbf{p} \cdot \hat{e}_y + \nabla V_{zx} \times \mathbf{p} \cdot \hat{e}_z)$
Γ^5	$\hat{\mathrm{O}}^5_{\mathrm{VIa};1} = \frac{\sqrt{3}\hbar}{8m_0^2c^2}\nabla(V_{yy} - V_{zz}) \times \mathbf{p} \cdot \hat{e}_x$ $\hat{\mathrm{O}}^5_{\mathrm{VIb};1} = \frac{\sqrt{2}\hbar}{4m_0^2c^2}(\nabla V_{zx} \times \mathbf{p} \cdot \hat{e}_z - \nabla V_{xy} \times \mathbf{p} \cdot \hat{e}_y)$

Table A.3.: Symmetrized operators (continued)

$\hat{H}_{\mathrm{VII}}$	
Γ^5	$\hat{\mathrm{O}}^5_{\mathrm{VII};1} = \hat{\mathrm{O}}^5_{\mathrm{III};1} = \frac{\hbar}{m_0} p_x$
$\hat{H}_{\mathrm{VIII}}$	
Γ^1	$\hat{\mathrm{O}}^1_{\mathrm{VIII}} = -\frac{\sqrt{2}\hbar}{6m_0^2c^2}(\partial_x V_{yz} + \partial_y V_{zx} + \partial_z V_{xy})$
Γ^3	$\hat{\mathrm{O}}^3_{\mathrm{VIII};1} = \frac{\hbar}{2\sqrt{6}m_0^2c^2}(2\partial_z V_{xy} - \partial_x V_{yz} - \partial_y V_{zx})$
Γ^4	$\hat{\mathrm{O}}^4_{\mathrm{VIIIa};1} = -\frac{\hbar}{4m_0^2c^2}\partial_x(V_{yy} - V_{zz})$ $\hat{\mathrm{O}}^4_{\mathrm{VIIIb};1} = \frac{\sqrt{3}\hbar}{2m_0^2c^2}(\partial_y V_{xy} - \partial_z V_{zx})$
Γ^5	$\hat{\mathrm{O}}^5_{\mathrm{VIIIa};1} = \frac{\sqrt{2}\hbar}{12m_0^2c^2}\partial_x(V_{xx} + V_{yy} + V_{zz} - V_0)$ $\hat{\mathrm{O}}^5_{\mathrm{VIIIb};1} = \frac{\sqrt{3}\hbar}{24m_0^2c^2}\partial_x(2V_0 - 2V_{xx} + V_{yy} + V_{zz})$ $\hat{\mathrm{O}}^5_{\mathrm{VIIIc};1} = -\frac{\hbar}{4m_0^2c^2}(\partial_y V_{xy} + \partial_z V_{zx} - \partial_x V_0)$

A.2. Symmetrized parameters

Table A.4.: Symmetrized parameters (Einstein's summation convention always implied).

$\mathcal{K}^1_0 = 1$	$\mathrm{K}^{s;4}_{\mathrm{I};\gamma} = \mathcal{K}^1_0 \mathrm{X}^{44;1}_{s\gamma}$
$\mathcal{K}^5_{\mathbf{k};\gamma} \equiv \mathcal{K}^5_{\mathrm{III};\gamma} = \mathcal{K}^5_{\mathrm{IV};\gamma} = k_\gamma$	$\mathrm{K}^{s,5}_{\mathrm{IV};\gamma} = \mathcal{K}^5_{\mathbf{k};\lambda} \mathrm{X}^{45;5}_{\lambda;s\gamma}$
$\mathcal{K}^1_{\boldsymbol{\varepsilon}} \equiv \mathcal{K}^1_{\mathrm{V}} = \mathcal{K}^1_{\mathrm{VI}} = \mathrm{Tr}\boldsymbol{\varepsilon}$ $\mathcal{K}^3_{\boldsymbol{\varepsilon};\lambda} \equiv \mathcal{K}^3_{\mathrm{V};\gamma} = \mathcal{K}^3_{\mathrm{VI};\gamma} =$ $\left(\frac{2\varepsilon_{zz}-\varepsilon_{xx}-\varepsilon_{yy}}{\sqrt{6}}, \frac{\varepsilon_{xx}-\varepsilon_{yy}}{\sqrt{2}}\right)$ $\mathcal{K}^5_{\boldsymbol{\varepsilon};\lambda} \equiv \mathcal{K}^5_{\mathrm{V};\gamma} = \mathcal{K}^5_{\mathrm{VI};\gamma} =$ $(\varepsilon_{yz}, \varepsilon_{zx}, \varepsilon_{xy})$	$\mathrm{K}^{s;2}_{\mathrm{VI}} = \mathcal{K}^5_{\boldsymbol{\varepsilon};\lambda} \mathrm{X}^{42;5}_{\lambda;s}$ $\mathrm{K}^{s;3}_{\mathrm{VI};\gamma} = \mathcal{K}^5_{\boldsymbol{\varepsilon};\lambda} \mathrm{X}^{43;5}_{\lambda;s\gamma}$ $\mathrm{K}^{s;4}_{\mathrm{VIa};\gamma} = \mathcal{K}^1_{\boldsymbol{\varepsilon}} \mathrm{X}^{44;1}_{1;s\gamma}$ $\mathrm{K}^{s;4}_{\mathrm{VIb};\gamma} = \mathcal{K}^3_{\boldsymbol{\varepsilon};\lambda} \mathrm{X}^{44;3}_{\lambda;s\gamma}$ $\mathrm{K}^{s;4}_{\mathrm{VIc};\gamma} = \mathcal{K}^5_{\boldsymbol{\varepsilon};\lambda} \mathrm{X}^{44;5}_{\lambda;s\gamma}$ $\mathrm{K}^{s;5}_{\mathrm{VIa};\gamma} = \mathcal{K}^3_{\boldsymbol{\varepsilon};\lambda} \mathrm{X}^{45;3}_{\lambda;s\gamma}$ $\mathrm{K}^{s;5}_{\mathrm{VIb};\gamma} = \mathcal{K}^5_{\boldsymbol{\varepsilon};\lambda} \mathrm{X}^{45;5}_{\lambda;s\gamma}$
$\mathcal{K}^1_{\mathbf{k}\boldsymbol{\varepsilon}} = \mathcal{K}^5_{\mathbf{k};\gamma} \mathrm{X}^{55;1}_{\gamma\gamma'} \mathcal{K}^5_{\boldsymbol{\varepsilon};\gamma'}$ $\mathcal{K}^3_{\mathbf{k}\boldsymbol{\varepsilon};\lambda} = \mathcal{K}^5_{\mathbf{k};\gamma} \mathrm{X}^{55;3}_{\lambda;\gamma\gamma'} \mathcal{K}^5_{\boldsymbol{\varepsilon};\gamma'}$ $\mathcal{K}^4_{\mathbf{k}\boldsymbol{\varepsilon}1;\lambda} = \mathcal{K}^5_{\mathbf{k};\gamma} \mathrm{X}^{53;4}_{\lambda;\gamma\gamma'} \mathcal{K}^3_{\boldsymbol{\varepsilon};\gamma'}$ $\mathcal{K}^4_{\mathbf{k}\boldsymbol{\varepsilon}2;\lambda} = \mathcal{K}^5_{\mathbf{k};\gamma} \mathrm{X}^{55;4}_{\lambda;\gamma\gamma'} \mathcal{K}^5_{\boldsymbol{\varepsilon};\gamma'}$ $\mathcal{K}^5_{\mathbf{k}\boldsymbol{\varepsilon}1;\lambda} = \mathcal{K}^5_{\mathbf{k};\gamma} \mathrm{X}^{51;5}_{\lambda;\gamma} \mathcal{K}^1_{\boldsymbol{\varepsilon}}$ $\mathcal{K}^5_{\mathbf{k}\boldsymbol{\varepsilon}2;\lambda} = \mathcal{K}^5_{\mathbf{k};\gamma} \mathrm{X}^{53;5}_{\lambda;\gamma\gamma'} \mathcal{K}^3_{\boldsymbol{\varepsilon};\gamma'}$ $\mathcal{K}^5_{\mathbf{k}\boldsymbol{\varepsilon}3;\lambda} = \mathcal{K}^5_{\mathbf{k};\gamma} \mathrm{X}^{55;5}_{\lambda;\gamma\gamma'} \mathcal{K}^5_{\boldsymbol{\varepsilon};\gamma'}$	$\mathrm{K}^5_{\mathrm{VII};\gamma} = -\frac{1}{3}\mathcal{K}^5_{\mathbf{k}\boldsymbol{\varepsilon}1;\gamma} - \sqrt{\frac{2}{3}}\mathcal{K}^5_{\mathbf{k}\boldsymbol{\varepsilon}2;\gamma} - \sqrt{2}\mathcal{K}^5_{\mathbf{k}\boldsymbol{\varepsilon}3;\gamma}$ $\mathrm{K}^{s;1}_{\mathrm{VIII}} = \mathcal{K}^4_{\mathbf{k}\boldsymbol{\varepsilon}2;\lambda} \mathrm{X}^{41;4}_{\lambda;s}$ $\mathrm{K}^{s;3}_{\mathrm{VIII};\gamma} = \frac{1}{\sqrt{3}}\mathcal{K}^4_{\mathbf{k}\boldsymbol{\varepsilon}2;\lambda} \mathrm{X}^{43;4}_{\lambda;s\gamma} + \mathcal{K}^5_{\mathbf{k}\boldsymbol{\varepsilon}3;\lambda} \mathrm{X}^{43;5}_{\lambda;s\gamma}$ $\mathrm{K}^{s;4}_{\mathrm{VIIIa};\gamma} = \mathcal{K}^4_{\mathbf{k}\boldsymbol{\varepsilon}1;\lambda} \mathrm{X}^{44;4}_{\lambda;s\gamma} - \sqrt{3}\mathcal{K}^5_{\mathbf{k}\boldsymbol{\varepsilon}2;\lambda} \mathrm{X}^{44;5}_{\lambda;s\gamma}$ $\mathrm{K}^{s;4}_{\mathrm{VIIIb};\gamma} = \mathcal{K}^1_{\mathbf{k}\boldsymbol{\varepsilon}} \mathrm{X}^{44;1}_{1;s\gamma} - \frac{\sqrt{3}}{2}\mathcal{K}^3_{\mathbf{k}\boldsymbol{\varepsilon};\lambda} \mathrm{X}^{44;3}_{\lambda;s\gamma}$ $+ \frac{1}{2\sqrt{3}}\mathcal{K}^4_{\mathbf{k}\boldsymbol{\varepsilon}2;\lambda} \mathrm{X}^{44;4}_{\lambda;s\gamma} - \frac{1}{2\sqrt{3}}\mathcal{K}^5_{\mathbf{k}\boldsymbol{\varepsilon}3;\lambda} \mathrm{X}^{44;5}_{\lambda;s\gamma}$ $\mathrm{K}^{s;5}_{\mathrm{VIIIa};\gamma} = \mathcal{K}^5_{\mathbf{k}\boldsymbol{\varepsilon}1;\lambda} \mathrm{X}^{45;5}_{\lambda;s\gamma}$ $\mathrm{K}^{s;5}_{\mathrm{VIIIb};\gamma} = \sqrt{3}\mathcal{K}^4_{\mathbf{k}\boldsymbol{\varepsilon}1\lambda} \mathrm{X}^{45;4}_{\lambda;s\gamma} + \mathcal{K}^5_{\mathbf{k}\boldsymbol{\varepsilon}2;\lambda} \mathrm{X}^{45;5}_{\lambda;s\gamma}$ $\mathrm{K}^{s;5}_{\mathrm{VIIIc};\gamma} = \sqrt{3}\mathcal{K}^3_{\mathbf{k}\boldsymbol{\varepsilon};\lambda} \mathrm{X}^{45;3}_{\lambda;s\gamma} - \mathcal{K}^4_{\mathbf{k}\boldsymbol{\varepsilon}2;\lambda} \mathrm{X}^{45;4}_{\lambda;s\gamma}$ $+ \mathcal{K}^5_{\mathbf{k}\boldsymbol{\varepsilon}3;\lambda} \mathrm{X}^{45;5}_{\lambda;s\gamma}$

A.3. Invariant matrices

Table A.5.: Symmetrized matrices $\mathrm{X}^{ab;\mu}_{\gamma;\delta\delta'} = \left(\mathrm{X}^{ba,\mu}_{\gamma;\delta'\delta}\right)^*$ of the symemtry group T_d which transform according to the representation Γ^μ. The matrices σ^i, J_i and T_i are defined in Tab. A.10.

Representations	Symmetrized matrices
$\Gamma^{1*} \otimes \Gamma^1$	Γ^1 : $\mathrm{X}_1^{11;1} = 1$
$\Gamma^{1*} \otimes \Gamma^2$	Γ^2 : $\mathrm{X}_1^{12;2} = 1$
$\Gamma^{1*} \otimes \Gamma^3$	Γ^3 : $\mathrm{X}_1^{13;3} = (1,0)\,, \mathrm{X}_2^{13;3} = (0,1)$
$\Gamma^{1*} \otimes \Gamma^4$	Γ^4 : $\mathrm{X}_1^{14;4} = (1,0,0)\,, \mathrm{X}_2^{14;4} = (0,1,0)\,,$ $\mathrm{X}_3^{14;4} = (0,0,1)$
$\Gamma^{1*} \otimes \Gamma^5$	Γ^5 : $\mathrm{X}_1^{15;5} = \mathrm{X}_1^{14;4}, \mathrm{X}_2^{15;5} = \mathrm{X}_2^{14;4}, \mathrm{X}_3^{15;5} = \mathrm{X}_3^{14;4}$
$\Gamma^{2*} \otimes \Gamma^2$	Γ^1 : $\mathrm{X}_1^{22;1} = 1$
$\Gamma^{2*} \otimes \Gamma^3$	Γ^3 : $\mathrm{X}_1^{23;3} = (0,-1)\,, \mathrm{X}_2^{23;3} = (1,0)$
$\Gamma^{2*} \otimes \Gamma^4$	Γ^5 : $\mathrm{X}_1^{24;5} = \mathrm{X}_1^{14;4}, \mathrm{X}_2^{24;5} = \mathrm{X}_2^{14;4},$ $\mathrm{X}_3^{24;5} = \mathrm{X}_3^{14;4}$
$\Gamma^{2*} \otimes \Gamma^5$	Γ^4 : $\mathrm{X}_1^{25;4} = \mathrm{X}_1^{14;4}, \mathrm{X}_2^{25;4} = \mathrm{X}_2^{14;4}, \mathrm{X}_3^{25;4} = \mathrm{X}_3^{14;4}$

Table A.6.: Symmetrized matrices (continued)

$\Gamma^{3^*} \otimes \Gamma^3$	Γ^1 :	$\mathrm{X}_1^{33;1} = 1/\sqrt{2}\,\mathbb{1}_{2\times 2}$
	Γ^2 :	$\mathrm{X}_1^{33;2} = \mathrm{i}/\sqrt{2}\,\sigma^y$
	Γ^3 :	$\mathrm{X}_1^{33;3} = -1/\sqrt{2}\,\sigma^z, \mathrm{X}_2^{33;3} = 1/\sqrt{2}\,\sigma^x$
$\Gamma^{3^*} \otimes \Gamma^4$	Γ^4 :	$\mathrm{X}_1^{34;4} = \frac{1}{2}\begin{pmatrix} -1 & 0 & 0 \\ \sqrt{3} & 0 & 0 \end{pmatrix}$, $\mathrm{X}_2^{34;4} = \frac{1}{2}\begin{pmatrix} 0 & -1 & 0 \\ 0 & -\sqrt{3} & 0 \end{pmatrix}$, $\mathrm{X}_3^{34;4} = \begin{pmatrix} 0 & 0 & 1 \\ 0 & 0 & 0 \end{pmatrix}$
	Γ^5 :	$\mathrm{X}_1^{34;5} = \frac{1}{2}\begin{pmatrix} -\sqrt{3} & 0 & 0 \\ -1 & 0 & 0 \end{pmatrix}$, $\mathrm{X}_2^{34;5} = \frac{1}{2}\begin{pmatrix} 0 & \sqrt{3} & 0 \\ 0 & -1 & 0 \end{pmatrix}$, $\mathrm{X}_3^{34;5} = \begin{pmatrix} 0 & 0 & 0 \\ 0 & 0 & 1 \end{pmatrix}$
$\Gamma^{3^*} \otimes \Gamma^5$	Γ^4 :	$\mathrm{X}_1^{35;4} = \mathrm{X}_1^{34;5}, \mathrm{X}_2^{35;4} = \mathrm{X}_2^{34;5}, \mathrm{X}_3^{35;4} = \mathrm{X}_3^{34;5}$
	Γ^5 :	$\mathrm{X}_1^{35;5} = \mathrm{X}_1^{34;4}, \mathrm{X}_2^{35;5} = \mathrm{X}_2^{34;4}, \mathrm{X}_3^{35;5} = \mathrm{X}_3^{34;4}$

Table A.7.: Symmetrized matrices (continued)

$\Gamma^{4*} \otimes \Gamma^4$	Γ^1 :	$\mathrm{X}_1^{44;1} = \frac{1}{\sqrt{3}} \mathbb{1}_{3\times 3}$
	Γ^3 :	$\mathrm{X}_1^{44;3} = \frac{1}{\sqrt{6}} \begin{pmatrix} -1 & 0 & 0 \\ 0 & -1 & 0 \\ 0 & 0 & 2 \end{pmatrix}$, $\mathrm{X}_2^{44;3} = \frac{1}{\sqrt{2}} \begin{pmatrix} 1 & 0 & 0 \\ 0 & -1 & 0 \\ 0 & 0 & 0 \end{pmatrix}$
	Γ^4 :	$\mathrm{X}_1^{44;4} = \begin{pmatrix} 0 & 0 & 0 \\ 0 & 0 & \frac{-1}{\sqrt{2}} \\ 0 & \frac{1}{\sqrt{2}} & 0 \end{pmatrix}, \mathrm{X}_2^{44;4} = \begin{pmatrix} 0 & 0 & \frac{1}{\sqrt{2}} \\ 0 & 0 & 0 \\ \frac{-1}{\sqrt{2}} & 0 & 0 \end{pmatrix}$, $\mathrm{X}_3^{44;4} = \begin{pmatrix} 0 & \frac{-1}{\sqrt{2}} & 0 \\ \frac{1}{\sqrt{2}} & 0 & 0 \\ 0 & 0 & 0 \end{pmatrix}$
	Γ^5 :	$\mathrm{X}_1^{44;5} = \begin{pmatrix} 0 & 0 & 0 \\ 0 & 0 & \frac{1}{\sqrt{2}} \\ 0 & \frac{1}{\sqrt{2}} & 0 \end{pmatrix}, \mathrm{X}_2^{44;5} = \begin{pmatrix} 0 & 0 & \frac{1}{\sqrt{2}} \\ 0 & 0 & 0 \\ \frac{1}{\sqrt{2}} & 0 & 0 \end{pmatrix}$, $\mathrm{X}_3^{44;5} = \begin{pmatrix} 0 & \frac{1}{\sqrt{2}} & 0 \\ \frac{1}{\sqrt{2}} & 0 & 0 \\ 0 & 0 & 0 \end{pmatrix}$
$\Gamma^{4*} \otimes \Gamma^5$	Γ^2 :	$\mathrm{X}_1^{45;2} = \mathrm{X}_1^{44;1}$
	Γ^3 :	$\mathrm{X}_1^{45;3} = -\mathrm{X}_2^{44;3}, \mathrm{X}_2^{45;3} = \mathrm{X}_1^{44;3}$
	Γ^4 :	$\mathrm{X}_1^{45;4} = \mathrm{X}_1^{44;5}, \mathrm{X}_2^{45;4} = \mathrm{X}_2^{44;5}, \mathrm{X}_3^{45;4} = \mathrm{X}_3^{44;5}$
	Γ^5 :	$\mathrm{X}_1^{45;5} = -\mathrm{X}_1^{44;4}, \mathrm{X}_2^{45;5} = -\mathrm{X}_2^{44;4}, \mathrm{X}_3^{45;5} = -\mathrm{X}_3^{44;4}$
$\Gamma^{5*} \otimes \Gamma^5$	Γ^1 :	$\mathrm{X}_1^{55;1} = \mathrm{X}_1^{44;1}$
	Γ^3 :	$\mathrm{X}_1^{55;3} = \mathrm{X}_1^{44;3}, \mathrm{X}_2^{55;3} = \mathrm{X}_2^{44;3}$
	Γ^4 :	$\mathrm{X}_1^{55;4} = \mathrm{X}_1^{44;4}, \mathrm{X}_2^{55;4} = \mathrm{X}_2^{44;4}, \mathrm{X}_3^{55;4} = \mathrm{X}_3^{44;4}$
	Γ^5 :	$\mathrm{X}_1^{55;5} = \mathrm{X}_1^{44;5}, \mathrm{X}_2^{55;5} = \mathrm{X}_2^{44;5}, \mathrm{X}_3^{55;5} = \mathrm{X}_3^{44;5}$

Table A.8.: Symmetrized matrices of the double group $T_d \otimes D_{\frac{1}{2}}$.

Representations	Symmetrized matrices
$\Gamma^{1*} \otimes \Gamma^6$	Γ^6 : $\mathrm{X}_1^{16;6} = (1,0)\,, \mathrm{X}_2^{16;6} = (0,1)$
$\Gamma^{2*} \otimes \Gamma^6$	Γ^7 : $\mathrm{X}_1^{26;7} = \mathrm{X}_1^{16;6}, \mathrm{X}_2^{26;7} = \mathrm{X}_2^{16;6}$
$\Gamma^{3*} \otimes \Gamma^6$	Γ^8 : $\mathrm{X}_1^{36;8} = \begin{pmatrix} 0 & -1 \\ 0 & 0 \end{pmatrix}, \mathrm{X}_2^{36;8} = \begin{pmatrix} 0 & 0 \\ -1 & 0 \end{pmatrix},$ $\mathrm{X}_3^{36;8} = \begin{pmatrix} 0 & 0 \\ 0 & 1 \end{pmatrix}, \mathrm{X}_4^{36;8} = \begin{pmatrix} 1 & 0 \\ 0 & 0 \end{pmatrix}$
$\Gamma^{4*} \otimes \Gamma^6$	Γ^6 : $\mathrm{X}_1^{46;6} = \begin{pmatrix} 0 & \frac{-1}{\sqrt{3}} \\ 0 & \frac{-\mathrm{i}}{\sqrt{3}} \\ \frac{-1}{\sqrt{3}} & 0 \end{pmatrix}, \mathrm{X}_2^{46;6} = \begin{pmatrix} \frac{-1}{\sqrt{3}} & 0 \\ \frac{\mathrm{i}}{\sqrt{3}} & 0 \\ 0 & \frac{1}{\sqrt{3}} \end{pmatrix}$
	Γ^8 : $\mathrm{X}_1^{46;8} = \begin{pmatrix} \frac{1}{\sqrt{6}} & 0 \\ \frac{-\mathrm{i}}{\sqrt{6}} & 0 \\ 0 & \frac{2}{\sqrt{6}} \end{pmatrix}, \mathrm{X}_2^{46;8} = \begin{pmatrix} 0 & \frac{-1}{\sqrt{2}} \\ 0 & \frac{\mathrm{i}}{\sqrt{2}} \\ 0 & 0 \end{pmatrix},$ $\mathrm{X}_3^{46;8} = \begin{pmatrix} \frac{1}{\sqrt{2}} & 0 \\ \frac{\mathrm{i}}{\sqrt{2}} & 0 \\ 0 & 0 \end{pmatrix}, \mathrm{X}_4^{46;8} = \begin{pmatrix} 0 & \frac{-1}{\sqrt{6}} \\ 0 & \frac{-\mathrm{i}}{\sqrt{6}} \\ \frac{2}{\sqrt{6}} & 0 \end{pmatrix},$
$\Gamma^{5*} \otimes \Gamma^6$	Γ^6 : $\mathrm{X}_1^{56;7} = \mathrm{X}_1^{46;6}, \mathrm{X}_2^{56;7} = \mathrm{X}_2^{46;6}$
	Γ^8 : $\mathrm{X}_1^{56;8} = -\mathrm{X}_3^{46;8}, \mathrm{X}_2^{56;8} = \mathrm{X}_4^{46;8},$ $\mathrm{X}_3^{56;8} = \mathrm{X}_1^{46;8}, \mathrm{X}_4^{56;8} = -\mathrm{X}_2^{46;8},$

Table A.9.: Symmetrized matrices (continued). The anticomutator is defined by $\{A, B\} = (AB + BA)/2$.

$\Gamma^{6*} \otimes \Gamma^{6}$	Γ^1 :	$\mathrm{X}_1^{66;1} = \frac{1}{\sqrt{2}} \mathbb{1}_{2\times 2}$
	Γ^4 :	$\mathrm{X}_1^{66;4} = \frac{1}{\sqrt{2}}\sigma^x, \mathrm{X}_2^{66;4} = \frac{1}{\sqrt{2}}\sigma^y, \mathrm{X}_3^{66;4} = \frac{1}{\sqrt{2}}\sigma^z$
$\Gamma^{6*} \otimes \Gamma^{7}$	Γ^2 :	$\mathrm{X}_1^{67;2} = \frac{1}{\sqrt{2}} \mathbb{1}_{2\times 2}$
	Γ^5 :	$\mathrm{X}_1^{67;5} = \frac{1}{\sqrt{2}}\sigma^x, \mathrm{X}_2^{67;5} = \frac{1}{\sqrt{2}}\sigma^y, \mathrm{X}_3^{67;5} = \frac{1}{\sqrt{2}}\sigma^z$
$\Gamma^{6*} \otimes \Gamma^{8}$	Γ^3 :	$\mathrm{X}_1^{68;3} = \frac{\sqrt{3}}{2}(T_{xx} - T_{yy}), \mathrm{X}_2^{68;3} = -\frac{1}{2}(2T_{zz} - T_{xx} - T_{yy})$
	Γ^4 :	$\mathrm{X}_1^{68;4} = \sqrt{3}\, T_{yz}, \mathrm{X}_2^{68;4} = \sqrt{3}\, T_{zx}, \mathrm{X}_3^{68;4} = \sqrt{3}\, T_{xy}$
	Γ^5 :	$\mathrm{X}_1^{68;5} = \frac{3}{2}T_x, \mathrm{X}_2^{68;5} = \frac{3}{2}T_y, \mathrm{X}_3^{68;5} = \frac{3}{2}T_z$
$\Gamma^{7*} \otimes \Gamma^{7}$	Γ^1 :	$\mathrm{X}_1^{77;1} = \frac{1}{\sqrt{2}} \mathbb{1}_{2\times 2}$
	Γ^4 :	$\mathrm{X}_1^{77;4} = \frac{1}{\sqrt{2}}\sigma^x, \mathrm{X}_2^{77;4} = \frac{1}{\sqrt{2}}\sigma^y, \mathrm{X}_3^{77;4} = \frac{1}{\sqrt{2}}\sigma^z$
$\Gamma^{7*} \otimes \Gamma^{8}$	Γ^3 :	$\mathrm{X}_1^{78;3} = -\mathrm{X}_2^{68;3}, \mathrm{X}_2^{78;3} = \mathrm{X}_1^{68;3}$
	Γ^4 :	$\mathrm{X}_1^{78;4} = \mathrm{X}_1^{68;5}, \mathrm{X}_2^{78;4} = \mathrm{X}_2^{68;5}, \mathrm{X}_3^{78;4} = \mathrm{X}_3^{68;5}$
	Γ^5 :	$\mathrm{X}_1^{78;5} = \mathrm{X}_1^{68;4}, \mathrm{X}_2^{78;5} = \mathrm{X}_2^{68;4}, \mathrm{X}_3^{78;5} = \mathrm{X}_3^{68;4}$
$\Gamma^{8*} \otimes \Gamma^{8}$	Γ^1 :	$\mathrm{X}_1^{88;1} = \frac{1}{2}\mathbb{1}_{4\times 4} = \frac{2}{15}J^2$
	Γ^2 :	$\mathrm{X}_1^{88;2} = \frac{1}{\sqrt{3}}\left(J_x J_y J_z + J_z J_y J_x\right)$
	Γ^3 :	$\mathrm{X}_1^{88;3} = \frac{1}{6}(2J_z^2 - J_x^2 - J_y^2), \mathrm{X}_2^{88;3} = \frac{1}{2\sqrt{3}}(J_x^2 - J_y^2)$
	Γ^4 :	$\mathrm{X}_{\mathrm{A};1}^{88,4} = \frac{1}{\sqrt{5}}J_x, \mathrm{X}_{\mathrm{A};2}^{88,4} = \frac{1}{\sqrt{5}}J_y, \mathrm{X}_{\mathrm{A};3}^{88,4} = \frac{1}{\sqrt{5}}J_z;$ $\mathrm{X}_{\mathrm{B};1}^{88,4} = \frac{1}{\sqrt{5}}(\frac{5}{3}\,J_x^3 - \frac{41}{12}\,J_x), \mathrm{X}_{\mathrm{B};2}^{88,4} = \frac{1}{\sqrt{5}}(\frac{5}{3}\,J_y^3 - \frac{41}{12}\,J_y),$ $\mathrm{X}_{\mathrm{B};3}^{88,4} = \frac{1}{\sqrt{5}}(\frac{5}{3}\,J_z^3 - \frac{41}{12}\,J_z)$
	Γ^5 :	$\mathrm{X}_{\mathrm{A};1}^{88,5} = \frac{1}{\sqrt{3}}\{J_y, J_z\}, \mathrm{X}_{\mathrm{A};2}^{88,5} = \frac{1}{\sqrt{3}}\{J_z, J_x\},$ $\mathrm{X}_{\mathrm{A};3}^{88,5} = \frac{1}{\sqrt{3}}\{J_x, J_y\}$ $\mathrm{X}_{\mathrm{B};1}^{88,5} = \frac{1}{\sqrt{3}}\{(J_y^2 - J_z^2), J_x\},$ $\mathrm{X}_{\mathrm{B};2}^{88,5} = \frac{1}{\sqrt{3}}\{(J_z^2 - J_x^2), J_y\},$ $\mathrm{X}_{\mathrm{B};3}^{88,5} = \frac{1}{\sqrt{3}}\{(J_x^2 - J_y^2), J_z\}$

Table A.10.: Symmetrized matrices which are frequently used in the theory of invariants (see, e.g., Ref. [35, 39])

$$\mathbb{1}_{2\times 2} = \begin{pmatrix} 1 & 0 \\ 0 & 1 \end{pmatrix}, \sigma^x = \begin{pmatrix} 0 & 1 \\ 1 & 0 \end{pmatrix},$$
$$\sigma^y = \begin{pmatrix} 0 & -\mathrm{i} \\ \mathrm{i} & 0 \end{pmatrix}, \sigma^z = \begin{pmatrix} 1 & 0 \\ 0 & -1 \end{pmatrix}$$

$$J_x = \frac{1}{2}\begin{pmatrix} 0 & \sqrt{3} & 0 & 0 \\ \sqrt{3} & 0 & 2 & 0 \\ 0 & 2 & 0 & \sqrt{3} \\ 0 & 0 & \sqrt{3} & 0 \end{pmatrix}, J_y = \frac{\mathrm{i}}{2}\begin{pmatrix} 0 & -\sqrt{3} & 0 & 0 \\ \sqrt{3} & 0 & -2 & 0 \\ 0 & 2 & 0 & -\sqrt{3} \\ 0 & 0 & \sqrt{3} & 0 \end{pmatrix}$$
$$J_z = \frac{1}{2}\begin{pmatrix} 3 & 0 & 0 & 0 \\ 0 & 1 & 0 & 0 \\ 0 & 0 & -1 & 0 \\ 0 & 0 & 0 & -3 \end{pmatrix}, \mathbb{1}_{4\times 4} = \begin{pmatrix} 1 & 0 & 0 & 0 \\ 0 & 1 & 0 & 0 \\ 0 & 0 & 1 & 0 \\ 0 & 0 & 0 & 1 \end{pmatrix}$$

$$T_x = \frac{1}{3\sqrt{2}}\begin{pmatrix} -\sqrt{3} & 0 & 1 & 0 \\ 0 & -1 & 0 & \sqrt{3} \end{pmatrix}, T_y = \frac{-\mathrm{i}}{3\sqrt{2}}\begin{pmatrix} \sqrt{3} & 0 & 1 & 0 \\ 0 & 1 & 0 & \sqrt{3} \end{pmatrix}$$
$$T_z = \frac{\sqrt{2}}{3}\begin{pmatrix} 0 & 1 & 0 & 0 \\ 0 & 0 & 1 & 0 \end{pmatrix}$$

$$T_{xx} = \frac{1}{3\sqrt{2}}\begin{pmatrix} 0 & -1 & 0 & \sqrt{3} \\ \sqrt{3} & 0 & 1 & 0 \end{pmatrix}, T_{yy} = \frac{1}{3\sqrt{2}}\begin{pmatrix} 0 & -1 & 0 & -\sqrt{3} \\ \sqrt{3} & 0 & 1 & 0 \end{pmatrix}$$
$$T_{zz} = \frac{\sqrt{2}}{3}\begin{pmatrix} 0 & 1 & 0 & 0 \\ 0 & 0 & -1 & 0 \end{pmatrix}$$

$$T_{yz} = \frac{\mathrm{i}}{2\sqrt{6}}\begin{pmatrix} -1 & 0 & -\sqrt{3} & 0 \\ 0 & \sqrt{3} & 0 & 1 \end{pmatrix}, T_{zx} = \frac{1}{2\sqrt{6}}\begin{pmatrix} -1 & 0 & \sqrt{3} & 0 \\ 0 & \sqrt{3} & 0 & -1 \end{pmatrix}$$
$$T_{xy} = \frac{\mathrm{i}}{\sqrt{6}}\begin{pmatrix} 0 & 0 & 0 & -1 \\ -1 & 0 & 0 & 0 \end{pmatrix}$$

B. Löwdin partitioning

The Löwdin perturbation theory [31, 32, 35, 129] is particularly useful for the derivation of effective Hamiltonians (see Chap. 3). In conventional stationary perturbation theory one has to distinguish rigorously between degenerate and non-degenerate states. The quasi-degenerate Löwdin perturbation theory circumvents this problem and is therefore especially suited for the $\mathbf{k} \cdot \mathbf{p}$-model, in which all states of the same band are degenerate. In this section we present a short introduction to Löwdin perturbation theory where we mainly follow the lines of [35].

Similar to conventional stationary perturbation theory, the Hamiltonian is divided into a main part H_0 with known eigenvalues and eigenfunctions, and into a perturbation H':

$$H = H_0 + H' \tag{B.1}$$

The intention of Löwdin perturbation theory is to bring the Hamiltonian into a block-diagonal form (see Fig. 2.1) with vanishing matrix elements – at least up to a given order in H' – between states $|\Psi_m\rangle$ of the set A, and the states $|\Psi_l\rangle$ of the set B. The transition of the Hamiltonian into

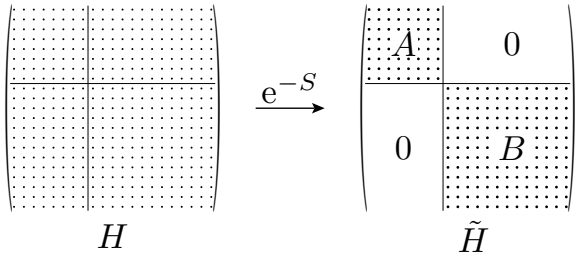

Figure 2.1.: The unitary operator e^{-S} transforms the Hamiltonian into a block-diagonalized form.

the block-diagonal form is achieved by the transformation

$$\tilde{H} = \mathrm{e}^{-S} H \mathrm{e}^{S}, \tag{B.2}$$

where $S^\dagger = -S$ denotes an anti-Hermitian operator. In order to obtain this operator S, one separates the Hamiltonian of the perturbation

$$H' = H_1 + H_2, \tag{B.3}$$

into two parts. The first one, H_1, possesses non-vanishing matrix elements only between states of the same set A or B, respectively. H_2 includes, on the contrary, all residual matrix elements that couple states of the set A with those of B. We depicted this in Fig. 2.2. Using the Baker-Campbell-

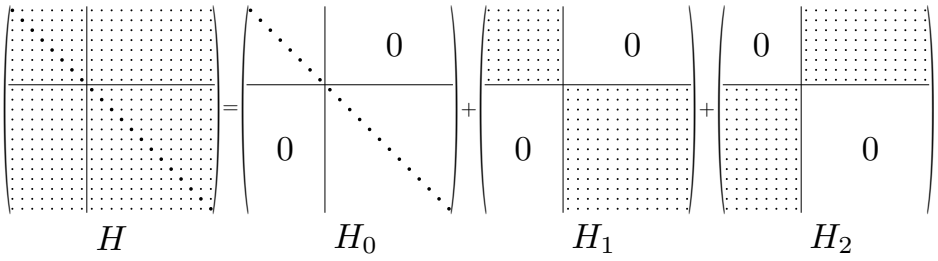

Figure 2.2.: Within Löwdin perturbation theory the Hamiltonian splitts up into H_0 as well as the perturbations H_1 and H_2.

Hausdorff formula the Hamiltonian (B.2) can be written as

$$\tilde{H} = \sum_{j=0}^{\infty} \frac{1}{j!} \left[H, S\right]_j = \sum_{j=0}^{\infty} \frac{1}{j!} \left[H_0 + H_1, S\right]_j + \sum_{j=0}^{\infty} \frac{1}{j!} \left[H_2, S\right]_j , \tag{B.4}$$

where the commutators $[H, S]_j$ are defined according to

$$\left[H, S\right]_j \equiv \left[\left[H, S\right]_{j-1}, S\right], \tag{B.5}$$

with $[H, S]_0 = H$. Equation (B.4) can apparently only be solved if S possesses the same non-block-diagonal form as H_2. The block-diagonal Hamiltonian $\tilde{H}$ consists therefore only of the terms $[H_0 + H_1, S]_j$ with even j, and $[H_2, S]_j$ with odd j:

$$\tilde{H} = \sum_{j=0}^{\infty} \frac{1}{(2j)!} \left[H_0 + H_1, S\right]_{2j} + \sum_{j=0}^{\infty} \frac{1}{(2j+1)!} \left[H_2, S\right]_{2j+1} . \tag{B.6}$$

With the help of the residual non-block-diagonal terms

$$\sum_{j=0}^{\infty} \frac{1}{(2j+1)!} \left[H_0 + H_1, S\right]_{2j+1} + \sum_{j=0}^{\infty} \frac{1}{(2j)!} \left[H_2, S\right]_{2j} = 0, \tag{B.7}$$

one could in principle derive the operator S. In general this is, however, not possible and one has to approximate S. This is accomplished by expanding S into a series

$$S = S^{(1)} + S^{(2)} + S^{(3)} + \ldots + S^{(i)} + \ldots, \tag{B.8}$$

where the operators $S^{(i)} \sim (H'/H_0)^i$ are, just as in conventional perturbation theory, assumed to converge quickly. Substituting this ansatz into (B.7) one obtains successively the operators $S^{(i)}$:

$$[H_0, S^{(1)}] = -H_2, \tag{B.9}$$
$$[H_0, S^{(2)}] = -[H_1, S^{(1)}], \tag{B.10}$$
$$[H_0, S^{(3)}] = -[H_1, S^{(2)}] - \frac{1}{3}[[H_2, S^{(1)}], S^{(1)}], \ldots \qquad = \ldots \tag{B.11}$$

Or explicitly:

$$S^{(1)}_{ml} = -\frac{H'_{ml}}{E_m - E_l}, \tag{B.12}$$
$$S^{(2)}_{ml} = \frac{1}{E_m - E_l}\left[\sum_{m'} \frac{H'_{mm'}H'_{m'l}}{E_{m'} - E_l} - \sum_{l'} \frac{H'_{ml'}H'_{l'l}}{E_m - E_{l'}}\right], \tag{B.13}$$
$$\ldots = \ldots \tag{B.14}$$

where E_j denotes the eigenenergies of H_0, and $H'_{ml} = \langle \Psi_m | H' | \Psi_l \rangle$ are the matrix elements of H'. In the following, we will stick to the notation that the indices m, m' belong to states of the set A, whereas states with indices l, l' correspond to the set B.

Eventually the expansion of the Hamiltonian

$$\tilde{H} = H^{(0)} + H^{(1)} + H^{(2)} + \ldots \tag{B.15}$$

into powers of $H^{(i)} \sim (H'/H_0)^i$ can be deduced by inserting the operators

$S^{(i)}$ (B.12), (B.13) into (B.6). Up to third order they read:

$$H^{(0)}_{mm'} = H_{0mm'}, \tag{B.16}$$

$$H^{(1)}_{mm'} = H'_{mm'}, \tag{B.17}$$

$$H^{(2)}_{mm'} = \frac{1}{2}\sum_{l} H'_{ml}H'_{lm'}\left[\frac{1}{E_m - E_l} + \frac{1}{E_{m'} - E_l}\right], \tag{B.18}$$

$$\begin{aligned} H^{(3)}_{mm'} = &-\frac{1}{2}\sum_{l,m''}\left[\frac{H'_{ml}H'_{lm''}H'_{m''m'}}{(E_{m'} - E_l)(E_{m''} - E_l)} + \frac{H'_{mm''}H'_{m''l}H'_{lm'}}{(E_m - E_l)(E_{m''} - E_l)}\right] \\ &+ \frac{1}{2}\sum_{l,l'} H'_{ml}H'_{ll'}H'_{l'm'}\left[\frac{1}{(E_m - E_l)(E_m - E_{l'})}\right. \\ &\left. + \frac{1}{(E_{m'} - E_l)(E_{m'} - E_{l'})}\right]. \end{aligned} \tag{B.19}$$

Note that the sets A and B have to be chosen in such a way that their states correspond to different eigenenergies $E_m \neq E_l$ of the Hamiltonian H_0. Contrary to conventional perturbation theory, states of the same set can, however, be degenerate.

Bibliography

[1] G. E. Moore, "Progress in digital integrated electronics," *IEEE text speech*, 1975.

[2] S. A. Wolf, D. D. Awschalom, R. A. Buhrman, J. M. Daughton, S. von Molnár, M. L. Roukes, A. Y. Chtchelkanova, and D. M. Treger, "Spintronics: a spin-based electronics vision for the future," *Science*, vol. 294, no. 5546, pp. 1488–1495, 2001.

[3] D. D. Awschalom and M. E. Flatté, "Challenges for semiconductor spintronics," *Nature Phys.*, vol. 3, p. 153, 2007.

[4] S. Datta and B. Das, "Electronic analog of the electro-optic modulator," *Appl. Phys. Lett.*, vol. 56, pp. 665–667, Feb. 1990.

[5] I. Žuti ć, J. Fabian, and S. Das Sarma, "Spintronics: fundamentals and applications," *Rev. Mod. Phys.*, vol. 76, pp. 323–410, 2 Apr. 2004.

[6] Knill, E., Laflamme, R., and Milburn, G. J., "A scheme for efficient quantum computation with linear optics," *Nature*, vol. 409, no. 6816, pp. 46–52, Jan. 2001.

[7] G. L. Bir, A. G. Aronov, and G. E. Pikus, "Spin relaxation of electrons due to scattering by holes," *Sov. Phys. JETP*, vol. 42, no. 4, p. 705, 1975.

[8] M. Z. Maialle, E. A. de Andrada E Silva, and L. J. Sham, "Exciton spin dynamics in quantum wells," *Phys. Rev. B*, vol. 47, pp. 15 776–15 788, 23 Jun. 1993.

[9] M. Dyakonov and V. Perel, "Spin relaxation of conduction electrons in noncentrosymmetric semiconductors," *Sov. Phys. Solid State*, vol. 13, no. 12, pp. 3023–3026, 1972.

[10] Rayleigh, "On waves propagated along the plane surface of an elastic solid," *Proc. London Math. Soc.*, vol. 4, no. 42, 1885.

[11] A. E. H. Love, *Some problems of geodynamics*. London: Cambridge University Press, 1911, p. 160.

[12] R. Stoneley, *Mon. Not. R. Astr. Soc. Geophys. Suppl.*, no. 5, p. 343, 1949.

[13] R. Stoneley, "The propagation of surface elastic waves in a cubic crystal," *Proc. Roy. Soc. (London)*, vol. 232, no. 1191, pp. 447–458, 1955.

[14] L. Gold, "Rayleigh wave propagation on anisotropic (cubic) media," *Phys. Rev.*, vol. 104, no. 6, pp. 1532–1536, 1956.

[15] J. L. Synge, *J. Math. Phys.*, no. 35, p. 323, 1957.

[16] H. Deresiewicz and R. D. Mindlin, "Waves on the surface of a crystal," *J. Appl. Phys.*, vol. 28, no. 6, pp. 669–671, 1957.

[17] D. C. Gazis, "Surface elastic waves in Cubic Crystals," *Phys. Rev.*, vol. 119, no. 2, p. 533, 1960.

[18] C.-C. Tseng and R. M. White, "Propagation of piezoelectric and elastic surface waves on the basal plane of hexagonal piezoelectric crystals," *J. Appl. Phys.*, vol. 38, no. 11, p. 4274, 1967.

[19] S. Adachi, "GaAs, AlAs, and AlxGa1-xAs material parameters for use in research and device applications," *J. Appl. Phys.*, vol. 58, no. 3, R1, 1985.

[20] Ioffe-Institute. (2015). New semiconductor materials. characteristics and properties. [accessed 5-August-2015], [Online]. Available: `http://www.ioffe.ru/SVA/NSM/Semicond/AlGaAs/ebasic.html`.

[21] A. Hernández-Mínguez, K. Biermann, S. Lazić, R. Hey, and P. V. Santos, "Kerr detection of acoustic spin transport in GaAs (110) quantum wells," *Appl. Phys. Lett.*, vol. 97, no. 24, p. 242 110, 2010.

[22] A. Hernández-Mínguez, K. Biermann, R. Hey, and P. V. Santos, "Spin transport and spin manipulation in GaAs (110) and (111) quantum wells," *Phys. Status Solidi B*, vol. 251, no. 9, pp. 1736–1752, 2014.

[23] T. Sogawa, P. V. Santos, S.-C. Zhang, S. Eshlaghi, A. D. Wieck, and K. H. Ploog, "Transport and lifetime enhancement of photoexcited spins in GaAs by surface acoustic waves," *Phys. Rev. Lett.*, vol. 87, no. 27, p. 276 601, 2001.

[24] F. Alsina, P. V. Santos, and R. Hey, "Spatial-dispersion-induced acoustic anisotropy in semiconductor structures," *Phys. Rev. B*, vol. 65, no. 19, p. 193 301, 2002.

[25] F. Alsina, P. V. Santos, H.-P. Schönherr, R. Nötzel, and K. H. Ploog, "Real-time dynamics of the acoustically induced carrier transport in GaAs quantum wires," *Phys. Rev. B*, vol. 67, no. 16, p. 161 305, 2003.

[26] F. Alsina, J. A. H. Stotz, R. Hey, and P. V. Santos, "Acoustically induced potential dots in GaAs quantum wells," *Solid State Commun.*, vol. 129, no. 7, pp. 453–457, 2004.

[27] O. Couto, F. Iikawa, J. Rudolph, R. Hey, and P. V. Santos, "Anisotropic spin transport in (110) GaAs quantum wells," *Phys. Rev. Lett.*, vol. 98, no. 3, p. 036 603, 2007.

[28] O. Couto, R. Hey, and P. V. Santos, "Spin dynamics in (110) GaAs quantum wells under surface acoustic waves," *Phys. Rev. B*, vol. 78, no. 15, p. 153 305, 2008.

[29] R. J. Elliott, "Theory of the effect of spin-orbit coupling on magnetic resonance in some semiconductors," *Phys. Rev.*, vol. 96, pp. 266–279, 2 Oct. 1954.

[30] Y. Yafet, "Conduction electron spin relaxation in the superconducting state," *Phys. Lett.*, vol. 98A, no. 5, pp. 287–290, 1983.

[31] J. Luttinger and W. Kohn, "Motion of electrons and holes in perturbed periodic fields," *Phys. Rev.*, vol. 97, no. 4, p. 869, 1955.

[32] G. Bir and G. E. Pikus, *Symmetry and strain-induced effects in semiconductors*. New York: Wiley, 1974, ISBN: 978-0706513677.

[33] T. B. Bahder, "Eight-band *kp* model of strained zinc-blende crystals," *Phys. Rev. B*, vol. 41, no. 17, 1990.

[34] Y. Zhang, "Motion of electrons in semiconductors under inhomogeneous strain with application to laterally confined quantum wells," *Phys. Rev. B*, vol. 49, no. 20, pp. 14 352–14 366, 1994.

[35] R. Winkler, *Spin-orbit coupling effects in two-dimensional electron and hole systems*. Berlin, New York: Springer, 2003, ISBN: 978-3540011873.

[36] K. Suzuki and J. Hensel, "Quantum resonances in the valence bands of germanium. I. Theoretical considerations," *Phys. Rev. B*, vol. 9, no. 10, 1974.

[37] J. Bardeen and W. Shockley, "Deformation potentials and mobilities in non-polar crystals," *Phys. Rev.*, vol. 80, no. 1, p. 72, 1950.

[38] G. Whitfield, "Theory of electron-phonon interactions," *Phys. Rev.*, vol. 121, p. 720, 1961.

[39] H.-R. Trebin, U. Rössler, and R. Ranvaud, "Quantum resonances in the valence bands of zinc-blende semiconductors. I. Theoretical aspects," *Phys. Rev. B*, vol. 20, no. 2, 1979.

[40] W. Commons. (2008). Crystal structure of GaAs, [Online]. Available: `http://upload.wikimedia.org/wikipedia/commons/2/21/Sphalerite_polyhedra..png`.

[41] O. Chalaev, "Matrices and characteristic polynomials for double crystallographic point groups," *ArXiv e-prints*, 2012. arXiv:`arXiv:1206.0292v3`.

[42] G. Dresselhaus, "Spin-orbit coupling effects in zinc blende structures," *Phys. Rev.*, vol. 100, p. 580, 1955.

[43] F. V. der Lage and H. Bethe, "A method for obtaining electronic eigenfunctions and eigenvalues in solids with an application to sodium," *Phys. Rev.*, vol. 9, 1947.

[44] P. Yu and M. Cardona, *Fundamentals of semiconductors physics and materials properties*. Berlin, New York: Springer, 2001, ISBN: 3-540-25470-6.

[45] I. Bronstein, K. A. Semendjajew, G. Musiol, and H. Mühlig, *Taschenbuch der Mathematik*. Frankfurt am Main: Deutsch, 2005, ISBN: 978-3-8171-2006-2.

[46] G. F. Koster, *Properties of the thirty-two point groups*. M.I.T. Press, 1963.

[47] E. O. Kane, "Band structure of indium antimonide," *J. Phys. Chem. Solids*, vol. 1, no. 4, pp. 249–261, 1957.

[48] M. Cardona, "Band parameters of semiconductors with zincblende, wurtzite, and germanium structure," *J. Phys. Chem. Solids*, vol. 24, no. 12, pp. 1543–1555, 1963.

[49] M. Braun and U. Rossler, "Magneto-optic transitions and nonparabolicity parameters in the conduction band of semiconductors," *J. Phys. Chem. Solids*, vol. 18, p. 3365, 1985.

[50] H. Mayer and U. Rössler, "Spin splitting and anisotropy of cyclotron resonance in the conduction band of GaAs," *Phys. Rev. B*, vol. 44, no. 16, pp. 9048–9051, 1991.

[51] J. J. Sakurai, *Modern quantum mechanics*. Reading, Massachusetts: Addison-Wesley Pub. Co, 1994, ISBN: 9780201539295.

[52] F. Schwabl, *Quantum mechanics*. Berlin, New York: Springer, 2007, ISBN: 9783540719328.

[53] M. Cardona, N. Christensen, and G. Fasol, "Relativistic band structure and spin-orbit splitting of zinc-blende-type semiconductors," *Phys. Rev. B*, vol. 38, no. 3, p. 1806, 1988.

[54] I. Vurgaftman, J. R. Meyer, and L. R. Ram-Mohan, "Band parameters for III-V compound semiconductors and their alloys," *J. Appl. Phys.*, vol. 89, no. 11, p. 5815, 2001.

[55] J. M. Luttinger, "Quantum theory of cyclotron resonance in semiconductors," *Phys. Rev.*, vol. 102, no. 4, p. 1030, 1954.

[56] B. Bernevig and S.-C. Zhang, "Spin splitting and spin current in strained bulk semiconductors," *Phys. Rev. B*, vol. 72, no. 11, p. 115 204, 2005.

[57] B. M. Norman, C. J. Trowbridge, J. Stephens, A. C. Gossard, D. D. Awschalom, and V. Sih, "Mapping spin-orbit splitting in strained (In,Ga)As epilayers," *Phys. Rev. B*, vol. 82, p. 081 304, 2010.

[58] Y. Kato, R. C. Myers, A. C. Gossard, and D. D. Awschalom, "Coherent spin manipulation without magnetic fields in strained semiconductors," *Nature*, vol. 427, no. 6969, p. 50, Jan. 2004.

[59] F. Michelini, N. Cavassilas, R. Hayn, and M. Szczap, "Multiband k p models for strained zincblende crystals: Application to the fine structure of ZnO," *Phys. Rev. B*, vol. 80, p. 245 210, 2009.

[60] M. Hruška, Š. Kos, S. A. Crooker, A. Saxena, and D. L. Smith, "Effects of strain, electric, and magnetic fields on lateral electron-spin transport in semiconductor epilayers," *Phys. Rev. B*, vol. 73, p. 075 306, 2006.

[61] M. Beck, C. Metzner, S. Malzer, and G. H. Döhler, "Spin lifetimes and strain-controlled spin precession of drifting electrons in zinc blende type semiconductors," *Europhys. Lett.*, vol. 75, p. 597, 2005.

[62] A. Hernández-Mínguez, K. Biermann, R. Hey, and P. V. Santos, "Electrical suppression of spin relaxation in GaAs(111)B quantum Wells," *Phys. Rev. Lett.*, vol. 109, no. 26, p. 266 602, 2012.

[63] X. Cartoixà, D. Ting, and Y.-C. Chang, "Suppression of the Dyakonov-Perel spin-relaxation mechanism for all spin components in [111] zincblende quantum wells," *Phys. Rev. B*, vol. 71, no. 4, p. 045 313, 2005.

[64] S. W. Chang and S. L. Chuang, "Strain-induced enhancement of spin relaxation times in [110] and [111] grown quantum wells," *Phys. Rev. B*, vol. 72, no. 11, pp. 1–9, 2005.

[65] R. Lassnig, "Kp theory, effective-mass approach, and spin splitting for two-dimensional electrons in GaAs-GaAlAs heterostructures," *Phys. Rev. B*, vol. 31, no. 12, pp. 8076–8086, 1985.

[66] L. V. Keldysh, "Diagram technique for nonequilibrium processes," *Sov. Phys. JETP*, vol. 20, no. 4, pp. 1018–1026, 1965.

[67] J. Rammer, *Quantum Transport Theory*. New York: Westview Press, 2004, ISBN: 0-7382-0048-4.

[68] C. Gorini, P. Schwab, R. Raimondi, and A. L. Shelankov, "Non-abelian gauge fields in the gradient expansion: generalized boltzmann and eilenberger equations," *Phys. Rev. B*, vol. 82, p. 195 316, 2010.

[69] J. Rammer, *Quantum field theory of non-equilibrium states*. Cambridge New York: Cambridge University Press, 2007, ISBN: 978-0-521-87499-1.

[70] H. Haug, *Quantum kinetics in transport and optics of semiconductors*. Berlin, New York: Springer, 1996, ISBN: 9783540616023.

[71] U. Eckern and A. Schmid, "Quasiclassical Green's function in the BCS pairing theory," *J. Low Temp. Phys.*, vol. 45, no. 1-2, pp. 137–166, 1981.

[72] P. Schwab and R. Raimondi, "Quasiclassical theory of charge transport in disordered interacting electron systems," *Ann. Phys. (Berlin)*, vol. 12, no. 7-8, pp. 471–516, 2003.

[73] J. Rammer and H. Smith, "Quantum field-theoretical methods in transport theory of metals," *Rev. Mod. Phys.*, vol. 58, no. 2, pp. 323–359, 1986.

[74] J. Schwinger, "Brownian motion of a quantum oscillator," *J. Math. Phys.*, vol. 2, no. 3, p. 407, 1961.

[75] H. Bruus, *Many-body quantum theory in condensed matter physics*. Oxford New York: Oxford University Press, 2004, ISBN: 9780198566335.

[76] P. Mello, *Quantum transport in mesoscopic systems*. Oxford New York: Oxford University Press, 2004, ISBN: 9780198525820.

[77] A. Zagoskin, *Quantum theory of many-body systems*. New York: Springer, 1998, ISBN: 9780387983844.

[78] T. Brandes, *Low-dimensional systems*. Berlin, New York: Springer, 2000, ISBN: 9783540672371.

[79] G. Mahan, *Many-particle physics*. New York: Plenum Press, 1990, ISBN: 9780306434235.

[80] J. Negele, *Quantum many-particle systems*. Reading, MA: Perseus Books, 1998, ISBN: 9780738200521.

[81] A. Altland, *Condensed Matter Field Theory*. Leiden: Cambridge University Press, 2010, ISBN: 9780521769754.

[82] S. Datta, *Electronic transport in mesoscopic systems*. Cambridge New York: Cambridge University Press, 1995, ISBN: 9780521416047.

[83] I. A. Larkin and Y. N. Ovchinnikov, "Nonlinear conductivity of superconductors in the mixed state," *Sov. Phys. JETP*, vol. 41, no. 5, pp. 960–965, 1975.

[84] R. E. Prange and L. P. Kadanoff, "Transport theory for electron-phonon interactions in metals," *Phys. Rev.*, vol. 134, no. 3A, A566–A580, 1964.

[85] A. B. Migdal, "Interaction between electrons and lattice vibrations in a normal metal," *Sov. Phys. JETP*, vol. 34, no. 6, pp. 966–1001, 1958.

[86] G. Eilenberger, "Transformation of Gorkov's equation for type II superconductors into transport-like equations," *Z. Phys.*, vol. 214, p. 195, 1968.

[87] M. Peskin and D. V. Schroeder, *An introduction to quantum field theory*. Cambridge: Perseus Books, 1995, ISBN: 9780201503975.

[88] R. Raimondi, C. Gorini, P. Schwab, and M. Dzierzawa, "Quasiclassical approach to the spin Hall effect in the two-dimensional electron gas," *Phys. Rev. B*, vol. 74, no. 3, p. 35 340, 2006.

[89] P. Schwab, M. Dzierzawa, C. Gorini, and R. Raimondi, "Spin relaxation in narrow wires of a two-dimensional electron gas," *Phys. Rev. B*, vol. 74, no. 15, p. 155 316, 2006.

[90] R. Raimondi, P. Schwab, C. Gorini, and G. Vignale, "Spin-orbit interaction in a two-dimensional electron gas: A SU(2) formulation," *Ann. Phys. (Berlin)*, vol. 524, p. 153, 2012.

[91] A. Wixforth, J. P. Kotthaus, and G. Weimann, "Quantum oscillations in the surface-acoustic-wave attenuation caused by a two-dimensional electron system," *Phys. Rev. Lett.*, vol. 56, pp. 2104–2106, 19 1986.

[92] A. Wixforth, J. Scriba, M. Wassermeier, J. P. Kotthaus, G. Weimann, and W. Schlapp, "Surface acoustic waves on GaAs/Al_x $Ga_{1-x}As$ heterostructures," *Phys. Rev. B*, vol. 40, pp. 7874–7887, 11 1989.

[93] C. Rocke, S. Zimmermann, A. Wixforth, J. P. Kotthaus, G. Böhm, and G. Weimann, "Acoustically driven storage of light in a quantum well," *Phys. Rev. Lett.*, vol. 78, no. 21, pp. 4099–4102, 1997.

[94] C. Rocke, A. Govorov, A. Wixforth, G. Böhm, and G. Weimann, "Exciton ionization in a quantum well studied by surface acoustic waves," *Phys. Rev. B*, vol. 57, no. 12, R6850–R6853, 1998.

[95] M. Rotter, A. V. Kalameitsev, A. O. Govorov, W. Ruile, and A. Wixforth, "Charge conveyance and nonlinear acoustoelectric phenomena for intense surface acoustic waves on a semiconductor quantum well," *Phys. Rev. Lett.*, vol. 82, pp. 2171–2174, 10 1999.

[96] A. O. Govorov, A. V. Kalameitsev, A. Wixforth, and M. Rotter, "Electron wires driven by a surface acoustic wave and nonlinear acoustoelectric interactions in quantum wells," *Proc. 25th Int. Conf. Phys. Semicond.*, 2000.

[97] T. Sogawa, P. V. Santos, S.-C. Zhang, S. Eshlaghi, A. D. Wieck, and K. H. Ploog, "Dynamic band-structure modulation of quantum wells by surface acoustic waves," *Phys. Rev. B*, vol. 63, no. 12, p. 121 307, 2001.

[98] F. Alsina, P. V. Santos, H.-P. Schönherr, W. Seidel, K. H. Ploog, and R. Nötzel, "Surface-acoustic-wave-induced carrier transport in quantum wires," *Phys. Rev. B*, vol. 66, no. 16, p. 165 330, 2002.

[99] A. García-Cristóbal, A. Cantarero, F. Alsina, and P. V. Santos, "Spatiotemporal carrier dynamics in quantum wells under surface acoustic waves," *Phys. Rev. B*, vol. 69, no. 20, p. 205 301, 2004.

[100] J. A. H. Stotz, F. Alsina, R. Hey, and P. V. Santos, "Acoustically induced dynamic potential dots," *Physica E*, vol. 26, no. 1-4, pp. 67–71, 2005.

[101] J. A. H. Stotz, R. Hey, P. V. Santos, and K. H. Ploog, "Coherent spin transport through dynamic quantum dots," *Nature Mat.*, vol. 4, no. 8, p. 585, 2005.

[102] O. Couto, F. Iikawa, J. A. H. Stotz, R. Hey, and P. V. Santos, "Coherent spin transport by acoustic fields in GaAs quantum wells," *Phys. Stat. Sol. C*, vol. 3, no. 12, pp. 4307–4312, 2006.

[103] J. A. H. Stotz, R. Hey, P. V. Santos, and K. H. Ploog, "Spin transport and manipulation by mobile potential dots in GaAs quantum wells," *Physica E*, vol. 32, no. 1-2, pp. 446–449, 2006.

[104] J. Rudolph, R. Hey, and P. V. Santos, "Long-range exciton transport by dynamic strain fields in a GaAs quantum well," *Phys. Rev. Lett.*, vol. 99, no. 4, p. 47 602, 2007.

[105] F. Alsina, J. A. H. Stotz, R. Hey, U. Jahn, and P. V. Santos, "Acoustic charge and spin transport in GaAs quantum wires," *Phys. Stat. Sol. C*, vol. 5, no. 9, pp. 2907–2910, Jul. 2008.

[106] J. A. H. Stotz, R. Hey, P. V. Santos, and K. H. Ploog, "Enhanced spin coherence via mesoscopic confinement during acoustically induced transport," *New J. Phys.*, vol. 10, no. 9, p. 093 013, 2008.

[107] O. Couto, S. Lazić, F. Iikawa, J. A. H. Stotz, U. Jahn, R. Hey, and P. V. Santos, "Photon anti-bunching in acoustically pumped quantum dots," *Nature Photon.*, vol. 3, no. 11, pp. 645–648, 2009.

[108] T. Sogawa, H. Sanada, H. Gotoh, H. Yamaguchi, S. Miyashita, and P. V. Santos, "Spatial and temporal modulation of exciton photoluminescence properties in GaAs/AlAs dynamic quantum dots formed by surface acoustic waves," *Phys. Rev. B*, vol. 80, no. 7, p. 75 304, 2009.

[109] O. Couto, S. Lazić, F. Iikawa, J. A. H. Stotz, U. Jahn, R. Hey, and P. V. Santos, "Evidence for photon anti-bunching in acoustically pumped dots," *Physica E*, vol. 42, no. 10, pp. 2497–2500, 2010.

[110] J. B. Kinzel, D. Rudolph, M. Bichler, R. Hey, J. J. Finley, G. Koblmüller, A. Wixforth, and H. J. Krenner, "Directional and dynamic modulation of the optical emission of an individual GaAs nanowire using surface acoustic waves," *Nano Lett.*, vol. 11, no. 4, pp. 1512–1517, 2011.

[111] H. Sanada, T. Sogawa, H. Gotoh, K. Onomitsu, M. Kohda, J. Nitta, and P. V. Santos, "Acoustically induced spin-orbit interactions revealed by two-dimensional imaging of spin transport in GaAs," *Phys. Rev. Lett.*, vol. 106, no. 21, p. 216 602, 2011.

[112] S. Völk, F. Knall, F. J. R. Schülein, T. A. Truong, H. Kim, P. M. Petroff, A. Wixforth, and H. J. Krenner, "Direct observation of dynamic surface acoustic wave controlled carrier injection into single quantum posts using phase-resolved optical spectroscopy," *Appl. Phys. Lett.*, vol. 98, no. 2, p. 23 109, 2011.

[113] T. Sogawa, H. Sanada, H. Gotoh, H. Yamaguchi, and P. V. Santos, "Dynamic control of photoluminescence polarization properties in GaAs/AlAs quantum wells by surface acoustic waves," *Phys. Rev. B*, vol. 86, no. 3, p. 35 311, 2012.

[114] H. J. Krenner, S. Völk, and F. J. R. Schülein, "Surface acoustic wave controlled carrier injection into self-assembled quantum dots and quantum posts," *Phys. Stat. Sol. C*, vol. 10, no. 2, pp. 407–410, 2012.

[115] F. J. R. Schülein, J. Pustiowski, K. Müller, M. Bichler, G. Koblmüller, J. J. Finley, A. Wixforth, and H. J. Krenner, "Surface acoustic wave controlled charge dynamics in a thin InGaAs quantum well," *JETP Lett.*, vol. 95, no. 11, pp. 575–580, 2012.

[116] H. Sanada, Y. Kunihashi, H. Gotoh, K. Onomitsu, M. Kohda, J. Nitta, P. V. Santos, and T. Sogawa, "Manipulation of mobile spin coherence using magnetic-field-free electron spin resonance," *Nature Phys.*, vol. 9, no. 5, pp. 280–283, 2013.

[117] F. J. R. Schülein, K. Müller, M. Bichler, G. Koblmüller, J. J. Finley, A. Wixforth, and H. J. Krenner, "Acoustically regulated carrier injection into a single optically active quantum dot," *Phys. Rev. B*, vol. 88, no. 8, p. 85 307, 2013.

[118] B. K. Ridley, "Kinetics of radiative recombination in quantum wells," *Phys. Rev. B*, vol. 41, pp. 12 190–12 196, 17 1990.

[119] C. Piermarocchi, F. Tassone, V. Savona, A. Quattropani, and P. Schwendimann, "Exciton formation rates in GaAs/$Al_xGa_{1-x}As$ quantum wells," *Phys. Rev. B*, vol. 55, pp. 1333–1336, 3 Jan. 1997.

[120] D. A. B. Miller, D. S. Chemla, T. C. Damen, A. C. Gossard, W. Wiegmann, T. H. Wood, and C. A. Burrus, "Electric field dependence of optical absorption near the band gap of quantum-well structures," *Phys. Rev. B*, vol. 32, pp. 1043–1060, 2 Jul. 1985.

[121] J. Wanner, C. Gorini, P. Schwab, and U. Eckern, "Driving spin and charge in quantum wells by surface acoustic waves," *Adv. Mater. Interfaces*, vol. 1, no. 8, p. 1 400 181, 2014.

[122] A. Cameron, P. Riblet, and A. Miller, "Spin gratings and the measurement of electron drift mobility in multiple quantum well semiconductors," *Phys. Rev. Lett.*, vol. 76, no. 25, p. 4793, 1996.

[123] G. Wang, B. L. Liu, A. Balocchi, P. Renucci, C. R. Zhu, T. Amand, C. Fontaine, and X. Marie, "Gate control of the electron spin-diffusion length in semiconductor quantum wells," *Nature Comm.*, vol. 4, p. 2372, 2013.

[124] M. V. Fischetti and S. E. Laux, "Monte Carlo simulation of transport in technologically significant semiconductors of the diamond and zinc-blende structures–I: homogeneous transport," *IEEE Transactions on Electron Devices*, vol. 38, no. 3, pp. 650–660, 1991.

[125] J. Požela and A. Reklaitis, "Diffusion coefficient of hot electrons in GaAs," *Solid State Commun.*, vol. 27, no. 11, pp. 1073–1077, 1978.

[126] M. Dyakonov and V. Perel, "Current-induced spin orientation of electrons in semiconductors," *Phys. Lett.*, vol. 35A, no. 6, pp. 459–460, 1971.

[127] J. D. Koralek, C. P. Weber, J. Orenstein, B. A. Bernevig, S.-C. Zhang, S. Mack, and D. D. Awschalom, "Emergence of the persistent spin helix in semiconductor quantum wells," *Nature*, vol. 458, no. 7238, pp. 610–3, 2009.

[128] M. Kohda, V. Lechner, Y. Kunihashi, T. Dollinger, P. Olbrich, C. Schönhuber, I. Caspers, V. V. Bel'kov, L. E. Golub, D. Weiss, K. Richter, J. Nitta, and S. D. Ganichev, "Gate-controlled persistent spin helix state in (In,Ga)As quantum wells," *Phys. Rev. B*, vol. 86, no. 8, p. 081 306, 2012.

[129] P.-O. Löwdin, "A Note on the quantum-mechanical perturbation theory," *J. Chem. Phys.*, vol. 19, no. 11, pp. 1396–1401, 1951.

Acknowledgements

At this point I would like to thank all the people that were involved in the successful completion of this thesis, especially:

- Prof. Dr. Ulrich Eckern for giving me the opportunity to work in his group and particularly for his patient way to guide me through this work
- Prof. Dr. Gert-Ludwig Ingold for agreeing to be my "Zweitgutachter" and for all his friendly support over the last years
- PD Dr. Peter Schwab for his useful help during the first two years
- Dr. Michael Dzierzawa for many interesting discussions as well as improving my English
- PD Dr. Karl-Heinz Höck for his invaluable support to the topic of group theory
- Dr. Cosimo Gorini for his collaboration
- All other people of the group for the pleasant atmosphere